UNIVERSITAT POLITÈCNICA DE VALÈNCIA

DEPARTAMENT DE QUÍMICA

Organic-inorganic hybrid materials for boron removal from aqueous media

PhD. THESIS

Submitted by

Cristina Sanfeliu Cano

PhD. Supervisors:

Prof. Mª Dolores Marcos Martínez
Prof. Félix Sancenón Galarza

Valencia Febrero de 2016

Instituto Interuniversitario de Reconocimiento Molecular y Desarrollo Tecnológico

Mª DOLORES MARCOS MARTÍNEZ, PhD in Chemistry and Professor at the Universitat Politècnica de València, and FÉLIX SANCENÓN GALARZA, PhD in Chemistry and Lecturer at the *Universitat Politècnica de València*.

CERTIFY:

That the work *"Organic-inorganic hybrid materials for boron removal in aqueous media."* has been developed by Cristina Sanfeliu Cano under their supervision in the Centro de Reconocimiento Molecular y Desarrollo Tecnológico de la *Universitat Politècnica de València*, as a thesis Project in order to obtain the degree of PhD in Chemistry at the *Universitat Politècnica de València.*

Valencia, *February of 2016*.

Prof. Mª Dolores Marcos Martínez Dr. Félix Sancenón Galarza

Agradecimientos

Me gustaría dar las gracias a todas las personas que han hecho posible la realización de esta tesis doctoral.
En primer lugar a mis directores, por ayudarme en todo momento a resolver los problemas que surgen durante la investigación, que no han sido pocos. Al instituto de reconocimento molecular y desarrollo tecnológico por acogerme nada más terminar la carrera. Al ministerio de educación y ciencia, por concederme una beca FPU, que hizo posible que me dedicara a la investigación.

A mis compañeros y amigos del lab 2.6, una de las mejores cosas que me llevo de estos años. Al grupo de orgánica de la Universidad de Valencia, por acogerme durante un año de exilio. Al centro "Chimie de la matière condensée de Paris" de la "Université Pierre et Marie Curie", por tratarme como si estuviera en casa durante mi estancia en el extrangero.

A mis amigos, de toda la vida, de Cañamares, del Erasmus,… porque de una manera u otra todos me han acompañado durante estos años.

A nivel personal, me gustaría darles las gracias a mis padres, por apoyarme siempre en todas mis decisiones.

Y por último, pero no menos importante, a Toni, sin ti no hubiera sido capaz de soportar los momentos más duros que hemos vivido juntos.

A mi familia

Resumen

La presente tesis doctoral está dedicada al diseño (empleando conceptos de química supramolecular), síntesis y caracterización de diferentes materiales híbridos orgánico-inorgánicos para la eliminación de boro en medios acuosos. También se ha procedido a estudiar detalladamente la interacción del boro con las agrupaciones orgánicas, polialcoholes, empleadas en el desarrollo de estos nuevos adsorbentes.

En la primera parte de la tesis se presenta una introducción en la que se revisan los conceptos de química supramolecular, química del boro y los principales métodos de eliminación de boro (primer capítulo) y, también, se exponen los objetivos de la tesis (segundo capítulo).

Ya en el tercer capítulo se exponen los resultados obtenidos empleando una esponja cerámica como soporte macroscópico para los materiales activos frente a la eliminación de boro. Este soporte se "impregna" previamente con un material inorgánico silíceo mesoporoso (UVM-7) y, en una fase posterior, se funcionaliza con un grupo orgánico con alta afinidad hacia el boro (gluconamida). El grupo orgánico que funcionará como adsorbente queda así anclado a un soporte de tamaño macroscópico que facilitará la aplicación de estos materiales a gran escala. Una vez preparado y caracterizado se estudió la capacidad del material para adsorber y eliminar boro de medios acuosos y su posterior reutilización.

En el cuarto capítulo de la tesis doctoral se aborda la preparación de materiales adsorbentes de bajo coste económico para la eliminación de boro en medios acuosos. En primer lugar se emplea, como soporte inorgánico, UVM-7, una sílice mesoporosa con un sistema bimodal de poros. Este material tiene una capacidad de adsorción de boro muy elevada una vez funcionalizado con el correspondiente polialcohol (tal y como se expone en el capítulo anterior) sin embargo los reactivos para su síntesis, tetraetilortosilicato como fuente de sílice y bromuro de cetiltrimetilamonio, como agente director de estructura son muy caros con lo que el material final presenta un elevado coste. En este capítulo se presenta como

alternativa otros materiales que puedan actuar como soportes inorgánicos: UVM-11, material mesoporoso que no requiere de agente director de estructura en su síntesis, dos xerogeles con poros en el rango meso y una sílice comercial nanoparticulada de elevada superficie específica. Una vez sintetizados y caracterizados los cinco soportes se funcionalizaron con gluconamidas, que son los componentes activos frente a la adsorción de boro. Finalmente, se realiza un estudio comparativo de la capacidad de eliminación de boro de los cinco materiales preparados. Los materiales de bajo coste estudiados presentan una capacidad de eliminación de boro comparable a los materiales de mayor coste y a los materiales comercialmente disponibles.

Por último, en el capítulo cinco de esta tesis doctoral, se aborda el estudio del mecanismo de adsorción del boro en los materiales activos preparados (basados en UVM-7 como soporte inorgánico) mediante medidas de resonancia magnética nuclear de sólidos, tanto de ^{13}C como de ^{11}B empleando las técnicas de rotación en ángulo mágico, polarización cruzada, y el desacoplamiento dipolar heteronuclear. Para ello se prepara un material híbrido formado por una matriz de UVM-7 funcionalizada con gluconamidas y este sólido se pone en contacto con diferentes cantidades de boro. Los sólidos finales se caracterizan mediante RMN de ^{13}C y de ^{11}B, observándose la formación de boroesteres entre los grupos diol de las gluconamidas ancladas y el boro adsorbido. Cuando la concentración de boro empleada es baja se forman complejos bisquelados (B:glucosa = 1:2) mientras que a concentraciones altas empiezan a formarse complejos monoquelados (B:glucosa = 1:1). Este trabajo se llevó a cabo en colaboración con el grupo de investigación de "Materiales sol-gel y RMN", perteneciente al centro "Chimie de la matière condensée de Paris" de la "Université Pierre et Marie Curie".

Resum

La present tesi doctoral està dedicada al disseny (empreant conceptes de química supramolecular), síntesi i caracterització de diferents materials híbrids orgànico-inorgànics per a la el·liminació de bor en medi aquòs. També s'ha precedit a estudiar detalladament la interacció del bor amb les agrupacions orgàniques, polialcohols, empreats en el desenvolupament d'aquestos nous adsorbents.

En la primera part de la tesi es presenta una introducció en la que es revisen els conceptes de química supramolecular, química del bor i els principals mètodes de el·liminació de bor (primer capítol) i, també, s'exposen els objectius de la tesi (segon capítol).

Ja en el tercer capítol s'exposen els resultats obtinguts empreant una esponja ceràmica com a suport macroscòpic per als materials actius front a l'el·liminació del bor. Aquest suport s'impregna prèviament amb un material inorgànic de sílice mesoporós (UVM-7) i, en una següent fase, es funcionalitza amb un grup orgànic amb alta afinitat cap al bor (gluconamida). El grup orgànic que funcionarà com a adsorbent queda aixina anclat a un suport de tamany macroscòpic que facil·litarà l'aplicació d'aquestos materials a gran escala. Una vegada preparat i caracteritzat s'estudia la capacitat del material per a adsorber i el·liminar bor en medi aquós i la seua posterior reutilització.

Al quart capítol de la tesi doctoral s'aborda la preparació de materials adsorbents de baix cost econòmic per a l'eliminació de bor en medi aquòs. En primer lloc, s'empra, com a suport inorgànic, UVM-7 una sílice mesoporosa amb un sistema bimodal de porus. Aquest material té una capacitat d'adsorció molt elevada després de la seua funcionalització amb el corresponent polialcohol (tal i com s'exposa al capítol anterior), no obstant això els reactius que s'utilitzen per a la seua síntesi tetraetilortosilicat, com a font de sílice i bromur de cetiltrimetilamoni, com agent director d'estructura són molt cars, per tant el material final presenta un elevat cost. En aquest capítol es presenta com alternativa altres materials que puguen actuar com a suports inorgànics: UVM-11, material mesoporós que no

requereix d'agent director d'estructura durant la seua síntesi, dos xerogels en porus en el rang meso i una sílice comercial nanoparticulada amb elevada superfície específica. Una vegada sintetitzats i caracteritzats els cinc suports es funcionalitzen en gluconamides, que són els components actius front a la adsorció de bor. Finalment, es realitza un estudi comparatiu de la capacitat d'el·liminació de bor dels cinc materials preparats. Els materials de baix cost estudiats presenten una capacitat de eliminació de bor semblant als materials de major cost i als materials comercialment disponibles.

Per últim, al capítol cinc d'aquesta tesi doctoral, s'aborda l'estudi del mecanisme d'adsorció de bor als materials actius preparats (basats en UVM-7 com a suport inorgànic) mitjançant medides de resonància magnética nuclear de sólids, tant de ^{13}C com de ^{11}B emprant tècniques de rotació en àngul màgic, polarització creuada, i el desacoplament dipolar heteronuclear. Per a ell es prepara un material híbrid format per una matriu de UVM-7 funcionalitzada amb gluconamides i aquest sòlid es posa en contacte amb diferents quantitats de bor. Els sòlids finals es caracteritzen mitjançant RMN de ^{13}C i de ^{11}B observant-se la formació de borésters entre els grups diol de les gluconamides anclades i el bor adsorbit. Quan la concentració de bor emprada és baixa es formen complexos bisquelats (B:glucosa = 1:2) mentre que a concentracions més altes comencen a formar-se complexos monoquelats (B:glucosa = 1:1). Aquest treball es va realitzar en col·laboració amb el grup d'investigació de "Materials sol-gel i RMN", perteneixent al centre "Chimie de la matière condensée de Paris" de la "Université Pierre et Marie Curie".

Abstract

The present PhD thesis is centred in the design (using concepts of supramolecular chemistry), synthesis and characterization of different hybrid organic-inorganic materials for boron removal from aqueous media. The interaction between boron and organic groups, polyols, used in the development of these new adsorbents is also studied.

In the first part of the thesis it is presented a brief review of supramolecular chemistry concepts, chemistry of boron and also the main methods for boron removal (first chapter) and, also, the objectives of this thesis (second chapter).

The third chapter exposes the results obtained by using a ceramic foam as macroscopic support for active materials for boron removal. This support is previously "impregnated" with an inorganic silica mesoporous material (UVM-7) and, in a second step, it is functionalized with an organic group with high boron affinity (gluconamide). This organic group, which works as an adsorbent, remains anchored to a macroscopic support, which will facilitate the use of these materials in industrial applications. Once the material is synthetized their boron adsorption and elimination abailability in aqueous media is studied and its ulterior reutilization.

The fourth chapter of the PhD thesis is focused on the preparation of low cost materials for boron adsorption from water. In first place, it is used, as inorganic scaffolding, UVM-7 material, a mesoporous silica phase with a bimodal pore system. This material has a high boron adsorption capacity after its functionalization with the polyalcohol (as it is shown in the previous chapter) nevertheless, the reagents used in the synthesis tetraethylorthosilicate, as silica source, and hexadecyltrimethylammonium bromide, as templating agent are so expensive that they induce a high cost of final materials. In this chapter is presented as an alternative another materials which are able to perform as inorganic scaffolds: UVM-11 (surfactant-free mesoporous material), two silica xerogels with pores within the mesoporous range and comercial high surface area silica fume were

prepared. Once all the materials are synthetized they are functionalized with gluconamides which are the active compounds for boron adsorption. Finally, a comparative study of the boron adsorption capacities in water is carried out. Low-cost materials present comparable boron removal to those of higher cost and comercially abailable materials.

Finally, in the fith chapter of this PhD thesis, the adsorption mechanism of boron on the active materials (based on UVM-7 as inorganic support) is studied using solid Nuclear Magnetic Resonance measures of ^{11}B and ^{13}C and using techniques as Magic Angle Spinning, crossed polarization and heteronuclear polarization disacoplament. To do that, a hybrid material composed by UVM-7 matrix grafted with gluconamide is prepared and then the solid is put in contact with different boron quantities. Final solids are characterized through ^{13}C and ^{11}B NMR, showing the formation of boronesters between gluconamide diol groups and boron adsorbed. When low boron concentration is used, bisquelate complexes are formed (B:glucosa = 1:2), however with higher concentrations monoquelate complexes are formed (B:glucosa = 1:1). This work was carried out in collaboration with the research group of “sol-gel materials and NMR”, appertaining to the center of “Chimie de la matière condensée de Paris” of the “Université Pierre et Marie Curie”.

"Il faut faire de la vie un rêve
et faire d'un rêve une réalité"
Pierre Curie

PUBLICATIONS

1. Cristina Sanfeliu, Ramón Martínez-Máñez, Félix Sancenón, Juan Soto, Pedro Amorós, Mª Dolores Marcos. *Ceramic foam supported active materials for boron remediation in water.* Desalination, 2015, 374, 10-19.

2. Cristina Sanfeliu, Ramón Martínez-Máñez, Félix Sancenón, Juan Soto, Victoria Puchol, Pedro Amorós, M. Dolores Marcos. *Low-cost materials for boron adsorption from water.* Journal of Materials Chemistry, 2012, 22, 25362-25372.

3. Cristina Sanfeliu, Ramón Martínez-Máñez, Félix Sancenón, Juan Soto, Pedro Amorós, Thierry Azaïs, Mª Dolores Marcos. *Boron Adsorption Mechanism Study in UVM-7 Gluconamide Adsorbent.* Submitted

Abbreviations

ACN	Acetonitrile
AEM	Anion Exchange Membrane
APTES	(3-aminopropyl)triethoxysilane
BET	Brunauer, Emmett and Teller Model
BJH	Barret, Joyner and Halenda Model
CEM	Cation Exchange Membrane
CF	Ceramic Foam
CTAB	Hexadecyltrimethylammonium bromide
DD	Donan Dialysis
EA	Elemental Analyser
EC	Electrocoagulation
ED	Electro Dialysis
LC	Liquid Crystal
LCT	Liquid Crystal Templating
IEM	Ion Exchange Membrane
MAS	Magic Angle Spinning
M41S /MCM	Mobile Crystalline Material
NBS	Nanoparticulated Bimodal porous Silica
NMDG	*N*-methyl-*D*-glucamine
NMR	Nuclear Magnetic Resonance
PUF	Polyurethane Foam
RO	Reverse Osmosis
SBA	Santa Barbara Amorphous type material
SDTA	Single Differential Thermal Analysis
SEM	Scanning Electron Microscopy
SF	Silica Fume
$TEAH_3$/$TEAH_2$/TEA	Triethanolamine
TEM	Transmission Electron Microscopy
TEOS	Tetraethylorthosilicate
TGA	Thermogravimetric Analysis
UV	Ultraviolet
UVM	Universidad de Valencia Material
X	Xerogel
XRD	X-ray diffraction

1. General introduction

1.1 **Supramolecular chemistry**

Supramolecular Chemistry has become one of the most important branches of nanoscience and, therefore, of nanotechnology. This chemistry field is based on the interaction between two or more molecules that formed aggregates within the nanometric range.[1] It is defined as the science that studies the weak and reversible noncovalent interactions between molecules such as hydrogen bonding, metal coordination, hydrophobic forces, van der Waals forces, π-π interactions and electrostatic effects and which deals with the design and the study of unique complex nanostructured supermolecules joined by intermolecular interactions.

Dr. Jean-Marie Lehn, who received the Nobel Prize in 1987 for their contributions to the development of this new area inside chemistry, defined supramolecular chemistry as the "chemistry of molecular assemblies and of the intermolecular bonds". Lehn described a supermolecule as "an organized complex entity that is created from the association of two or more chemical species held together by intermolecular forces. Supermolecule structures are the result of not only additive but also cooperative interactions, including, hydrogen bonding, hydrophobic interactions and coordination, and their properties are different (often better) than the sum of the properties of each individual component".[2]

In all living organisms, nature provides a multiplicity of materials (organic, inorganic, hybrids and composites) wich are characterized by hierarchical constructions at scales ranging from nanometers, micrometers to milimeters that introduce the capacity to answer the physical or chemical demands occurring at these different levels. Thus, this area of chemistry has been developed with the aim of chemical construccion and patterning of "biomimetic and bioinspired" materials with long-range order architectures (beyond nanometer size).

---

[1] Taylor & Francis Group, Encyclopedia of Supramolecular Chemistry, Vols. 1, 2 (Ed.: Atwood, J.L.; Steed, J.W.), LLC, New York, **2004**.

[2] J.M. Lehn, Supramolecular Chemistry, Ed. VCH, 1995; J.-M. Lehn, Nobel lecture, **1987**

Supramolecular chemistry is an interdisciplinar science combining physical, biological and chemical concepts in its bases. Its most important characteristic is the wide range of possibilities that offers the combination of various concepts in the same system where the top limit is the creativity of the researcher.

1.1.1 Molecular recognition

Molecular recognition is the basis of supramolecular chemistry and it is based on the ability of the mutual recognition of different molecules. It can be defined as the selective interaction between a host or receptor molecule and a guest or substrate through non-covalent interactions (See Figure 1).

Host-guest interaction is based in the affinity between the properties of both molecules like shape, size, polarity, hydrophobic forces, Van der Waals forces, ...[3]

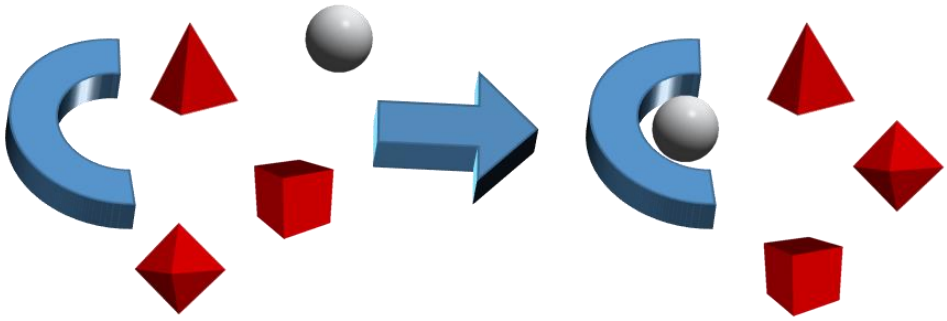

Figure 1. Scheme of molecular recognition process typical of supramolecular chemistry

In supremolecular chemistry, first studies were based in the selective coordination of cations and anions by macrocyclic and macropolyciclic ligands as crown ethers and criptands. When molecular recognition takes place, a host-guest complex is formed. One of the more important drawbacks of the molecular recognition processes is the separation of the complex from the individual components, so the

[3] G.V. Oshovsky, D. N. Reinhoudt, W. Verboom, *Angew. Chem. Int. Ed.*, **2007**, 46, 2366.

regeneration process of the receptor could be very difficult. Therefore, it is important to achieve these recognition processes in heterogeneous phase. In the last decades, many advances have been achieved in this area, resulting in the synthesis and development of new hybrid organic-inorganic materials for detection and adsorption of target molecules.[4]

1.2 **Hybrid organic-inorganic materials**

Hybrid organic-inorganic materials can be broadly defined as synthetic materials with organic and inorganic components, intimately mixed. Such materials could be either homogeneous (derived from monomers and miscible organic and inorganic components) or heterogeneous and phase-separated where at least one of the component domains a dimension ranging from few Å to several nanometers. Hybrid nanocomposites had an explosive development since the 1980's, with the expansion of soft chemistry processes.[5]

1.2.1 Mesoporous materials

"Porous materials created by nature or by synthetic design have found great utility in all aspects of human activity". This sentence introduces perfectly the great importance that this kind of materials has gained in the last few years.[6]

In 1992, researchers of the Mobil Company reported the synthesis of a new mesoporous silica family, known as M41S phases.[7] This group of materials consists of three different phases: MCM-41 (Mobile Crystalline Material having a *hexagonally* packed cylindrical mesopores), MCM-48 (*cubic*) and MCM-50 (*lamellar*). (See Figure 2)

---

[4] (a) R. Martínez-Máñez, F. Sancenón, *Chem. Rev*., **2003**, 103, 4419. (b) P. D. Beer, P. A. Gale, *Angew. Chem. Int. Ed.* **2001**, *40*, 486. (c) C.R. Bondy, S. Loeb, *J. Coord. Chem. Rev*. **2003**, 240, 77-99. (d) J. F. Callan, A. P. de Silva, D. C. Magri, *Tetrahedron,* **2005**, 61, 8551.

[5] (a) J. Livage, M.Henry, C. Sanchez, *Prog. Solid State Ch.*, **1988**, 18, 259 (b) P. Gómez-Romero, C. Sanchez, *Functional Hybrid Materials*, *Wiley-VCH*, Weinheim, **2004**.

[6] P.T. Tanev, J. Butruille, T.J. Pinnavaia, in: L.V. Interrante, M.J. Hampden-Smith (Eds.), *Chemistry of Advanced Materials: An Overview, Wiley–VCH*, New York, **1998**, p. 329.

[7] C. T. Kresge, M. E. Leonowicz, W. J. Roth, J. C. Vartuli, J. S. Beck, *Nature*, **1992**, 359, 710.

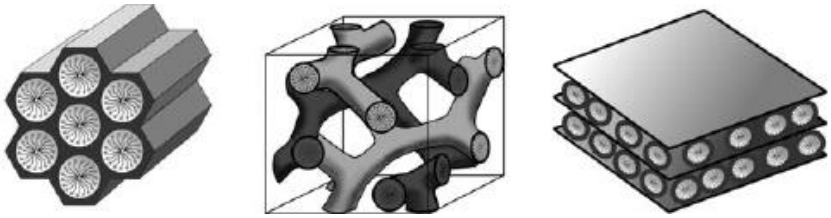

MCM-41 ***MCM-48*** ***MCM-50***

Figure 2. Schematic of structures of mesoporous M41S phase materials. (Reprinted with permission from F. Hoffmann et al., Angew. Chem. Int. Ed., 2006, 45, 3216.Copyright © 2006 Wiley-VCH Verlag GmbH & Co. KGaA, Weinheim).

The distinctive characteristics of mesoporous silica supports such as the very high specific surface of ca. 1200 m^2/g, inertness, thermal stability, the presence of tunable pore sizes with a diameter of ca. 2– 10 nm, high pore volume (*ca*. 1 cm^3/g) and the possibility to easily functionalise their surface, make these scaffolds ideal for the design of highly effective active materials with applications in remediation processes, controlled release or detection of target molecules.[8]

1.2.1.1 *Surfactant templated mesoporous materials*

- **MCM-41 (Mobile Crystalline Material)**

The original MCM-41 phase, as the representative M41S material, was synthesized by the combination of appropriate amounts of a silica source (tetraethylorthosilicate (TEOS)), an alkyltrimethylammonium halide surfactant (hexadecyltrimethylammonium bromide (CTAB)), a base (sodium hydroxide) and water.

There have been several models proposed to explain the formation of mesoporous materials and to provide rational basis for the various synthesis routes.[9] On the

[8] (a) E. Aznar, C. Coll, M.D. Marcos, R. Martínez-Máñez, F. Sancenón, J. Soto, P. Amorós, J. Cano, E. Ruiz, *Chem. Eur. J.*, **2009**, 15, 6877. (b) I. Candel, A. Bernardos, E. Climent, M.D. Marcos, R. Martínez-Máñez, F. Sancenón, J. Soto, A. Costero, S. Gil, M. Parra, *Chem. Commun*., **2011**, 47, 8313. (c) K. Sarkar, Y. Salinas, I. Campos, R. Martínez-Máñez, F. Sancenón, P. Amorós, *Chem. Plus. Chem*., **2013**, 78, 684.
[9] J.Y. Ying, C.P. Mehnert, M.S. Wong, *Angew. Chem. Int. Ed.*, **1999**, 38, 56.

most common level, these models are based on the presence of surfactants in a solution to guide the formation of the inorganic mesostructure from the solubilized inorganic precursors.

A “liquid crystal templating” (LCT) mechanism was proposed by the Mobil researchers, based on the similarity between liquid crystalline surfactant assemblies and M41S. As shown in Figure 3, two mechanistic pathways were postulated by the Mobil researchers:
a) The inorganic precursor species occupied the space between a pre-existing hexagonal lyotropic liquid crystal (LC) phase and deposited on the micellar rods of the LC phase.
b) Cooperative self-assembling procedures involved the formation of composite (inorganic-organic) micelles. These composite micelles were those that organise to form particle nuclei that flocculate after a more or less lengthy growing stage.

In either case, the inorganic components (wich were negatively charged at the high pH values used) preferentially interacted with the positively charged ammonium head groups of the surfactants and condensed into a solid, continuos framework.

Finally, the removal of the surfactant, either by high temperature calcinations procedures or by solvent extraction methods,[10] produced the open, mesoporous MCM-41 material.

[10] (a) J. S. Beck, J. C. Vartuli, W. J. Roth, M. E. Leonowicz, C. T. Kresge, K. D. Schmitt, C. T. W. Chu, D. H. Olson, E. W. Sheppard, *J. Am. Chem. Soc.*, **1992**, 114, 10834. (b) G. S. Attard, J. C. Glyde, C. G. Göltner, *Nature,* **1995**, 378, 366. (c) F. Hoffmann, M. Cornelius, J. Morell, M. Fröba, *Angew. Chem. Int. Ed.* **2006**, 45, 3216.

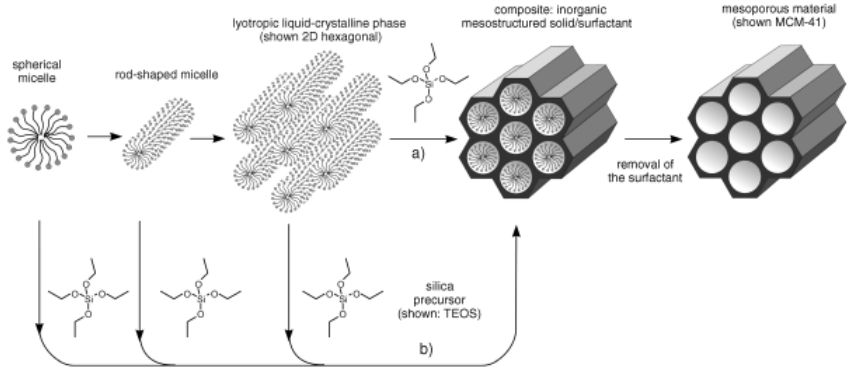

Figure 3. Formation of mesoporous materials by structure-directing agents: a) true liquid-crystal template mechanism, b) cooperative liquid-crystal template mechanism. *Adapted from Angew. Chem. Int. Ed. 2006, 45, 3216. Copyright © 2006 Wiley.*

The obtained materials using this procedure show several advantages such as versatility (it is possible to modify their final properties by changing small features of the synthetic process) and homogeneus porosity (not only in size but also in form).

Besides, this porous solids show some other advantages that make them suitable to act as scaffolding for the preparation of hybrid organic-inorganic materials: The regular, homogeneus, fair-sized pore system can be loaded with different size molecules and the inner and outer surface of the pores can be easily functionalized using appropriate organic molecules.

Silica chemistry has been extensively studied and, nowadays, it is almost possible to control the amount and density of the organic moieties incorporated to the solid as well as their arrangement on the siliceous surface since these materials show a high silanol groups density (Si-OH) capable to react covalently with molecules having trialkoxysilane moieties. Being able to functionalize the siliceous surface of MCM-41 materials with organic molecules, it is possible to control its surface properties.

- **UVM-7 material (University of Valencia Materials-7)**

It has been noted that the principal feature of the M41S and related solids, namely their periodic and ordered unimodal mesoporous structure, could suffer from poor accessibility to the interior of the pores because of pore blocking.[11] Materials presenting hierarchical multimodal porosity offer the possibility of combining an enhanced accessibility to the functional active groups (across large pores) with the conservation of high surface area and pore volume. Thus, L. Huerta et al. succeeded in synthesizing a novel Nanoparticulated Bimodal porous Silica (NBS) based on the control of experimental factors (pH conditions and modulation of the Si/surfactant ratio in dilute conditions).[12] These materials can be described as bimodal porous silicas constructed by aggregation of pseudo-spherical mesoporous primary nanoparticles whose average diameter is ca. 15–20 nm (see Fig.4). The small intra-particle mesopore system has its origin in the template effect of the surfactant aggregates (acting as porogens, as consequence of their ulterior elimination). This pore system is defined by regular mesopores organized in a disordered hexagonal array (see inset in Figure 4).

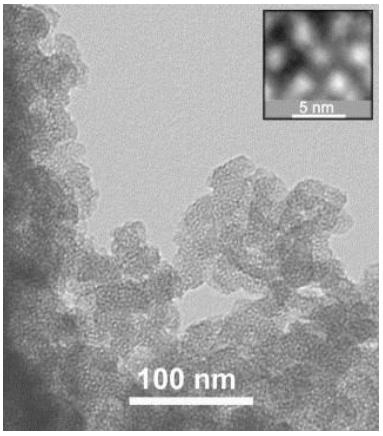

Figure 4. Representative TEM micrograph of the bimodal porous UVM-7-like Materials. An image of the intra-nanoparticle mesopore system is showed in the inset

[11] (a) D.R. Rolinson, *Science,* **2003**, 299, 1698. (b) M. Antonietti, G.A. Ozin, *Chem. Eur. J.,* **2004**, 10, 28.
[12] L. Huerta, C. Guillem, J. Latorre, A. Beltrán, R. Martínez-Máñez, M. D. Marcos, D. Beltrán, P. Amorós, *Solid State Sci.*, **2006**, 8, 940.

On the other hand, the large inter-particle pores must be generated as the nucleation and growth of the primary mesoporous nanoparticles proceeds. In practice, the formation of a continuous network from the soldered nanoparticles generates a disordered system of large void-pores (ranging from large-meso to macropores) accounting for the observed textural porosity. The non-ordered nature of this large pore system is consistent with a formation mechanism implying collision and aggregation of primary nanoparticles, in which does not participate any supramolecular template able to transfer a certain organization. The most relevant feature of these solids is the presence of a quasi mono-sized system of soldered mesoporous nanoparticles describing a secondary (meso) pore system, as it is shown in the schematic model (Figure 5) for UVM-7 materials.

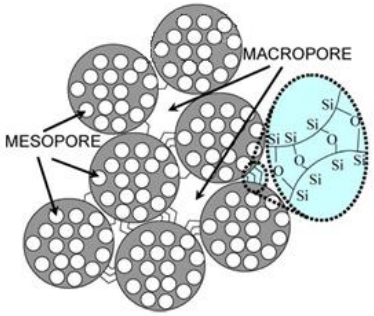

Figure 5. Propossed schematic model for the hierarchic bimodal UVM-7 materials.

In spite of the disordered nature of the mesopore system, UVM-7 materials, presenting hierarchical multimodal porosity, offer the possibility of combining an enhanced accesibility to the functinal active groups (across large pores) with the conservation of high surface area and pore volume.

1.2.1.2 *Non templated mesoporous materials*

Since the publication of the surfactant-assisted preparation of M41S solids, a high amount of reports dealing with the synthesis and characterization of these supports have been published. In spite of this interest the use of these materials in real applications has failed to a great extent. The use of surfactants implies additional costs of production when the key factor for industrial exploitation lies on the

development of cost-effective, large-scale manufacturing processes. At this point, in recent years, there has been increasing interest in the implementation of alternative ''non-surfactant'' routes to mesoporous materials. In fact, sol-gel chemistry-based procedures have received considerable attention for preparing porous materials (xerogels, aerogels) requiring a fine control of the microstructure and surface properties.

- **Mesoporous xerogels**

The structural characteristics of silica gels mainly depend on the size of the primary particles. Iler[13] showed that the size to which the particles grow before they form the gel is a function of the pH used during the hydrolysis-condensation processes. Thus, for low pH the size of the primary particles is very small and consequently the silica gels obtained have a large surface area (>500 m^2/g), large pore volumes (>0.5 cm^3/g), and a porosity made up mainly of pores in the mesopore range with sizes below 20 nm. Recently, it has been demonstrated that mesoporous silica xerogels obtained by using inexpensive sodium silicate as the silica source have characteristics comparable to those obtained from expensive organosilica precursors (i.e., TEOS).[14]

- **UVM-11 (University of Valencia Materials-11)**

Following the previous work of Amorós and coworkers on mesoporous materials, mesoporous xerogel UVM-11 has been developed.[15] This material can be described as unimodal porous xerogels constructed by aggregation of pseudo-spherical primary nanoparticles whose average diameter is comprised in the ca. 4-20 nm range. The images clearly show the disordered nature of the pore system (inter-particle voids) generated by the nanoparticles' aggregation (See Figure 6). It is reported a scale-up and low-cost procedure for the preparation of this mesoporous

[13] Iler, R. K.The Chemistry of Silica; John Wiley Sons: New York, **1979**.
[14] A.B. Fuertes, *Chem. Mater.*, **2004**, 16, 449.
[15] D. Ortiz de Zárate, L. Fernández, A. Beltrán, C. Guillem, J. Latorre, D. Beltrán, P. Amorós, *Solid State Sci.*, **2008**, 10, 587.

xerogel including well-defined pore systems and high surface area and pore volume.

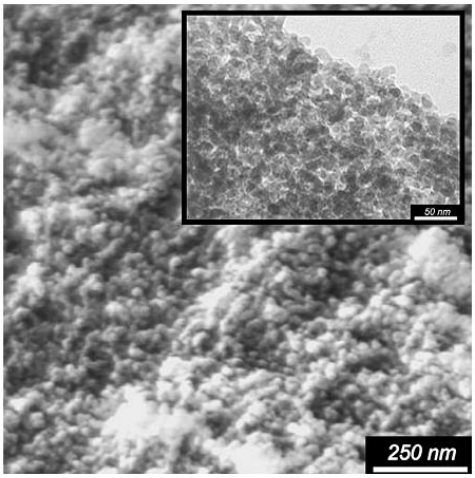

Figure 6. Typical SEM and TEM (in the inset) images of UVM-11 materials.

1.2.1.3 *Macroporous inorganic supports*

- **Monoliths with hierarchical pore systems**

Nowadays, materials with frameworks including hierarchical pore systems and complex macroscale forms are attracting much attention, given that they offer at first the possibility of combining an enhanced accessibility to the functional active groups (across large pores) with the conservation of a high surface area and pore structure.[16] So, these very open networks would favour diffusion of reagents and products while avoiding undesired pore blocking phenomena. Therefore, this class of materials could exhibit improved efficiency in classic separation and catalytic processes. In this context, ceramic foams represent an emerging category of hosts that can be used as structured supports. Ceramic foams (CF) possess a unique combination of physicochemical (high porosity and chemical stability) and mechanical (low thermal-expansion coefficients and high specific strength)

[16] (a) G.J.A.A. Soler-Illa, C. Sanchez, B. Lebeau, J. Patarin, *Chem.Rev*., **2002**, 102, 4093. (b) A. Stein, *Adv. Mater.*, **2003**, 15, 763.

properties.[17] In addition, CF can be easily manufactured by impregnation of an organic template foam with inorganic particles or by in situ polymerization followed by calcination.

However, the relatively low surface areas of CF (usually below 1 m^2/g) constitute a significant drawback. In order to overcome this drawback, a high-surface porous solid could be deposited onto the surface of the CF, as shown in Figure 7.[18]

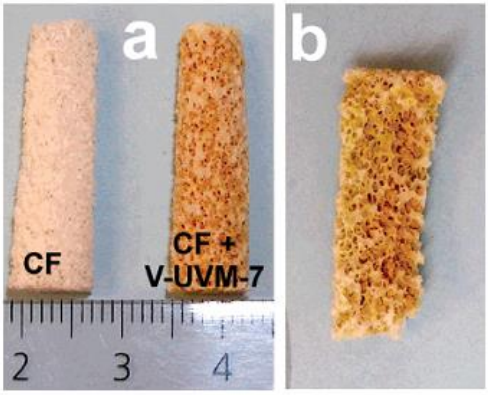

Figure 7. (a) Optical images of CF monoliths before and after coating with a V-UVM-7 colloid showing the homogeneity of the recovery. (b) Image of the interior of the (broken) coated monolith. Reprinted with permission from L. Huerta, J. El Haskouri, D. Vie, M. Comes, J. Latorre, C. Guillem, M. D. Marcos, R. Martínez-Mañez, A. Beltrán, D. Beltrán, P. Amorós, Chem. Mater., 2007, 19, 1082. Copyright 2007 American Chemical Society."

1.2.2 Functionalization of the mesoporous material surface.

An important number of techniques have been developed or adapted to add organic functions to the walls of mesoporous silica, combining the properties of a mesoporous inorganic structure with the surface organic groups.[19]

---

[17] (a) P. Colombo, *AdV. Eng. Mater.*, **1999**, 1, 203. (b) M. V. Twiggs, J. T. Richardson, *Chem. Eng. Res. Des.,* **2002**, 80, 183.

[18] L. Huerta, J. El Haskouri, D. Vie, M. Comes, J. Latorre, C. Guillem, M. D. Marcos, R. Martínez-Mañez, A. Beltrán, D. Beltrán, P. Amorós, *Chem. Mater*., **2007**, 19, 1082.

[19] (a) A. Stein, B. J. Melde, R.C. Schroden, *Adv. Mater.* **2000**, 12, 1403. (b) A. Vinu, K. Z. Hossain, K. Ariga, *Nanosci. Nanotech.,* **2005**, 5, 347.

The incorporation of the organic functions can, in principle, be carried out in two ways: by covalent binding on the inorganic walls of the material, during a post-functionalization process (grafting) and by direct incorporation of the organic functions, upon the synthesis process (co-condensation).

In the first approach, different organoalkoxysilanes have been widely used to graft specific organic moieties, by condensation reactions with silanol or silanolate groups of the silica framework. The mesoporous hosts (having previously removed the surfactant template by a calcination or extraction process); must be thoroughly dried before the addition of the organosilane precursors to avoid their autocondensation in the presence of water. The concentration and distribution control of the organic functions is restricted by the surface silanols and their accessibility. The grafting ratio depends on the precursor reactivity, being also limited by diffusion and steric factors (see Figure 8).

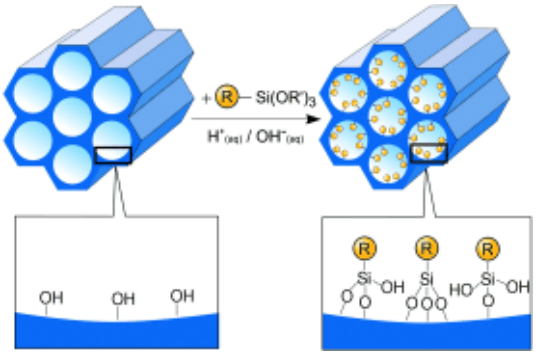

Figure 8. Grafting (postsynthetic functionalization) for organic modification of mesoporous pure silica phases with terminal organosilanes of the type $(R'O)_3SiR$. R=organic functional group. *Adapted from Angew. Chem. Int. Ed. 2006, 45, 3216. Copyright © 2006 Wiley.*

An alternative approach for pore functionalization relies on a direct synthesis, based on the co-condensation of siloxane and organosiloxane precursors in situ to yield modified MCM-41 in one step. Whereas the polymerization of the silicon precursor (TEOS) ensures the formation of the mineral network, organosiloxane moieties play a double role: they contribute as building blocks of the inorganic structure and they provide the organic groups. This one-pot pathway presents

several advantages, such as high modification ratios, homogeneous incorporation, and short preparation times (see Figure 9).

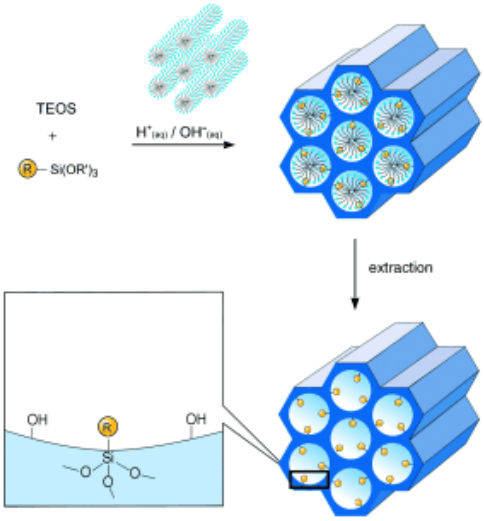

Figure 9. Co-condensation method (direct synthesis) for the organic modification of mesoporous pure silica phases. R=organic functional group. *Adapted from Angew. Chem. Int. Ed. 2006, 45, 3216. Copyright © 2006 Wiley.*

It is important to point out that, in this case, it is not possible to remove the surfactant template by calcination since the organic molecules attached to the structure would also be eliminated as a consecuence of the high temperature treatment.

1.2.3 Applications of Organic-Inorganic Mesoporous Hybrid Materials

The possibility to combine properties of inorganic and (bio)organic components in a unique material is an old challenge starting with the beginning of the industrial era. The development of innovative multi-functional advanced materials should have a major impact in future applications regarding several fields as optics, electronics, mechanics, membranes, protective coatings, catalysis, sensors,

biology, etc.[20] Mesoporous silica materials have been used as effective scaffoldings in a number of these applications due to their properties, such as chemical inertness, three dimensional structure, high external surface, high load capacity, biocompatibility etc.[21] Among these uses we are specially interested in the design of functionalised mesoporous materials for adsorption and remediation applications.

1.2.3.1 *Adsorptive materials*

Water pollution results in serious health and environmental problems. The considerable contamination of the aqueous environment by numerous pollutants still requires the development of quick and simple methods for the removal, separation, and determination of these compounds. A common problem in many industries is the disposal of large volumes of waste water with high toxicological potentials. Efficient techniques for the removal of highly toxic compounds from water have drawn significant interest. Among the possible techniques for water treatments, the adsorption process by solid adsorbents shows potential as one of the most attractive and efficient methods for the purification and separation of contaminant molecules in wastewater treatment. In fact, mesoporous functionalised solids have recently been used as scaffolding for the removal of toxic metal cations such as silver and copper,[22] gold,[23] mercury,[24] and for remediation studies of the toxic fluoride, nitrate, phosphate, arsenate, selenate, molybdate and chromate anions,[25] surfactants[26] and boron.

Inspired by the attractive properties of mesoporous solids for their use as matrices in remediation protocols, *Coll, Martínez-Máñez* and co-workers, reported a new

---

[20] (a) K. Sarkar, Y. Salinas, I. Campos, R. Martínez-Máñez, M. D. Marcos, F. Sancenón, P. Amorós, *Chem. Plus. Chem*, **2013**, 78, 684. (b) A.M. Ewlad-Ahmed, M. A. Morris, S. V. Patwardhan, L. T. Gibson, *Environ. Sci. Technol.,* **2012**, 46, 13354.

[21] (a) M. Vallet-Regi, A. Rámila, R. P. del Real, J. Pérez-Pariente, *J. Chem. Mater.* **2001**, 13, 308. (b) B. Muñoz, A. Rámila, J. Pérez-Pariente, I. Díaz, M. Vallet-Regi, *Chem. Mater.* **2003**, 15, 500.

[22] K. F. Lam, K. L. Yeung, G. McKay, *Langmuir*, **2006**, 22, 9632.

[23] K. F. Lam, K. L. Yeung, G. McKay, *J. Phys. Chem. B,* **2006**, 110, 2187.

[24] J. V. Ros-Lis, R. Casasús, M. Comes, C. Coll, M. D. Marcos, R. Martínez-Máñez, F. Sancenón, J. Soto, P. Amorós, J. El Haskouri, N. Garró, K.Rurack, *Chem. Eur. J.,* **2008**, 14, 8267.

[25] (a) S. Hamoudi, K. Belkacemi, *Fuel*, **2013**, 110,107; (b) H. Yoshitake, T. Yokoi, T. Tatsumi, *Chem. Mater.* **2002**, 14, 4603; (c) H. Yoshitake, T. Yokoi, T. Tatsumi, *Chem. Mater.,* **2003**, 15, 1713.

hybrid system for surfactant removal from water.[26] These solids consist of a mesoporous MCM-41-type support with the surface decorated by imidazolium, amine and pyridine binding groups. Therefore, the prepared solids contained different kinds of binding sites, all of them suitable for anion coordination (see Figure 10) but still showing different properties.

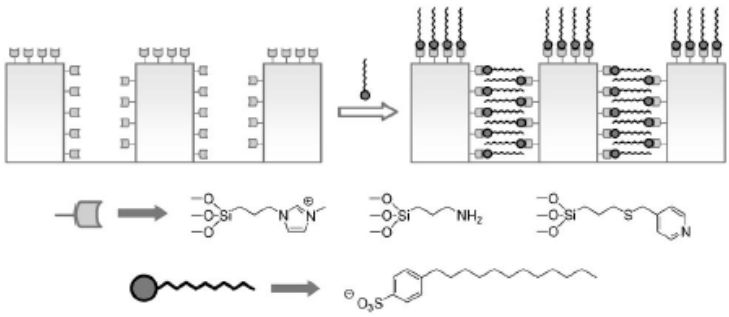

Figure 10. Protocol for surfactant removal in water using mesoporous solids containing nanoscopic binding pockets.

The high loading capacity found for solid treated with *N*-methyl-*N*-propyltrimethoxysilylimidazolium chloride, made this or similar functionalised mesoporous scaffolds promising candidates as new materials for anionic surfactant remediation in certain applications.

Ros-Lis, Casasús, and coworkers, reported a dual function hybrid material U1 for simultaneous chromofluorogenic detection and removal of Hg^{2+} in an aqueous environment. Mesoporous material UVM-7 was used as an inorganic support. The mesoporous solid is decorated with thiol groups that were treated with squaraine dye to give a 2,4-bis(4-dialkylaminophenyl)-3-hydroxy-4-alkylsulfanylcyclobut-2-enone (APC) derivative that is covalently anchored to the inorganic silica matrix. Hg^{2+} reacts with the APC fragment in U1 with release of the squaraine dye into the solution, which turns deep blue and fluoresces strongly (See Figure 11). Material

[26] C. Coll, R. Martínez- Máñez, M.D. Marcos, F. Sancenón, J. Soto, R. K. Mahajan, *Eur. J. Inorg. Chem*., **2009**, 25, 3770.

U1 acts not only as chemodosimeter that signals the presence of Hg^{2+} down to parts-per-billion concentrations, but at the same time is also an excellent adsorbent for the removal of mercury cations from aqueous solutions. The amount of adsorbed mercury ranges from 0.7 to 1.7 mmol/g, depending on the degree of functionalisation.

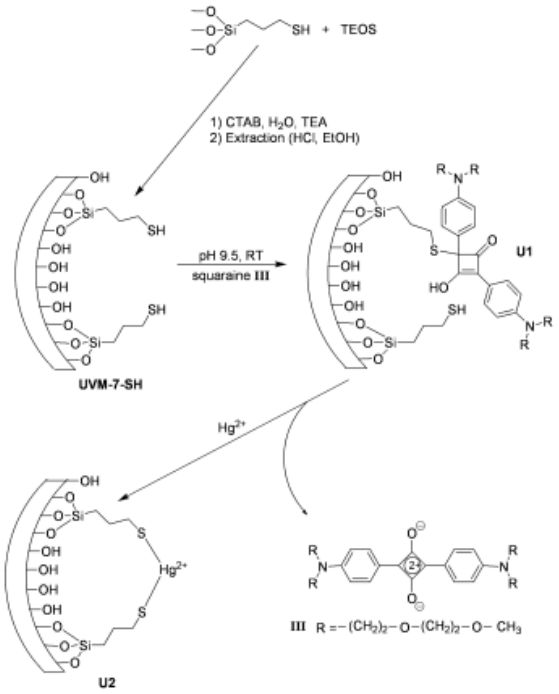

Figure 11. Route for the preparation of U1 material and detection and adsorption of Hg^{2+} mechanism.

U1 belongs to a new class of polyfunctional hybrid supports that can be used as both remediation and alarm systems by selective signalling and removal of target species of environmental importance.

S. Hamoudi and K. Belkacemi[25a] reported the synthesis of a variety of propylammonium functionalized mesoporous silica materials (MS—NH_3) and their efficiency to remove nitrate and phosphate anions in aqueous solution. The solids consisted of five different amino-functionalized mesostructured materials, i.e. MCM-41–NH_2, MCM-48–NH_2, SBA-15–NH_2, MS-56–NH_2 and MS-76–NH_2. Once the propylammonium functionalized mesoporous silica materials were synthesized they were applied for the adsorptive removal of nitrate and phosphate anions from

water. These materials demonstrated high adsorption performances in terms of anions removal, capacities and distribution coefficients. Moreover, the adsorption was shown to be very fast and can be accomplished in less than 5 min, as shown in Figure 12.

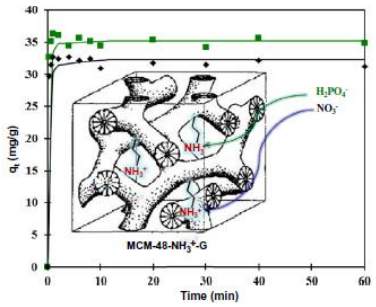

Figure 12. Experimental and theoretical adsorption kinetics on functionalised MCM-48-NH_3 for nitrate and phosphate with 5 g/L adsorbent loading. Solid lines showpseudo-second order kinetic model.

1.3 **Boron**

Boron is a nonmetallic element (atomic weight 10.811, solid state 298 K, melting point 2349 K, boiling point 4200 K) in group 13 of periodic table. The stable isotopes of boron are of mass 10 and 11 with estimated 20:80% ratio. Elemental boron has a high melting point, good hardness and is a rather poor conductor of electricity.[27] It is not found as a free element in nature, it always binds with oxygen to form both borate minerals (borax, ulexite and colemanite) and orthoboric acid. It is widely distributed in nature, but only in low and very low concentrations.[28] The average content of boron in the earth crust is 10 mg/Kg. In soils its average concentration is 30 mg/kg. Seawater contains an average of 4.6 mg/L boron that varies from 0.5 to 9.6 mg/L. The concentration of boron in fresh water is usually from less than 0.01 mg/L to 1.5 mg/L and increases significantly in areas where soils are boron enriched: the western part of the U.S., and a ground stretching from the Mediterranean Sea to Kazakhstan.[29] In general, the amount of boron in fresh water

[27] P.P. Power, W.G. Woods, *Plant Soil,* **1997**, 193, 1.
[28] F. Jay Murray, *Regul. Toxicol. Pharmacol.,* **1995**, 22, 221.
[29] J. Wolska, M. Bryjak, *Desalination*, **2010**, 310, 18.

depends on such factors as the geochemical nature of the drainage area, proximity to marine coastal regions and charges from industrial and urban effluents.

1.3.1 Uses of boron and related problems

In the recent years a significant increase in the concentration of boron in surface waters has been observed. The increase as well as concentration fluctuations at different areas are caused by many natural and anthropogenic factors. For the natural source one can count weathering of rocks and leaching of salt deposits. Because of the high volatility of this element, boron is found in the rainfall at coastal areas. The industrial activities are the next reason of boron increasing amount in surface waters. Boron has been used extensively in many industries, such as glass, ceramics, porcelain, cosmetics, semiconductors, carpets and fireproofing fabrics. Among them, the biggest user is the glass industry as more than half of the boron compounds are consumed in the glass industry. Because of all these factors, the concentration of boron in surface water at industrial and urban areas is still increasing.[30] Therefore, the problem of removing boron from water is not only related to the countries with natural deposits of this element but it has also become a critical issue for highly developed countries.

1.3.2 Effect of boron in plants, animals and humans

The essential role of boron in plants was first described in the 20's of the XX century.[31] Boron is an essential micronutrient for plants, humans and animals.

For plants, it is a structural component of cell wall, plays an important role in the structural stability, and relates to cell wall formation and lignifications. If boron deficiency occurs in the plant growth, it will lead to thick leaf, excessive branch, and poor germination.[32] For humans and animals, it is related with immune function of

[30] A.J. Wyness, R.H. Parkaman, C. Neal, *Sci. Total Environ*., **2003**, 314,255.
[31] J. Takano, K. Miwa, T. Fujiwara, *Trends Plant Sci.,* **2008**, 13 (8), 451.
[32] (a) H.E. Goldbach, M.A. Wimmer, *J. of Plant Nutr. Soil Sc.*, **2007**, 170, 39. (b) D.G. Blevins, K.M. Lukaszewski, *Annual Review of Plant Biology*, **1998**, 49, 481. (c) P. Brown, N. Bellaloui, M. Wimmer, E. Bassil, J. Ruiz, H. Hu, H. Pfeffer, F. Dannel, V. Römheld, *Plant Biology*, **2002**, 4, 205. (d) R. Reid, *Update*

the organism,[33] and affects hormone action and bone metabolism.[34] Boron deficiency disarranges embryo development for vertebrates,[35] and impedes absorption of elements such as calcium magnesium and phosphorus.

Although boron is an essential nutrient, the range between deficiency and toxicity is very narrow. In agricultural production, boron toxicity is more difficult to manage than boron deficiency which can be amended by proper fertilization. Excessive boron inhibits photosynthesis and root cell division, impedes deposition of lignin and chlorophyll, causes yellowish spots on the leaves, less fruit, dwarf even death for plants.[36] For humans and animals, a longterm chronic absorption of boron may cause a series of harmful impacts, such as growth retardation, the change of blood composition, nervous and reproductive system.[37]

The content of boron in drinking water, irrigation as well as in the wastewater, is regulated throughout the world. However, the recommended level of boron varies in different countries and regions. Boron compounds have not been considered as toxic hazards until not long ago. In 1993, the European Union (EU) initiated the first attempts to determine the risk caused by boron to the environment and to human health. In the same year the World Health Organization (WHO) identified this element on a list of drinking water standards and determined the permissible boron level at 0.3 mg/L. Later, in 2011, this standard was revised to 2.4 mg/L because it would be difficult to achieve in areas with high natural boron levels with the treatment technology available. Recently European Union has classified boron as a pollutant in drinking water, and adopted a standard of 1 mg/L.[38]

on Boron Toxicity and Tolerance in Plants, Advances in Plant and Animal Boron Nutrition, Springer, Dordrecht, The Netherlands, **2007**, pp. 83–90.

[33] J.W. Spears, T.A. Armstrong, *Dietary boron: evidence for a role in immune function, Advances in Plant and Animal Boron Nutrition*, Springer, Netherlands, **2007**, pp. 269–276.

[34] Y. Bai, C.D. Hunt, *J. Trace Elem.Exp. Med.*, **1996**, 9.

[35] D.J. Fort, E.L. Stover, P.L. Strong, F.J. Murray, C.L. Keen, *J. Nutr.*, **1999**, 129, 2055.

[36] P.D. Howe, *Biol. Trace Elem. Res.*, **1998**, 66, 153.

[37] R. F. Moseman, *Environ. Health Perspect*., **1994**, 102, 113.

[38] E.Weinthal, Y. Parag, A. Vengosh, A. Muti, W. Kloppmann, *The EU drinkingwater directive: the boron standard and scientific uncertainty, Eur. Environ*., **2005,** 15, 1.

1.3.3 Chemistry of boron in aqueous solutions

Boron is found as several species in water depending on their concentrations. In high boron concentrated aqueous solutions, several boron species are found, such as $B_2O(OH)_6^{2-}$, rings including $B_3O_3(OH)_4^-$, $B_4O_5(OH)_4^{2-}$, and $B_5O_6(OH)_4^-$.[39] As the boron concentration is below 290 mg/L, these ions are negligible. While the boron concentration is below 216 mg/L, $B(OH)_3$ and $B(OH)_4^-$ are found as the predominant boron species. In freshwater ecosystems, boric acid accounts for approximately 95% of the dissolved Boron, whereas the borate ion is approximately 5%.[40] Boric acid is moderately soluble in water and behaves as a very weak Lewis acid. The behavior of boric acid in water systems depends on other parameters such as temperature, pressure, pH and ionic strength.[41] Chemical spe-ciation of boric acid varies with acidity according to the flowing equilibrium equation:

$$B(OH)_3 + H_2O \rightleftarrows B(OH)_4^- + H^+ \qquad pKa = 9.15 \text{ at } 25^oC$$

1.4 **Technologies for boron removal**

Taking into account the increasing concentration of boron in surface waters and the need for treatment of seawater, which contains large amounts of this element, the current research focuses on the development of effective technologies for the removal of boron. Unfortunately, there is no simple and economic method for this task. The great difficulty in selecting such a method is the fact that boron appears in water as several chemical compounds and its concentration varies from place to place.[42] The methods commonly used in water purification as sedimentation, coagulation or adsorption on clays are not effective in the case of boron compounds, because they remove only small amounts or they do not remove it at all. Technologies for boron removal have been reviewed very recently.[43] Main

[39] P.H. Brown, H. Hu, *Plant soil*, **1997**, 196, 211.
[40] E. Dotsika, D. Poutouskis, W. Kloppmann, B. Raco, D. Psomadis, *Environ. Sec.*, **2011**, 209.
[41] N. Hilal, G.J. Kim, C. Somerfield, *Desalination*, **2011**, 273, 23.
[42] E. Loizou, P.N. Kanari, G. Kyracou, M. Aletrari, *J. Verbr. Lebensm*., **2010**, 5, 459.
[43] (a) J. Wolska, M. Bryjak, *Desalination*, **2013**, 310, 18. (b) B. Wang, X. Guo, P. Bai, *Colloid Surface A*, **2014**, 444, 338. (c) O.C. Türker, J. Vymazal, C. Türe, *Ecol. Eng.*, **2014**, 64, 350. (d) Y. Xu, J.Q. Jiang, *Ind. Eng. Chem. Res*., **2008**, 47, 16.

processes for boron removal include coagulation-electrocoagulation, absorption on oxides, absorption on active carbon, ion exchange with basic exchangers, electrodialysis, membrane filtration after complexation, use of boron selective resins, with diols as complexing agents. The removal of boron through the use of adsorption process and ion exchange systems seems to be the most effective treatment methods.

1.4.1 Membrane process

Membrane methods are the most common used in desalination of seawater and any other salted water. Although these methods are among the more widely used technologies for water deboronation, it has some limitation in practical application. These technologies are not able sometimes to reduce the boron content below the permissible level and it is necessary to introduce an additional process to the technological line. In order to remove residual boric acid, the pH of the media used in this method must be increased to the range of 10-11, and boric acid will be transformed to borate and be finally separated.[44] But this way will lead to another problem. Although the separation efficiency increased dramatically to 98-99%, some hydroxides (magnesium hydroxides) precipitate on the surface of the membrane. Therefore electrocoagulation or resin adsorption might be used as a pretreatment step for membrane process in order to remove the hydroxides present in the wastewaters.

1.4.2 Ion-exchange membranes (IEM)

Ion-exchange membranes (IEM) are a group of synthetic ion exchangers which are immobilized on membrane materials, including cation-exchange membrane (CEM), anion-exchange membrane (AEM), and bipolar membranes (BPMs). They are usually used in boron removal process such as electrodialysis (ED) and Donnan Dialysis (DD) systems.

[44] V.V. Goncharuk, Y.V. Babak, L.A. Melnik, V.V. Trachevskii, *J. Water Chem. Technol*., **2011**, 33, 307.

In an ED system, electric potential gradient is the driving force. Cations and anions will migrate across CEMs and AEMs respectively in the opposite directions along the electric field lines, and concentrate compartments are formed. Finally, the desalination process finishes and boron anions are removed from feed solution.[45]

Donnan dialysis (DD) is a kind of ion exchange process. Unlike ED, there is no external electric field. It is based in the difference of chemical potencial between two compartments separated by an ion exchange membrane. In the process, the AEMs are used to remove borate ions from aqueous solutions.[46] But the limitation of this method is that DD can only be used in the purification and concentration of diluted solutions.

1.4.3 Reverse Osmosis (RO)

Reverse osmosis is a membrane technology, which is widely used in seawater desalination and water treatment. This is an effective method for removing boron from drinking water. The membrane used in RO is semipermeable, only allows water to permeate while dissolved species are rejected under external pressure. The rejection of boron depends mainly on the pH of the feedwater. In high pH solutions, boron is presented in the form of borate anion, $B(OH)_4^-$, which can be separated easily by RO technology.[47] However, in seawater and other low pH solutions, the dominant form of boron is non-dissociated uncharged boric acid which can penetrate RO membranes; this results in the formation of the boron complexes and then larger molecules, tending to reduce membrane flux in the RO process. However, the primary disadvantage is the amount of water wasted by the process: about 2-20 gallons of water are lost as waste if 1 gallon of water is produced. Low-energy efficiency also restricts reverse osmosis techniques as a potential candidate for boron removal from water.

[45] P. Dydo, M. Turek, *Desalination,* **2013**, 310, 2.
[46] E. Kir., B. Gurler, A. Gulec, *Desalination*, **2011**, 267, 114.
[47] (a) C. Domínguez-Tagle, V.J. Romero-Ternero, A.M. Delgado-Torres, *Desalination*, **2011**, 265,43. (b) Y. Cengeloglu, G. Arslan, A. Tor, I. Kocak, N. Dursun, *Sep. Purif. Technol.*, **2008**, 64, 141.

1.4.4 Electrocoagulation (EC)

Electrocoagulation is often used before membrane process. It is an easy-to-operate method with simple equipment, which can be used in most rigorous situations even when the boron amount is negligible in the aqueous solutions. The EC process involves an electrolytic reactor with aluminum (or iron) electrodes and a separation tank. The water to be treated passes through the reactor and is subject to coagulation/flotation, by the Al or Fe ions dissolved from the electrodes, with the resulting flocs floating after being captured by hydrogen gas bubbles generated at cathode surfaces (see Figure 13).[48]

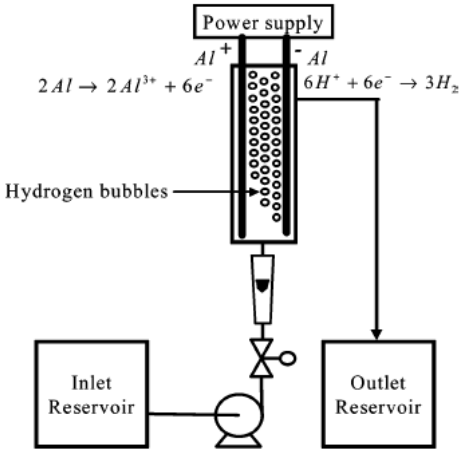

Figure 13. Schematic of laboratory-scale electrocoagulation system.

1.4.5 Adsorption process

The most effective method to remove boron from aqueous solutions is the adsorption technique, because the process requirements are simple and can be used in aqueous media with low boron concentration.

The boron adsorption method is based on complexation reactions. For the elimination of boron from aqueous media organic adsorbents with hydroxyl

[48] (a) M.H. Isaa, E.H. Ezechia, Z. Ahmedb, S.F. Magramb, S.R.M. Kuttya, *Water Res.*, **2014**, 51, 113. (b) A.E. Yilmaza, R. Boncukcuoğlua, M.M. Kocakerimb, B. Keskinlerc, *J. Hazard. Mater.*, **2005**, 125, 160.

moieties are used as active groups which may coordinate boron atoms with the subsequent formation of different borate esters .[49] Most of the synthetised adsorbents have at least three hydroxyl groups or two adjacent phenolic hydroxyl groups as ligands often located in the cis position. This type of structures have a high selectivity towards boron, and does not react with other elements due to the small size of boron atom. Several studies suggest that the presence of tertiary amine group is critical for boron chelating. It captures proton released during complexing of borate by hydroxyl functionalities.[50] Although boron chelating mechanism is not yet clarified, these materials have a promising performance in boron removal process. Furthermore, complexation mechanism onto functionalised materials will be discussed in the fifth chapter of the present PhD thesis.

Most of the synthesized adsorbents have been formed by modification of a material that acts as support such as an organic polymer (like styrene and divinylbenzene) a biopolymer (like chitosan or tannin gel) or finally an inorganic material (like SBA-15 or MCM-41).

1.4.5.1 *Organic polymer based materials*

Many synthesized resins are based on a macroporous polystyrene matrix, to which *N*-methyl-*D*-glucamine (NMDG) functional groups are attached. This functional group is a polyol with five hydroxyls and a tertiary amine end, which can offer more complexation sites, and form stable complexes with boron. The traditional polystyrene resin is a kind of anion exchange resin, the hydrophobic skeleton structure of which is not conducive to the mass transfer process in aqueous solutions, which effects boron removal from aqueous media. These materials are able to remove boron selectively to the effectiveness of 93-98%, even with highly

[49] (a) W.G. Henderson, M.J. How, G.R. Kennedy, E.F. Mooney, *Carbohydr. Res.*, **1973**, 28, 1. (b) H. van Duin, J.A. Peters, A.P.G. Kieboom, H. van Bekkum, *Tetrahedron,* **1984**, 40, 2901. (c) M. van Duin, J.A. Pfters, A.P.G. Kieboom, H. van Bekkum, *Tetrahedron,* **1985**, 41, 3411. (d) C.F. Bell, R.D. Beauchamp, E.L. Short, *Carbohydr. Res.*, **1989**, 185, 39.

[50] (a) B.M. Smith, P. Todd, C.N. Bowman, *Sep. Sci.Technol*., **1995**, 30, 3849. (b) B.M. Smith, J.L. Owens, C.N. Bowman, P. Todd*, Carbohydr. Res*., **1998**, 308, 173.

mineralized solutions.[51] This type of adsorbents are available on the market from different manufacturers as following, PWA10 and IRA743 (Amberlite), CRB01 and CRB02 (Diaion), BSR-1 (Dowex), S108 and S110 (Purolite).

Since the polystyrene resins with the functional groups of *N*-methyl-*D*-glucamine function emerged in boron removal process, more chelating resins with different functional groups have been developed. Recently, Wang et al.[52] reported a chloromethyl resin modified with pyrocatechol functional groups. The poor boron uptake capacity limited the use of this resin in water purification applications. Suzuki et al.[53] modified a type of strong base anion exchange resin – Lewattitt MP 500WS with chromotropic acid, obtaining a chelating resin containing two phenolic hydroxyl functional groups. The adsorption capacity of the resin was 8.87 mg/g, and it was more dependent on the solution pH compared with commercial resin.

However, boron chelating resins have many problems, such as limited surface area, unordered pore structure and poor chemical and thermal stability. At the same time, resin regeneration requires a large amount of acid and alkali, which increases the cost. Therefore, research in finding new boron absorbents with large surface area, good stability and low cost is essential.

1.4.5.2 *Biopolymer based materials*

For the last decade, great attention has been paid to the development of new low-cost adsorbents for boron removal. One option could be reusable waste materials from industries or even natural materials. Some authors have shown the potential of biopolymers for the immobilisation of active materials and the elaboration of composite adsorbents.

Chitosan is an abundant, cheap and environmental friendly biopolymer. It is obtained by deacetylation of chitin, a major component of shrimp, crab and other

[51] (a) L. Melnyk, V. Goncharuk, I. Butnyk, E. Tsapiuk, *Desalination*, **2005**, 185, 147. (b) M.F. Chillón, L. Valero i Bru, D. Prats, P. Varó, *Desalination,* **2011**, 278, 244.
[52] B. Wang, H. Lin, X. Guo, P. Bai, *Desalination*, **2014**, 347,138.
[53] T.M. Suzuki, D.P. Tanaka, T. Yokoyama, Y. Miyazaki, K. Yoshimura, *J. Chem. Soc. Dalton*, **1999**, 1639.

crustaceans.[54] Wei et al.[55] designed an environmentally friendly adsorbent for boron removal by functionalisation of chitosan with *N*-methylglucamine group through atom transfer radical polymerisation. Gazi et al.[56] synthesized a new boron chelating resin based on chitosan backbone functionalized with multi-hydroxyl iminobis (propylene glycol) (IBPG) groups. This organic resin was able to remove 29.19 mg/g of boron. However, these materials require a complex synthetic procedure and the recyclability is not reported. A good sorbent, especially for large-scale applications, need to be recyclable to be competitive.

Morisada et al.[57] reported an amine-modified tannin gel as boron adsorbent. The tannin molecule is an inexpensive and ubiquitous natural polymer extracted from leaves and barks of plants and has many hydroxyl groups. The obtained results show that tannin gel could be regarded as reasonable adsorbent for boron removal. Nevertheless, maximum boron uptake takes place at pH 8.8 which means a necessary pretreatment of wastewater.

Other conventional natural materials modified with saccarides as activated carbon,[58] or cellulose[59] have been also used for the removal of boron in aqueous solution.

1.4.5.3 *Inorganic based materials*

In addition to the use of organic polymers and biopolymers, boron removal can be performed using an inorganic support. Mesoporous Silica Materials (MSM) are supports of choice to introduce organic functional groups, because of their regular porosity, pore size, high surface area and large pore volume. Moreover, the amorphous nature of the structure offers a large number of silanols (Si/OH) that can react with condensable groups.

---

[54] (a) H. Demey, T. Vincent, M. Ruiz, A. M. Sastre, E. Guibal, *Chem. Eng. J.*, **2014**, 244, 576. (b) A. Sabarudin, K. Oshita, M. Oshima, S. Motomizu, *Talanta*, **2005**, 66, 136.
[55] Y.T. Wei, Y.M. Zheng, J.P. Chen, *Water Res.*, **2011**, 45, 2297.
[56] M. Gazi, S. Shahmohammadi, *React. Funct. Polym.,* **2012** , 72, 680.
[57] S. Morisada, T. Rin, T. Ogata, Y. Kim, Y. Nakano, *Water Res.*, **2011**, 45, 4028.
[58] Z. C. Çelik, B.Z. Can, M. M. Kocakerim, *J. Hazard. Mat.*, **2008**, 152, 415.
[59] Y. Inukai, Y. Tanaka, T. Matsuda, N. Mihara, K. Yamadac, N. Nambu, O. Itoh, T. Doi, Y. Kaida, S. Yasuda, *Anal. Chim. Acta*, **2004**, 511, 261.

Several studies have been developed using different MSM as inorganic scaffolding modified with polyols as boron adsorbents. Most of these adsorbents are based on SBA-15 and MCM-41 due to their textural properties, excellent hydrophilicity, thermal stability and the fact that they are the most extensively investigated mesoporous materials among the wide variety of silica mesophases.[60] Some studies have also been made with commercial silica gel as the support for organic groups.[61]

Moorthy et al.[62] prepared magnetic mesoporous silica hybrid nanoparticles for boron adsorption. The adsorbent material consisted of novel core–shell magnetic mesoporous silica hybrid nanoparticles composed of a Fe_3O_4 core, mesoporous silica shell and glycidol modified organosilica functional derivatives with cisdiol groups in the mesochannels as seen in Figure 14.

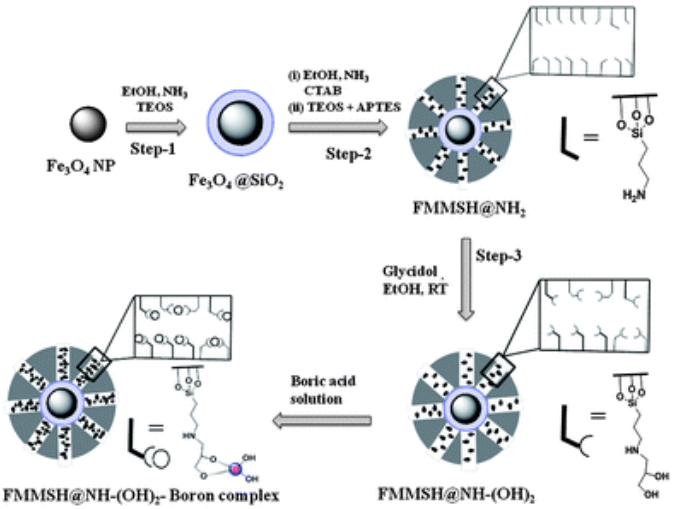

Figure 14. Synthesis of functional core–shell magnetic mesoporous silica hybrid FMMSH@NH-$(OH)_2$ nanoparticles. Reproduced from Ref. M. S. Moorthy, D. Seo, H. Song, S. S. Park, C. Ha, *J. Mater. Chem. A*, **2013**, 1, 12485, with permission from The Royal Society of Chemistry.

[60] (a) T. Ben Amor, I. Dhaouadi, B. Lebeau, M. Tlili, M. Ben Amor, *Desalination*, **2014**, 351, 82. (b) L. Wang, T. Qi, Y. Zhang, *Colloid. Surf. A.*, **2006**, 275, 73. (c) O. Kaftan, M. Acikel, A.E. Eroglu, T. Shahwan, L. Artok, C. Ni, *Anal. Chim. Acta.*,**2005**, 547, 31.

[61] L. Xu, Y. Liu, H. Hu, Z. Wu, Q. Chen, *Desalination*, **2012**, 294, 1.

[62] M. S. Moorthy, D. Seo, H. Song, S. S. Park, C. Ha, *J. Mater. Chem. A*, **2013**, 1, 12485.

Owing to the special magnetic properties of Fe_3O_4 cores, the mesoporous silica hybrid adsorbents are capable of easy separation by external magnetic attraction from a small magnet. Therefore, particles after boron adsorption can be removed easily from the aqueous media.

Fried et al.[63] reported covalent immobilization of glycopyranose-azide onto functionalized MCM-41 via a copper-catalyzed click-reaction (see Figure 15). The click-reaction produces strong and stable substrate-carbohydrate bonds. Based on the results obtained this material was shown to be a potential candidate for borate adsorption from wastewater.

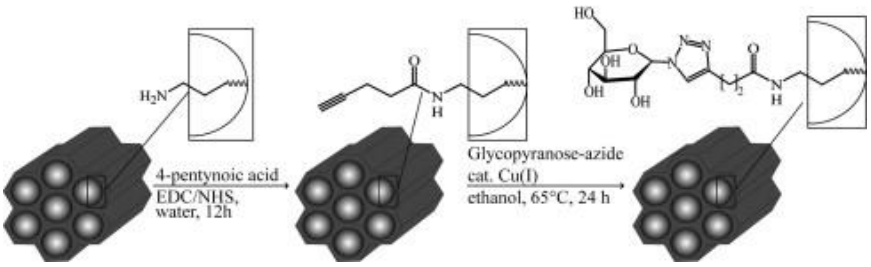

Figure 15. Covalent immobilization of glycopyranose-azide on acetylene-functionalized MCM-41 achieved by click-chemistry.

In a previous work,[64] Martínez-Máñez and coworkers presented a boron removal hybrid system based on a novel mesoporous silica material (UVM-7) grafted with different saccharides as shown in Figure 16. The high loading capacity found for S4 grafted with mannose, made this system promising candidates as new material for boron remediation.

[63] D. I. Fried, A. Schlossbauer, T. Bein, *Micropor. Mesopor. Mat.*, **2012**, 147, 5.
[64] G. Rodríguez-López, M.D. Marcos, R. Martínez-Máñez, F. Sancenón, J. Soto, L.A. Villaescusa, D. Beltrán, P. Amorós, *Chem. Commun*., **2004**, 2198.

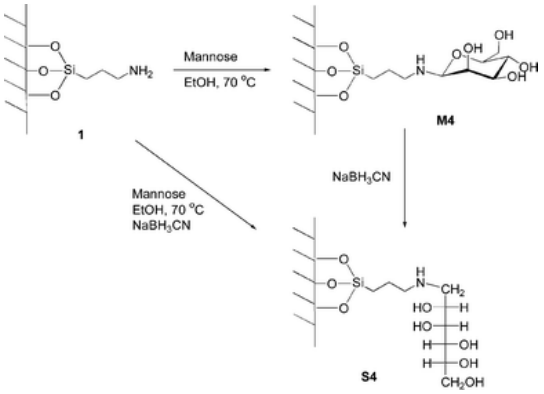

Figure 16. Reaction scheme for the synthesis of the functionalised mesoporous solid S4. Reproduced from Ref. G. Rodríguez-López, M.D. Marcos, R. Martínez-Máñez, F. Sancenón, J. Soto, L.A. Villaescusa, D. Beltrán, P. Amorós, *Chem. Commun*., **2004**, 2198, with permission from The Royal Society of Chemistry.

Adsorption methods and its boron sorption capacities of the reports mentioned in this general introduction are summarized in Table 1.

Type of base Material	Support material	Moiety	Sorption capacity (mmol/g)	Reference
Organic Polymer	Polystyrene	NMDG	0.62	L. Melnyk et al. (51 a)
	Chloromethyl	pyrocatechol	0.42	B. Wang et al. (52)
	anion exchange resin	chromotropic acid	0.82	T.M. Suzuki et al. (53)
Biopolymer	Chitosan	propyleneglycol	2.7	M. Gazi et al. (56)
	Chitosan	$Ni(OH)_2$	5.68	H. Demey et al. (54 a)
	Chitosan	NMDG	3.25	Y. Wei et al. (55)
	Tannin gel	amino	2.25	S. Morisada et al. (57)
	Activated carbon	Salicylic acid	0.03	Z.C. Çelik et al. (58)
	cellulose	NMDG	1.1	Y. Inukai et al. (59)
Inorganic	SBA-15	NMDG	0.92	T. Ben Amor et al. (60 a)
	Fe_3O_4@SiO_2	Glycidol	2.37	M.S. Moorthy et al. (62)
	Silica gel	NMDG	1.54	L. Xu et al. (61)
	MCM-41	Glycopyranose	0.50	D.I. Fried et al. (63)
	SBA-15	Glucose	0.63	L. Wang et al. (60 b)
	MCM-41	Glucose	0.25	
	MCM-41	NMDG	0.8	O. Kaftan et al. (60 c)
	UVM-7	glucose	0.67	G. Rodríguez-López et al. (64)
		fructose	0.76	
		galactose	0.49	
		mannose	1.85	

Table 1. Summary of Adsorption processes reported in boron removal

2. Objectives

Bearing in mind the exposed problems with boron contamination and the previous works reported, the main objective of this PhD thesis is the synthesis and characterization of hybrid organic-inorganic material for boron removal in aqueous media and the optimization of the involved adsorption procces.

Particulary, our aim is:

-To prepare and characterize mesoporous silica materials functionalized with polyols by reproducible methodology.
-To synthetise optimized boron adsorption “low-cost” materials.
-To study boron desorption from the adsorbents and their regeneration by simple acidic washing.
-To incorporate hybrid organic-inorganic materials for boron removal onto macroscopic systems in order to faciclitate the separation process from waste water after the adsorption process.
-To investigate the borate to polyols complexation process by solid ^{11}B NMR.

3. Ceramic foam supported active materials for boron

Ceramic foam supported active materials for boron remediation in water

Cristina Sanfeliu,[abc] Ramón Martínez-Máñez,[abc] Félix Sancenón,[abc] Juan Soto,[abc] Pedro Amorós,[d] Mª Dolores Marcos.[abc]

a Centro de Reconocimiento Molecular y Desarrollo Tecnológico (IDM), Unidad Mixta Universitat Politècnica de València, Universitat de València, Spain.

b Departamento de Química, Universitat Politècnica de València, Camino de Vera s/n E-46022 Valencia, Spain. (Tel.: (+34) 963877343)

c CIBER de Bioingeniería Biomateriales y Nanomedicina (CIBER-BBN), Spain.

d Institut de Ciència del Materials (ICMUV), Universitat de València, P.O. Box 22085, E-46071, Valencia, Spain. (Tel.: (+34) 963543617)

Received 20th February 2015, Accepted 24th June 2015

First published on the web 24th July 2015

Desalination, *2015*, ***374***, *10-19*

Abstract

Due to the narrow range between boron necessities and toxicity in the environment, there is a high interest in the design of effective boron remediation procedures. We have previously reported a promising boron adsorption material based on the affinity of boron aqueous species for cis-diol groups that were anchored on different mesoporous silica matrices. However, the small particle size of these systems makes them difficult to be applied on real remediation situations. In this context we report herein a novel system for boron adsorption from aqueous solutions in which the high boron affinity for functionalized mesoporous materials is combined with the mechanical properties of ceramic foams as macroscopic supports. The efficiency of these new composites for boron removal is very high and comparable with the parent microparticulated adsorbent.

3.1 **Introduction**

Boron is widely distributed in the environment, mainly in the form of borate salts which are very soluble and hence difficult to remove from water. The principal boron contamination is due to industrial wastewater discharge as for example the ceramic industry. In regions with a high concentration of such industries the contamination of ground and subsoil by boron is considered of maximum environmental concern.[1]

Boron is an important micronutrient for plants, animals and humans. It has a marked effect on plants in terms of both nutrition and toxicity, even 1-2 ppm in irrigation water can cause stunting of plant growth. Boron also has virulence for reproduction and causes disease in the nervous system of animals and humans.[2,3] Therefore, removal of boron from water is crucial for boron environmental protection.

The World Health Organization (WHO) guidelines for water quality recommend a 2.4 mgL^{-1} standard for boron in drinking water.[4] In the case of the European Union (EU) a standard of 1mgL^{-1} for drinking water[5] for boron has been adopted, though

in some countries derogations have been made due to a higher boron concentration in natural fresh water.[6]

There is no universal method for the removal of boron from water.[7] Main processes for boron removal include adsorption,[8,9] coagulation,[10] reverse osmosis,[11-14] electrodialysis,[15] etc. The adsorption process is extensively used.[16,17] Therefore, novel materials and methods are being developed. [18]

Previously, we presented an alternative system: a new generation of boron adsorption materials based on functionalized mesoporous silica.[19] This method was developed taking advantage, in one side, of the boron ability to produce esters with chemical compounds containing multiple hydroxyl groups (polyols)[20, 21] and, on the other, of the attractive properties of mesoporous solids such as very large capacity of functionalisation and very high specific surface.[22,23] Based on these ideas, it was envisaged that the grafting of mesoporous scaffolds with saccharides could yield highly efficient boron removal systems. Several of these mesoporous scaffolds with different porous structures have been obtained and compared with non-porous inorganic materials and though the best adsorption result was obtained for highly homogeneous scaffolds, other cheap matrices showed also a good performance.[24]

However, thinking on real applications, the relatively small particle size of these functionalized mesoporous materials constitute a significant disadvantage. At this point, we will pointed out that the grain size of the inorganic silicas we have used (50-300 nm) is significantly lower than the size of other materials used for boron remediation such as Dianion or Dowex ion exchange resins (in the micrometric-milimetric range).[25-27] The solid-liquid separation process becomes hard and difficult when nanometric particles are involved. This drawback can be solved by the incorporation of the active species onto a macroscopically structured support. In this context, ceramic foams (CF) represent an emerging category of hosts that possess a unique combination of physicochemical (high porosity and chemical stability) and mechanical (low thermal-expansion coefficients and high specific strength) properties.[28-30] In addition, CF can be easily manufactured by

impregnation of organic template foams with inorganic particles or by in situ polymerization followed by calcination.[31]

Preparation and characterization of "CF-mesoporous silica" composites in the form of rigid large monoliths having trimodal pore systems (small meso-, large meso-, and macroporous) has been described.[32] The monoliths have been synthesized by using preformed mesoporous nanoparticles and a CF as support. The surfactant-assisted synthesis of the silica-based nanoparticulate mesoporous materials, denoted as UVM-7 (a nanometric version of the MCM-41 silicas), has been reported elsewhere.[33] These UVM-7 materials show very open architectures consisting of micrometric aggregates of mesoporous nanoparticles connected through covalent bonds.

In this study, we present a novel system for boron adsorption from aqueous solutions in which the high accessibility of the UVM-7 mesoporous materials has been combined with the boron affinity towards diols and the mechanical properties of the ceramic foams as macroscopic supports. The efficiency of this new system in boron removal is also presented.

3.2 **Experimental**

3.2.1 Synthesis of the adsorbents

The synthesis of the ceramic foam (CF) was carried out through a typical organic foam replication, a technique that allows good control of the monolith shape and dimensions.[34] Commercially available inexpensive polyurethane foam (PUF) without cell forming membranes (average pore diameters around 600 μm (30 ppi)) was used as macro-scale template. The foam was impregnated with an optimally deflocculated casting slip for porcelain bodies prepared with two different kaolins, feldspar and quartz, which contained 67% of solid materials (19.4% kaolin A, 18.1% kaolin B, 10.7% quartz, 18.8% feldspar), and 33% of water, which included the deflocculant (0.45% with respect to solid kaolins), to give a slip density of 1.6 g/cm^3. As deflocculant, a mixture of sodium carbonate ($Na_2CO_3 \cdot 10H_2O$) and sodium silicate (aqueous solution with a density of 1.36) in a weight ratio of 2:1 was used. The

green body obtained with this slip had the following chemical composition: SiO_2, 68.0%; Al_2O_3, 21.5%; Na_2O, 0.8%; K_2O, 4.1%; ignition loss, 5.6%; distributed as kaolinite, quartz, and feldspar minerals. The impregnated PUF was passed through rollers preset at 80% compression to expel the excessive slurry and dried at room temperature to obtain a coated PUF. Then, the monolith was calcined in a two-step process (at 500 °C for 2 h, and later at 1200° for 5 h) to provoke PUF evolution and ceramic vitrification. The corresponding porcelain body contains two crystalline phases, mullite and quartz, and a vitreous phase containing sodium and potassium aluminosilicates.

The nanosized mesoporous UVM-7 silica was synthesized through a one-pot surfactant-assisted procedure using a homogeneous hydroalcoholyc reaction medium (water/triethanolamine).The general procedure, a modification of the so-called atrane route,[35] has been described in detail elsewhere. It is based on the use of a simple structural directing agent ((CTABr) cetyltrimethylammonium bromide) and a complexing polyalcohol (triethanolamine), which originates silatrane complexes (relatively inert complexes that include triethanolamine-related ligand species) as hydrolytic precursors. Together with its complexing ability, the presence of the cosolvent (triethanolamine) was a key in order to favor the formation of nanoparticulated materials. To open the intrananoparticle mesopores, the surfactant was extracted from the as-synthesized mesostructured solid by chemical exchange using an HCl/ethanol solution (CTA^+/H^+ exchange). Thus, 1 g of mesostructured UVM-7 powder was suspended in a solution containing 16 mL of HCl (37%) and 130 mL of ethanol (99%), and this mixture was heated at reflux (60 °C) for 2 h while stirring. Later, after renewal of the HCl/ethanol solution, and to complete the extraction process, the suspension was heated again at 60 °C for 16 h while stirring. The resulting mesoporous solid UVM-7-e was collected by filtration, washed with ethanol, and air-dried at 100 °C.

The large aggregates of UVM-7-e material were transformed into submicrometric or nanometric aggregates by means of high power ultrasound treatment (using a Branson instrument). In a typical preparation, a suspension containing 3g of UVM-7-e in 100 mL of distilled water (3% in weight) was irradiated for 15 min at a nominal power of 350 W. After irradiation, the suspension has colloidal character showing

the Tyndall effect. The CF coating was performed by successive impregnation cycles. In each cycle an immersion of the ceramic foam into an aqueous UVM-7-e colloidal suspension (ca. 3% in weight) was firstly performed, and afterwards, a soft thermal treatment (150 °C for 16 h) to favor water evolution and nanoparticles adhesion (formation of covalent Si-O-Si bonds with the CF surface). The solid CF-UVM-7-e was hence obtained. Mesoporous material anchored to the monolith was functionalised in order to build the active sites on the materials surface.[36] CF-UVM-7-e monoliths were immersed in anhydrous acetonitrile (500 mL) and heated at 120 ºC in a Dean-Stark apparatus to remove the adsorbed water by azeotropic distillation under an inert atmosphere (Ar gas). After this, 25.6 mmol (6mL) of APTES ((3-aminopropyl)-triethoxysilan), were added and the solution was stirred for 16h. Then, the monoliths (CF-UVM-7-N) were washed with acetonitrile, and ethanol. Finally, 0.5 L of a 0.07M solution of gluconolactone in methanol was added to the former mixture, and after stirring for 48 hours at room temperature the fully functionalized monoliths, named CF-G (-a, -b, -c for those used for adsorption essays and –d, -f , –g, to be used in the different analytical techniques), were achieved.

In order to compare the adsorption capacity of the supported active materials, a non-supported UVM-7-e material was also functionalized. Hence, 2 g of UVM-7-e were suspended in 70 mL of acetonitrile and heated at 120^{o}C in a dean-stark apparatus. Then, 3.4 mmol of APTES were added at room temperature following the same conditions as those described above for the CF-UVM-7-e. After 16 h., the solid was filtered and washed with acetonitrile and water reaching to UVM-7-N. Finally, in order to achieve the active sites UVM-7-N material was reacted with 6.8 mmol of gluconolactone in 100 mL of methanol. The mixture was stirred during 48h at room temperature. After that, the obtained S1 solid was filtered, washed with water and dried. A summary of the codes used for naming the prepared materials and composites.

CF	Non functionalised ceramic foam
UVM-7	Non functionalised mesostructured silica (including the template surfactant)
UVM-7-e	Non functionalised mesoporous silica (surfactant extracted)
CF-UVM-7-e	Ceramic foam coated with non functionalised mesoporous silica
CF-UVM-7-N	3-aminopropyl-functionalised mesoporous silica coated ceramic foam
CF-G-a	Fully functionalised mesoporous silica coated ceramic foam (including glucose moiety) –used in adsorption assays
CF-G-b	Fully functionalised mesoporous silica coated ceramic foam (including glucose moiety) –used in adsorption assays
CF-G-c	Fully functionalised mesoporous silica coated ceramic foam (including glucose moiety) –used in adsorption assays
CF-G-d	Fully functionalised mesoporous silica coated ceramic foam (including glucose moiety) –for analysis
CF-G-f	Fully functionalised mesoporous silica coated ceramic foam (including glucose moiety) –for analysis
CF-G-g	Fully functionalised mesoporous silica coated ceramic foam (including glucose moiety) –for analysis
UVM-7-N	3-aminopropyl-functionalised mesoporous silica
S1	Fully functionalised mesoporous silica (including glucose moiety)

Table 1. Summary of the codes used for the prepared materials and composites.

3.2.2 Boron adsorption assays

Adsorption studies of boron on CF-G were carried out dipping each monolith in 25 mL of distilled water while stirring. After two hours, an aliquot of 2 mL was extracted from the solution and another 2 mL aliquot of 75 ppm of boron was added resulting in a nominal concentration of 6 ppm of boron. Thus, every two hours an aliquot of 2 mL was extracted from the solution in contact with the monolith and another 2 mL aliquot of increasing boron solution was added in order to keep a constant volume of 25 mL. This protocol was kept on until the concentration of the solution reached 230 ppm with the aim of reaching the monolith saturation for boron adsorption. Boron adsorption studies on S1 were carried out suspending 30 mg of S1 solid in 12.5 mL of boron solution at a certain concentration in order to maintain the same conditions as those in the CF-G functionalisations. The suspensions were stirred during 16 h. and then the mixture was filtered. The boron concentration in the solutions was analyzed by azomethine-H as a colorimetric reagent according to the method described in references.[37,38]

Kinetic adsorption studies of boron on CF-G were carried out dipping the monolith in 25 mL of a 5 ppm boron solution. An aliquot of 1 mL was extracted from the solution at different times during 4h. Batch experiments were carried out for kinetic assays on the S1 solid. These involved suspension of 30 mg of S1 solid in 12.5 mL of a 5 ppm boron solution in order to maintain the same conditions as for CF-G material. The suspensions were stirred and an aliquot was taken and filtered at different times during 4h. Boron concentration was determined using Perkin Elmer Spectrophotometer with azomethine-H method.[37,38]

3.2.3 Characterization Techniques

X-ray powder diffraction (XRD) data were recorded on a Bruker D8 Advance diffractometer using Cu Kα radiation. Both low- and high-angle XRD patterns were recorded to analyze the diffraction signals typical of the UVM-7 mesoporous silicas and the peaks associated with the ceramic foam. Low angle XRD patterns were collected in steps of 0.02°2θ over the angular range 0.65-10°2θ and an acquisition time of 25 s/step. High-angle patterns were collected with a scanning step of 0.05°2θ over the angular range of 10-70°2θ and an acquisition time of 10 s/step. High and low-magnification SEM images were recorded by using a Jeol JSM 6300 microscope. Samples were previously coated with Au-Pd. A TEM study was carried out with a Philips CM10 instrument operating at 100 kV and equipped with a CCD camera. Samples were gently ground in dodecane, and microparticles were deposited on a holey carbon film supported on a Cu grid. Nitrogen adsorption-desorption isotherms (-196 °C) were recorded with a Micromeritics ASAP- 2010 automated instrument. Calcined samples were degassed at 120 °C and 10-6 Torr for 5h prior to measurement. Surface areas were estimated according to the BET model, and pore size dimensions and pore volumes were calculated by using the BJH method from the adsorption branch of the isotherms. Particle size measurements (DLS) were performed using a Malvern Zetasizer ZS instrument. Thermogravimetric analyses were carried out on a TGA/SDTA 851e Mettler Toledo balance, with a heating program consisting of a heating ramp of 10°C per minute from 393 to 1273 K and an isothermal heating step at this temperature over 30 min.

Spectrophotometric measurements were carried out with a Lambda 35 UV/Vis Spectrometer from Perkin–Elmer Instruments.

3.3 **Results and discussion**

3.3.1 Preparation of the adsorbent agents

As we have commented in the introduction, the system for boron adsorption we have designed is based on the capacity of boron ions to form boro-esters with molecules that present consecutive diols. Hence, our idea was to obtain an adsorbent material with the highest possible concentration of diols. This point can be easily reached by functionalisation of mesoporous silicas with saccharides moieties due to the high surface area these materials present and its ease functionalization. However, two important points must be also taken into account in order to get a good performance of the final adsorbent. In first place, the active sites (consecutive diols) should present maximum accessibility. This feature can be attained when using the materials denoted as UVM-7 as the mesoporous support. These materials are a nanometric version of the MCM-41 silicas and show very open architectures consisting of micrometric aggregates of mesoporous nanoparticles connected through covalent bonds. This organization defines two pore systems: the first one (intraparticle) is generated by the effect of the surfactant micelles and the second one (inter-particles) is formed as the nucleation and growth of the primary mesoporous nanoparticles proceeds. In this way, an improved accessibility to the active sites can be attained without losing the possibility of a high surface functionalisation of the mesoporous materials. The surfactant-assisted synthesis of the UVM-7 silica-based nanoparticulated mesoporous materials has been reported elsewhere. [33]

The second point to be contemplated to get a good performance of the adsorption system was the improvement of the adsorbent handling as the mesoporous materials usually are obtained as very fine powders (in the nanometric range) and then are not good candidates for real adsorption processes. In this case, the opted solution was to choose ceramic foam as macroscopic inorganic support. Hence, the

final adsorption system would be composed by a mesoporous silica matrix that after being supported on macroporous ceramic foam is being functionalized with saccharide moieties.

Additionally, the large aggregates of the as-synthesized UVM-7-e silica can be transformed into even smaller sub-micrometric or nanometric aggregates by means of high-power ultrasound treatment, which leads to stable colloids in water.[39] This is a key point in our preparative procedure because it allows us to have stable UVM-7-e colloidal particles able to cover the CF support by dip coating. Besides, UVM-7-e materials so treated still maintain the same high capacity to be easily derivatized with functional groups.[40] Then, the poliol group selected as the binding site will be attached to the silica framework by prior reaction with an alkoxysilane reactant.

The preparation of CF-G composites is shown in Scheme 1. The coating process of the CF support was performed by successive impregnation dip-coating cycles into an aqueous UVM-7-e colloidal suspension (ca. 3% in weight) followed by soft thermal treatment (150 °C for 16 h) to favor water evolution and nanoparticle adherence (formation of covalent Si-O-Si bonds both among nanoparticles and with the CF surface). The resulting monoliths CF-UVM-7-e were then weighted and the amount of impregnated material was determined to be approximately 0.05 g of UVM-7 per monolith (a mean value of 6.4% of increment). Then, surface organic functionalization was carried out through a two steps grafting protocol. The starting CF-UVM-7-e was first reacted with (3-aminopropyl)-triethoxysilane in acetonitrile to yield CF- UVM7-N, and then with gluconolactone in methanol to obtain the final CF-G composite. After the full functionalisation process an average increment of mass of 7.9% corresponding meanly to the adhered UVM-7-G active material was obtained. In Table 2 the main values for the coating and functionalisation process performed on several CF matrices are collected. It can be seen that even when the process presents some difficulties due to the mixing of three different phases, CF support, UVM-7 mesoporous solid and the components in the aqueous solution, the results on Table 1 show a quite acceptable reproducibility of the synthetic process.

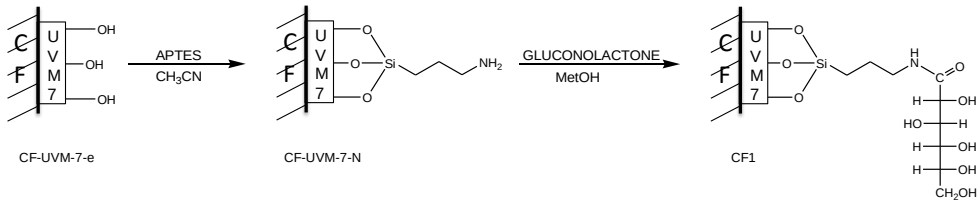

Scheme 1. Route for the preparation of CF-G composites.

	Initial mass (g)	1st adhesion of UVM-7-e (g)	2nd adhesion of UVM-7-e (g)	UVM-7-e adhered (%wt)	Final mass (g)[a]	UVM7-G adhered (% wt)[b]
CF-G-a	0.8816	0.9060	0.9293	5.13	0.9435	6.56
CF-G-b	0.8777	0.8999	0.9234	4.95	0.9362	6.25
CF-G-c	0.6716	0.6968	0.7168	6.31	0.7378	8.97
CF-G-d	0.4550	0.4732	0.4912	7.37	0.4940	7.89
CF-G-f	0.6662	0.6972	0.7242	8.01	0.7407	10.06
CF-G-g	0.6101	0.6250	0.6550	6.85	-	-

a Mass of the monolith after complete functionalisation

b Percentage of active material UVM7-G adhered in the final monolith.

Table 2. CF coating and functionalization process for several CF-G monoliths.

The non-supported UVM-7-e material was also functionalized following the same procedure: the silica mesoporous powder was treated with APTES in acetonitrile to yield UVM-7-N and then the resulting solid was treated with gluconolactone in methanol to yield S1. In this way, the adsorbent capacity of CF-G materials, in which the active mesoporous particles are stuck on the ceramic foam, can be compared with the capacity of the non-supported S1 material directly suspended in water.

3.3.2 Materials characterization

The inorganic material used as macroscopic support for the active material is a macroporous solid that can be described as ceramic foam (CF). This scaffolding was prepared through conventional polyurethane foam (PUF) replica technique described by Schwartzwalder,[31] which allows good control of the macroscopic monolith shape and dimensions. As expected from the SiO_2-Al_2O_3 phase diagram, the XRD data (Fig. 1) show that the final material is basically formed by two

crystalline phases, quartz (60%) and mullite (23%) (estimated composition from XRD phase analysis), and a vitreous phase including amorphous sodium and potassium aluminosilicates. The result is a rigid foamlike macroporous monolith (CF) (wt % composition, after calcination: SiO_2 72.0%, Al_2O_3 22.8%, Na_2O 0.9%, K_2O 4.3%). While it might be assumed that this monolith with high percentage of silica could be a good candidate for functionalizing directly with APTES and later with gluconolactone, there are two reasons to discard this strategy: its very low surface area (0.001 m^2/g) and the difficulty to anchor APTES groups considering the high degree of condensation of the monolith (as expected taking into account the high temperatures employed in its synthesis). Both factors, separately, and even more cooperatively, would lead to a material with low content of functional groups and consequently with a low capacity to capture boron species. Therefore, to increase the surface and facilitate the functionalization, we includes within the monolith a siliceous material of high surface area, easy to functionalize (due to its amorphous nature) and having small grain size (to invade easily the macropores of the monolith). These features are provided by the UVM-7 silica.

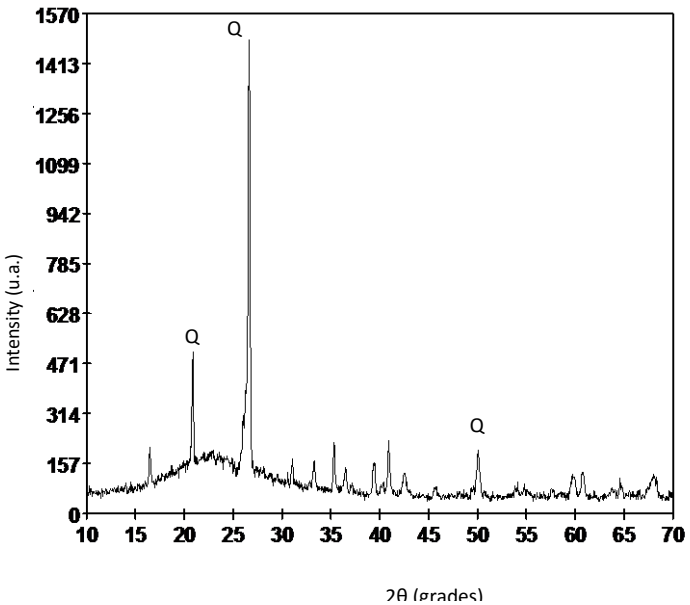

Figure 1. XRD pattern of the ceramic foam (CF). Q = quartz. The remaining peaks correspond to mullite.

The mesoporous and hybrid materials were characterized by standard procedures. X-ray diffraction (XRD) patterns of the materials UVM7, UVM-7-e and CF-UVM-7-e (Fig. 2) show that the intense peak at about 2°2θ, characteristic of surfactant-assisted mesoporous materials, does not suffer major changes, that is, the synthetic steps do not significantly affect the mesoporous structure of the silica mesoporous matrix even after the sticking process on the ceramic foam.

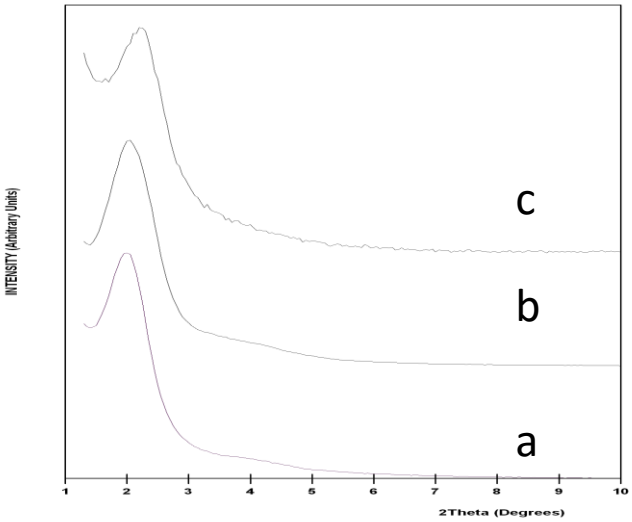

Figure 2. Low angle powder XRD patterns of (a) UVM7, (b) UVM-7-e and (c) CF-UVM-7-e.

The transformation of the large aggregates of the as-synthesized UVM-7-e solid into smaller sub-micrometric or nanometric aggregates after high power ultrasound treatment can be easily followed by direct observation. Indeed, after ultrasound irradiation, the suspension acquired colloidal character showing the Tyndall effect. Additionally, the decrease of the aggregate dimensions was studied by transmission electron microscopy. In Figure 3 representative TEM images of UVM-7-e material before and after ultrasound irradiation are shown. However, a more direct evidence of the true particle size that interacts with the ceramic support (and its evolution) is obtained by DLS. Thus, we measured the grain size of the UVM-7 silica dispersions (with concentration identical to that used in the impregnation cycles) before and after sonication. A decrease of the aggregate sizes

from 830 to 220 nm is induced through ultrasound irradiation (Figure 4). The low grain size achieved is adequate to ensure an efficient invasion along the macropores of the monolith.

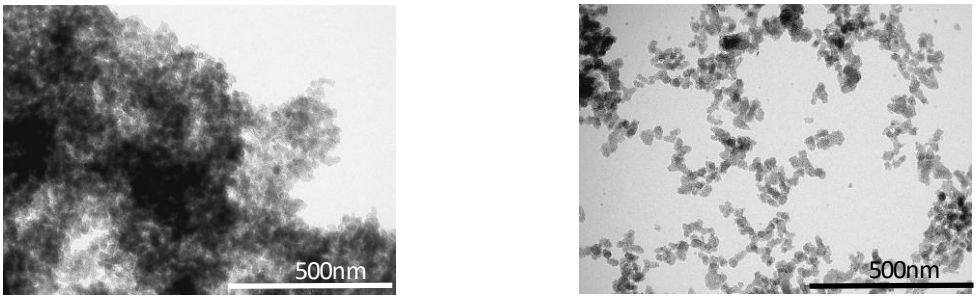

Figure 3. TEM micrographs of the UVM-7-e aggregates before (a) and after (b) ultrasound irradiation.

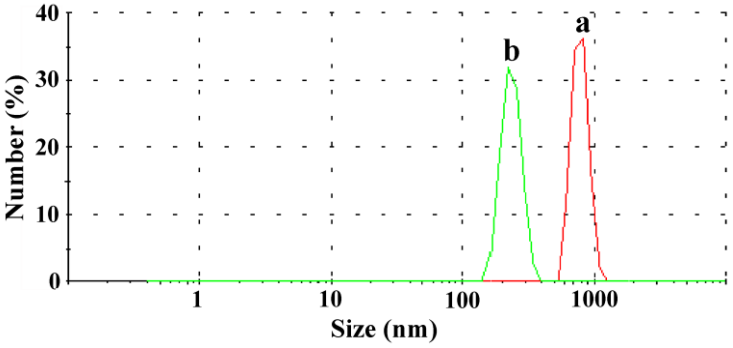

Figure 4. DLS curves of the UVM-7-e aggregates before (a) and after (b) ultrasound irradiation.

The coating process leading to CF-UVM-7-e can be appreciated in Figures 5 to 8. In Figure 5 an optical image of the ceramic foam before and after the coating process is shown. A closer insight of the coating process is shown in Figure 6 where Scanning Electron Microscope (SEM) images reveal the differences produced on the monolith surface during the process. The foam coating is rather homogeneous and can be described as formed by successive deposition of small UVM-7-e flakes in an imbricate way. These flakes are rather regular and have about 6-9 µm of thickness. The origin of these thick flakes is likely due to cracks generated during the drying process. Probably, the macrostructure generated by superposition of the UVM-7-e

flakes induces a “binder” effect favoring the cohesion of the particles among them. High-magnification SEM and TEM images (Figure 7) demonstrate that the UVM-7 organization is preserved. Thus, at micrometric scale, the deposited silica flakes present rough surfaces (Figure 7a) consisting of aggregates of pseudospherical clusters of mesoporous nanoparticles (Figure 7b), which define true textural large mesopores among them. The intraparticle disordered small mesopore system can be clearly appreciated in Figure 7b. This fact confirms that the intraparticle mesopore organization is preserved after the CF coating. These mesopore systems (small and large) typical of UVM-7 mesoporous material, together with the foam-like interconnected macropores (400-600 µm) define a very open hierarchical porous architecture.

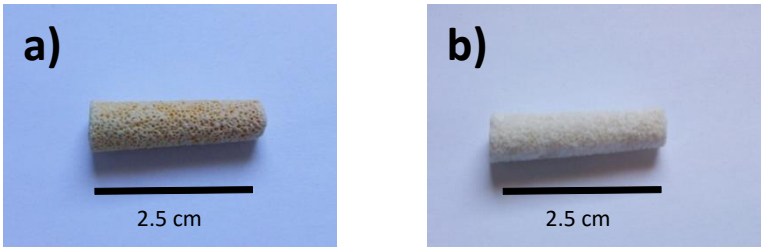

Figure 5. Optical images: (a) Starting foam, (b) CF-UVM-7-e composite.

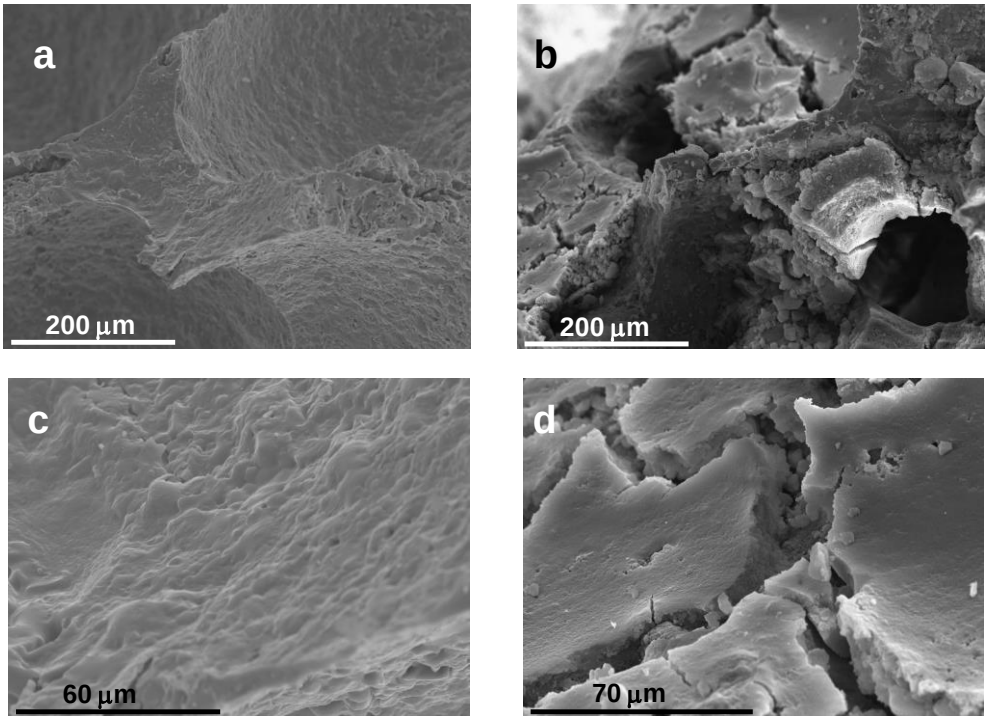

Figure 6. SEM images of the CF: (a) and (c) before coating, and (b) and (d) after two impregnation cycles.

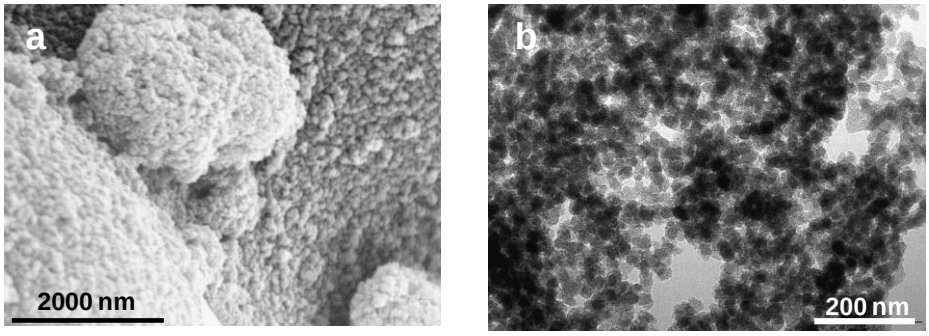

Figure 7. SEM (a) and TEM (b) images showing typical UVM-7 like aggregates of the mesoporous nanoparticles present in the CF monolith after two impregnations.

SEM image in Figure 8 shows the interior (transverse section) of a CF-coated monolith. Thus, it can be appreciated that the coating efficiency gets into the deepest part of the monolith and that the deposition of UVM-7-e particles is not

limited to the exterior of the ceramic foam. In practice there are no appreciable differences in the coating degree between the monolith surface and its interior.

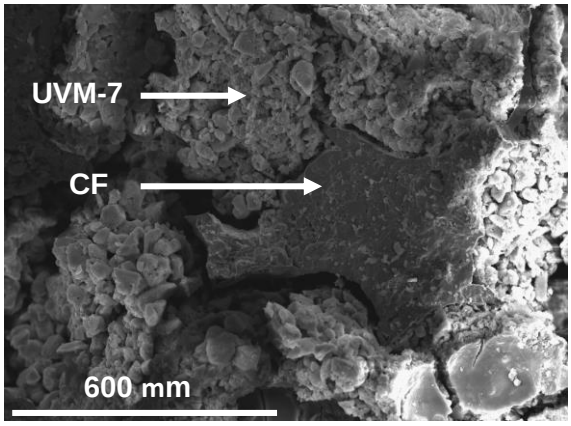

Figure 8. SEM image of a section of the CF after two impregnation cycles with UVM-7-e.

In Figure 9, the evolution of the N_2 adsorption with the ceramic foam impregnation process is shown. Isotherms of the resulting composites show the characteristic features of UVM7 materials: two well-defined adsorption steps at intermediate ($0.3 < P/P0 < 0.5$) and high ($P/P0 > 0.8$) relative pressure values, which can be respectively associated with the filling of the intra-nanoparticle (surfactant generated) small mesopores and the interparticle (generated by condensation of the primary nanoparticles) large mesopores.

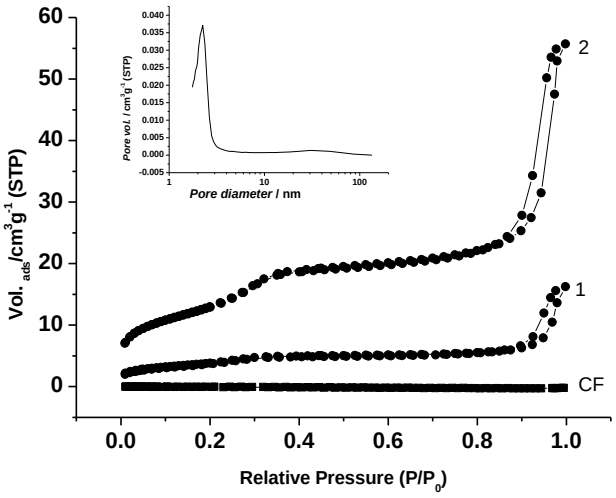

Figure 9. N2 isothermal absorption/desorption curves for: CF) non-impregnated ceramic foam; 1) ceramic foam after one UVM-7-e impregnation cycle; and 2) ceramic foam after two UVM-7-e impregnation cycles.

The physisorption data in Table 3 evidence that both the BET surface area, calculated from a Brunauer–Emmet–Teller (BET) treatment of the isotherms,[41] and volumes and the pore sizes, estimated by the Barrett–Joiner–Halenda (BJH) method,[42] in the composite monoliths increase with the number of impregnation cycles. Moreover, the N_2 adsorption ratio associated with the intra- and interparticle pores reminds that expected for a UVM-7 mesoporous material. After two cycles, the weight increase for the CF analyzed (CF-G-g, Table 1) was 6.85%, which corresponds to the incorporation of 0.045 g of UVM-7-e material. Assuming that the 47.1 m^2/g are basically due to the adhered UVM-7-e solid, we can estimate an average BET area of 687.1 m^2/g for the mesoporous active phase prior the final functionalisation. This value fits very well with typical BET area of UVM-7 bulk phases. Then, the high accessibility of the UVM-7 pore system is preserved even for nanoparticles close to the CF surface.

	Coating cycles	BET (m^2/g)	BJH intraparticle pore (nm)	BJH interparticle pore (nm)	Small pore volume (cm^3/g)	Large pore volume (cm^3/g)	Relative impreg-nation[a]	UVM7 content[b] (% wt)
UVM-7-e	-	877.7	2.73	48.6	0.71	1.58	-	-
CF	0	0.001	-	-	-	-	0	0
CF-UVM-7-e	1	13.7	2.43	43.3	0.01	0.02	2.44	2.38
CF-UVM-7-e	2	47.1	2.69	33.5	0.04	0.06	7.35	6.85

a increment of mass of the monolith after each impregnation process (referred to the initial monolith weight)

b Percentage of UVM-7 adhered in the CF- UVM-7-e monolith.

Table 3. Evolution of the textural properties and coverage level for UVM-7 mesoporous coated CF composites

The functionalisation degree of CF-G monoliths and S1 material was also assessed by elemental analysis and thermogravimetric studies. From the elemental contents (C, H, N), the amount of N-(3-triethoxysilylpropyl)gluconamide groups were calculated. In order to compare both type of solids the final functionalisation value is given as millimoles per mass unit of silica residue (αamine in mmol of amine/g SiO_2, and αglucose in mmol of glucose/g SiO_2). Hence, for S1 solid the silica residue was taken directly from thermogravimetric analysis. In the case of CF-G the data was taken from the thermogravimetric decomposition of the CF-G-f monolith and taking into account the amount of UVM-7-G adhered onto the corresponding CF support. The final functionalization value was referred to the silica residue of the adhered UVM-7-e. In this way, even when both materials CF-G-f and S1 are quite different, their functionalisation degree can be compared. Functionalisation data are collected in Table 4. It can be seen that CF-G-f and S1 present different functionalisation degree, while S1 solid contain 1.29 mmol of amino groups per gram of SiO_2, CF-G-f composite has 2.79 mmol of amino groups per gram of SiO_2 (silica residue of the active UVM-7-e adhered material). The contents on saccharide groups for both materials follow a similar tendency, S1 solid has lower functionalisation (0.77 mmol of saccharide groups per gram of SiO_2) while CF-G-f has higher amount of glucose groups (1.31 mmol of saccharide groups per gram of SiO_2). These differences in the functionalisation degree could be related with the different availability of reactants during the preparation of both materials. Even when the concentration of reactants (APTES and gluconolactone) are initially the same in both processes, the differences in shape and size between the initial

supports, CF-UVM-7-e and microparticulated UVM-7-e, compelled us to use a higher amount of the corresponding solutions for the functionalisation of the monoliths, and so higher amount of reactants were available in this case.

However the higher funtionalisation of the CF composite, from the values of these factors the difference in the yield of the reaction between the amino groups and glucolactone says that the final reaction has lower effectiveness in the case of the ceramic foam CF-G-f (48%) than in the case of the microparticulated S1 solid (60%). This fact could indicate that the access to the amine groups is somehow more intricate in the case of the ceramic foam.

Ads.	Total amine (mol)	Total glucose (mol)	Amine (mmol/g UVM7-G)	glucose (mmol/g UVM7-G)	α_{amine} (mmol/g SiO_2)	$\alpha_{glucose}$ (mmol /g SiO_2)	$\alpha_{glucose}/\alpha_{amine}$ (%)[d]	$\beta_{glucose}$ (molecules /nm^2)
CF-G-f	0.0163	0.0079	1.625[a]	0.786[a]	2.70[b]	1.31[b]	48	0.88[c]
S1	0.1003	0.0600	1.003	0.560	1.29	0.77	60	0.52

a Amine or glucose content of the adsorbent per mass unit of the active material UVM7-G.

b Amine or glucose content of the adsorbent per mass unit of SiO_2 of the active material UVM7-G.

c Glucose coverage of the adsorbent taking into account the surface of the active material UVM7-G.

d Yield of the second functionalization reaction.

Table 4. Amine and glucose contents and estimated average coverage for selected adsorbents

3.3.3 Boron sorption assays

Boron removal in functionalised materials is due to the complex formation between the boric acid and polyol groups incorporated into the pore structure of the sorbents. Although the reaction between gluconamide groups and boric acid molecules is not yet well clarified, boron is expected to form both bidentate and bisbidentate complexes with the consecutive alcohol groups of the glucose moieties attached to the surface of the adsorbent, as it is shown in Figure 10. Hence, functionalised materials will show the ability to remove boron from aqueous solutions depending meanly on the amount and distribution of the glucose groups on the adsorbent surface. In order to evaluate the adsorption capacity of the supported active material, both types of absorbents, monoliths and mesoporous solid S1, have been tested for their boron sorption efficiency.

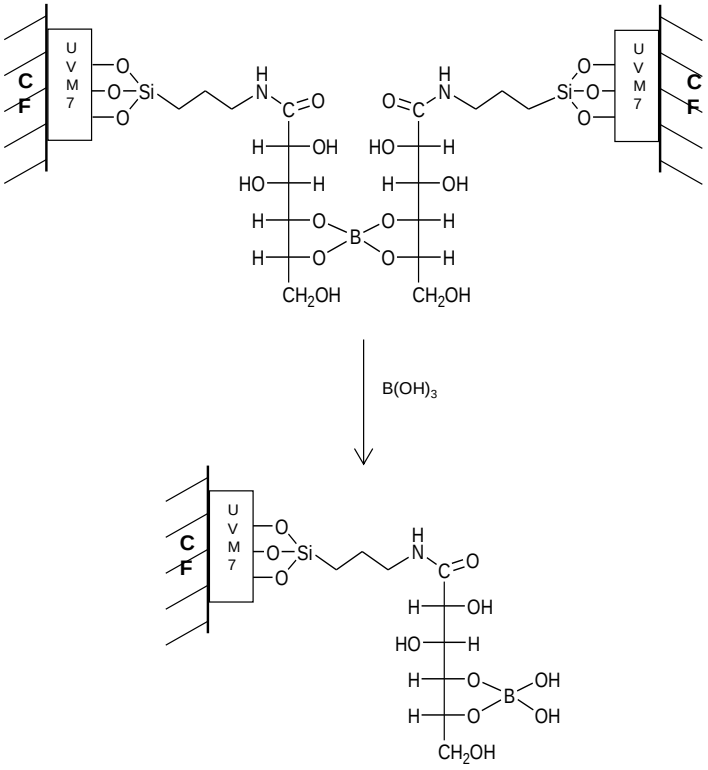

Figure 10. Proposed mechanism for the boron sorption by gluconamide-functionalized sorbents.

First parameter to be studied has been the variation of boron adsorption for both CF-G and S1 as a function of the contact time and the results are depicted in Figure 11. The experiment shows a very quick adsorption of boron by S1 solid as the 90% of the total adsorption was reached already during the first minute at the experimental conditions used. Then, the adsorption levels off after approximately 15 minutes. In comparison, it takes longer time, around 15 minutes, to CF-G-d to get the same 90% level of adsorption and it is not after 40 minutes that the monolith-supported material reaches the maximum level of adsorption. This different behavior may be related with the unlike pathways in both adsorbents for boric moieties to reach the active sites. In the case of S1 adsorbent the active material is directly suspended in the solution while in the case of CF-G-d composite boric moieties have to travel through the intricate structure of the monolith to reach the active groups.

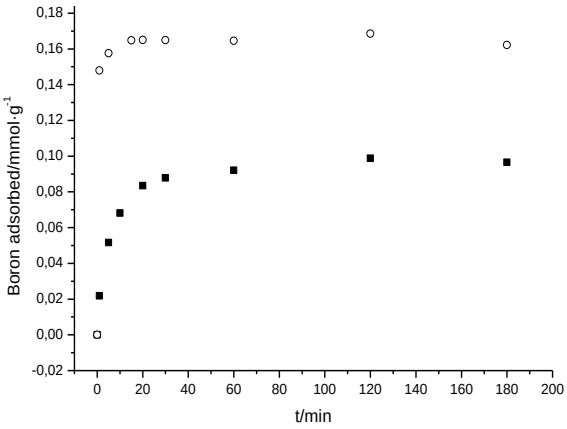

Figure 11. Evolution of the boron removal from a 5ppm B solution as a function of the contact time.

The borate adsorption behaviour for three monoliths (CF-G-a, CF-G-b and CF-G-c) and for S1 are shown in Figure 12 (a and b respectively) where the amount of boron adsorbed per unit mass of the sorbent (in the case of monoliths, per unit mass of supported UVM-7 already functionalized with the glucose) is shown as a function of the initial boron in solution. As can be seen from the curves, the amount of adsorbed boron increased as the boron equilibrium concentration in solution increased. The behaviour of the three monoliths is quite similar though different to the S1 material as the monoliths take longer in reaching the saturation level.

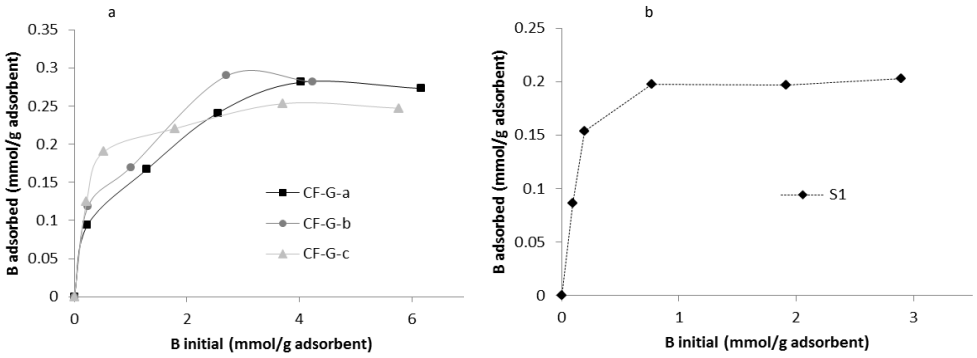

Figure 12. Boron adsorbed at 25ºC as function of the initial boron concentration a) for three different monoliths CF-G-a, CF-G-b, CF-G-c and b) for S1.

In a typical boron adsorption test, increasing amounts of boron were added to the solution in contact with the monolith while adsorbed boron was monitored. Saturation is reached at about 0.25 mmol of boron per gram of adsorbent. Consequently, bearing in mind the amount of saccharide present in the solid (see Table 3) it is possible to say that approximately a 32% of the binding sites are occupied. However, as each boron atom could be bonded to two glucose molecules the adsorption is not so far from full occupancy. Figure 12.b shows the performance of the material S1 in boron adsorption. Batch studies were carried out for the adsorption assays. In this case, the saturation is reached with much lower equilibrium concentration and so, the isotherm reaches the saturation very fast. Yet, the occupancy of the available binding sites when saturation is reached behaves similarly as in the case of monoliths. In S1 the 36% of the binding sites were occupied and thinking in a boron coordination through two glucose molecules, the system approaches the full occupancy.

In order to clarify the design of adsorption systems to remove boron species from aqueous solution, it is necessary to establish the most appropriate correlation for adsorption results. Several models have been published in the literature to describe experimental data of adsorption isotherms. In this work, Langmuir model was used to describe the relationship between the adsorbed amount of boron and its concentration in solution at the equilibrium conditions. The Langmuir isotherm is valid for monolayer sorption onto a surface with a finite number of identical sites and uniform adsorption energies. This model assumes that the isotherm coverage can be expressed in terms of the Langmuir adsorption constant (K) and the concentration Ce (in mol/L) of the adsorbate at the equilibrium:

$$\Theta t = \frac{\mathrm{K} \cdot Ce}{1 + \mathrm{K} \cdot Ce}$$

On the other hand, experimental coverage can be expressed by the following equation:

$$\Theta e = \frac{Cs}{Cm}$$

where Cm is the maximum sorption capacity corresponding to the complete monolayer coverage (mmol/g) and Cs is the amount of adsorbed boron (mmol/g). In Figure 13 the plot of experimental coverage (Θe) as a function of the equilibrium boron concentration in solution is presented and a typical Langmuir type adsorption can be appreciated.

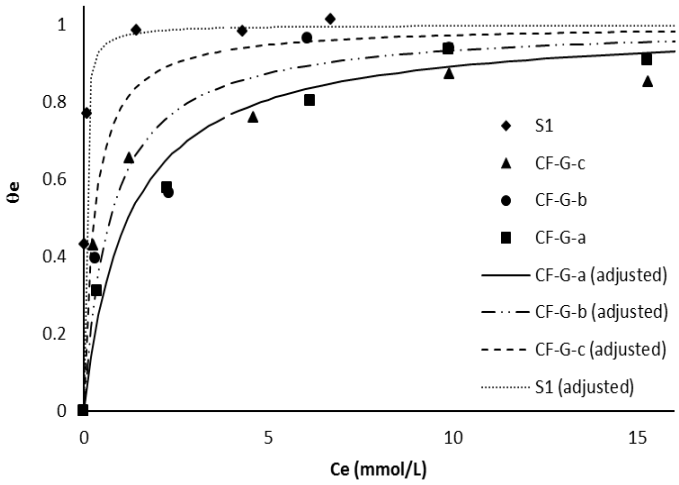

Figure 13. Boron adsorption isotherms for S1 solid and CF-G-(a, b,c) monoliths.

From the adjustment of the Figure 13 plots using the Langmuir model values of the adsorption constant (K) and the monolayer capacity (Cm) for the different monoliths and S1 can be obtained (see Table 5). The calculations have been performed with the Solver tool inside the Excel program by minimizing the quadratic average error between the theoretical (Θt) and experimental coverage (Θe). It can be seen that the three monoliths present similar constant values, with log K around 3. However, solid S1 shows a constant with a value one order of magnitude higher. Bearing in mind that the adsorption constant accounts for the interaction between the adsorbent and the adsorbate, we could say that the synthesis of the active material (glucose functionalized UVM-7 material) onto the ceramic foam induces a decrease in the interaction strength. The main difference between the two systems we have essayed in this paper is that the organic groups,

that give rise to the final active sites, have different pathways until they reach the surface of the corresponding inorganic matrix where they must anchor. This fact, that has been already discussed above when talking about the yield of the functionalization reactions, may have influenced also the final distribution of the glucose groups attached onto the surface. If the gluconamide groups had a somehow more intricate pathway towards the anchored amines in the case of the ceramic foam the resulting glucose groups may present some steric hindrance for the borate groups to form bisbidentate complexes and a higher amount of only bidentate complexes would form during the boron adsorption on CF-G. Hence, a different distribution of the glucose groups on the inorganic matrix could account for the differences in the constant values of the CF-G and S1 materials.

Adsorbent	Log K	C_m (mmol/g)	R^2
S1	4,48	0.20	0,9994
CF-G-a	2,91	0.30	0,9782
CF-G-b	3,10	0.29	0,9203
CF-G-c	3,25	0.25	0,9886

Table 5. Langmuir constants

According with our previous studies, the active material UVM-7-G could be regenerated by simple acidic washing which quantitatively would remove the loaded boron because of the hydrolysis of the boron esters generated during the adsorption process. In order to corroborate the regeneration possibility of our new composites, a monolith (CF-G-c) was immersed into 100mL of 0.1 M HCl solution and left there for 24 hours at room temperature. Then the monolith was extracted from the acidic solution and washed with distilled water until the acid was completely removed. It was then treated with a fresh boron solution under the same conditions as in the first adsorption test and the adsorbed boron was measured as before. This process was repeated several times. Figure 14 shows a plot of the adsorption capacity of CF-G-c over successive cycles. It is observed that approximately 50% of initial boron sorption capacity can be preserved after the acidic treatment. The fact that the complete sorption capacity cannot be recovered could be related with the loss of poorly attached active sites during the acidic

washing, as the more intricate morphology of the monoliths matrix may present more difficulties when producing a good functionalization of the surface. However, we remark that after the observed leaching of active sites (and the subsequent B adsorption decrease) during the first cycle, the material adsorption capacity is maintained in successive cycles.

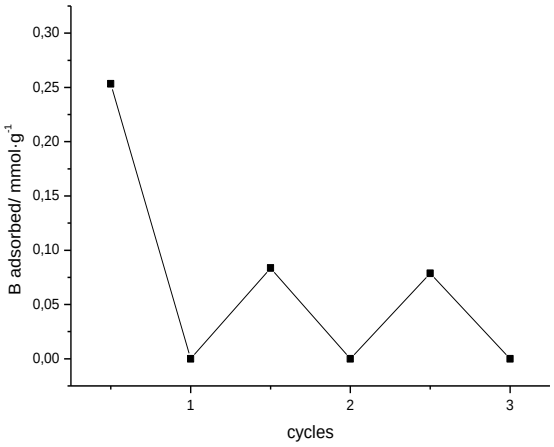

Figure 14. Evolution of the boron content for **CF-G-c** during several cycles of washing with HCl and boron adsorption.

3.4 **Conclusions**

We have shown that ceramic monoliths can act as proper supporting matrices to get a boron adsorbent easier to handle for applied proposals. The synthesis of this kind of composites shows a good reproducibility as all the monoliths essayed present similar behavior and adsorption properties. When comparing the CF-G composites with the parent adsorbent S1, monoliths present lower adsorption kinetics however they show comparable total adsorption capacity though at low boron concentrations the adsorption capacity is lower than for S1. The affinity of borate entities for the active sites in CF-G materials is lower than that for S1 which may indicate a different distribution of the active sites onto the CF-G composites related with a higher difficulty during the functionalization process due to a more intricate pathway for the organic moieties to reach the mesoporous surface. The capacity of CF-G composites to be recycled for new uses is quite good and makes

of this material a promising candidate to be essayed in a continuous boron elimination process.

Acknowledgements

Financial support from the Spanish Government (Project MAT2009-14564-C04-01 and MAT2009-14564-C04-04, and MAT2012-38429-C04-01 and MAT2012-38429-C04-02) and the Generalitat Valenciana (Project PROMETEO/2009/016) is gratefully acknowledged. C.S. thanks the MICINN for a predoctoral fellowship.

References

1 P.W.Howe, *Biol. Trace Elem. Res*., **1998**, 66, 153.

2 R.F. Moseman, *Environ. Health Perspect. Suppl*., **1994**, 102, 113.

3 V.M. Shorrocks, *Plant Soil*, **1997**, 193, 121.

4 WHO, *Guidelines for drinking-water quality, 4th ed., Malta*, **2011**. (ISBN 978 92 4 154815 1)

5 E.Weinthal, Y. Parag, A. Vengosh, A. Muti,W. Kloppmann, *Eur. Environ*., **2005**, 15, 1.

6 SCHER (Scientific Committee on Health and Environmental Risks) scientific opinion on request for derogations on the Drinking Water Directive (Directive 98/83/EC), 16 April 2010.

7 Y. Xu, Jia-Qian Jiang., *Ind. Eng. Chem. Res*., **2008**, 47, 16.

8 C. Yan, W. Yi, P. Ma, X. Deng, F. Li, *J. Hazard. Mater.,* **2008**, 154, 564.

9 C. Jacob, *Desalination,* **2007**, 205, 47.

10 A.E. Yilmaz, R. Boncukcuoglu, M.M.Kocakerim, M.T. Yilmaz, C. Paluluoglu, *J. Hazard. Mater.,* **2008**, 153, 146.

11 L. Melnyk, V. Goncharuk, I. Butnyk, E. Tsapiuk, *Desalination*, **2007**, 205, 206.

12 M. Turek, P. Dydo, J. Trojanowska, A. Campen, *Desalination,* **2007**, 205, 192.

13 W. Bouguerra, A. Mnif, B. Hamrouni, M. Dhahbi, *Desalination,* **2008**, 223, 31.

14 N. Ozturk, D. Kavak, T.E. Kose, *Desalination*, **2008**, 223, 1.

15 Y. Oren, C. Linder, N. Daltrophe, Y. Mirsky, J. Skorka, O. Kedem, *Desalination*, **2006**, 199, 52.

16 T.E. Kose, N. Ozturk, *J. Hazard. Mater*., **2008**, 152, 744.

17 S. Karahan, M. Yurdakoc, Y. Seki, K. Yurdakoc, *J. Colloid Interface Sci*., **2006**, 293, 36.

18 D.I. Fried, A. Schlossbauer, T. Bein, *Microporous and Mesoporous Materials,* **2012**, 147, 5.

19 G. Rodríguez-López, M.D. Marcos, R. Martínez- Máñez, F. Sancenón, J. Soto, L. A. Villaescusa, D. Beltrán and P. Amorós, *Chem. Commun*., **2004**, 2198.

20 D. Yu, D. Xue, Acta Crystallogr. B62, **2006**, 702.

21 B. M. Smith, J. L. Owens, C. N. Bowman, P. Todd, *Carbohydrate Research*, **1998**, 308, 173.

22 J. Aguado, J. M. Arsuaga, A. Arencibia, M. Lindo, V. Gascón, *Journal of Hazardous Materials,* **2009**, 163, 213.

23 C. Coll, R. Martínez-Máñez, M. D. Marcos, F. Sancenón, J. Soto, and R. K. Mahajan, *Eur. J. Inorg. Chem.,* 2009, 3770.

24 C. Sanfeliu, R. Martínez-Máñez, F. Sancenón, J. Soto, V. Puchol, P. Amorós, M. D. Marcos*, J. Mat. Chem.*, **2012**, 22, 25362.

25 N. Kabaya, S. Sarp, M. Yuksel, M. Kitis, H. Koseoglu, Ö. Arar, M. Bryjak, R. Semiat, *Desalination*, **2008**, 223, 49.

26 N. Kabaya, I. Yilmaz-Ipek, I. Soroko, M. Makowski, O. Kirmizisakal, S. Yag, M. Bryjak, M. Yuksel., *Desalination*, **2009**, 241, 167.

27 E. Güler, N. Kabay, M. Yüksel, N.Ö. Yigit, M. Kitis, M. Bryjak, *Journal of Membrane Science*, **2011**, 375, 249.

28 P. Colombo, *Adv. Eng. Mater*., **1999**, 1, 203.

29 M.V. Twigg, J.T. Richardson, *Chemical Engineering Research and Design*, **2002**, 80, 183.

30 A. Zamperi, P. Colombo, G.T.P. Mabande, T. Selvam, W. Schwieger, F. Scheffler, Zeolite, *Adv. Mater*., **2004**, 16, 819.

31 K. Schwartzwalder, H. Somers, A. V. Somers, U.S. Patent 3090094, **1963**.

32 L. Huerta, J. El Haskouri, D. Vie, M. Comes, J. Latorre, C. Guillem, M. D. Marcos, R. Martínez-Mañez, A. Beltrán, D. Beltrán, P. Amorós, *Chem. Mater*., **2007**, 19, 1082.

33 J. El Haskouri, D. Ortiz de Zárate, C. Guillem, J. Latorre, M. Caldés, A.Beltrán, D. Beltrán, A. B. Descalzo, G. Rodríguez, R. Martínez-Máñez, M. D. Marcos, P. Amorós, *Chem. Commun.,* **2002**, 330.

34 K. Schwartzwalder, A. V. Somers, U.S. Patent 30900941963.

35 S. Cabrera, J. El Haskouri, C. Guillem, J. Latorre, A. Betrán, D. Beltrán, M.D. Marcos, P. Amorós, *Solid State Sci.*, **2000**, 2, 405.

36 B. Burczyc, K. A. Wilk, A. Sokolowski, L. Syper, *J. of Colloid and Interface Science*, **2001**, 240, 552.

37 D.L. Harp, *Analytica Chimica Acta*, **1997**, 346, 373.

38 R. N. Sah and P. H. Brown, *Microchemical Journal*, **1997**, 56, 285.

39 L. Huerta, C. Guillem, J. Latorre, A. Beltrán, D. Beltrán, P. Amorós, *Chem. Commun*., **2003**, 1448.

40 J. V. Ros-Lis, R. Casasús, M. Comes, C. Coll, M. D. Marcos, R. Martínez-Máñez, F. Sancenón, J. Soto, P. Amorós, J. El Haskouri, N. Garró, K. Rurack, *Chem. Eur. J.*, **2008**, 14, 8267.

41 S. Brunauer, P. H. Emmet, E. Teller, *J. Am. Chem. Soc*., **1938**, 60, 309.

42 E. P. Barret, L. G. Joyner, P. P. Halenda, J. Am. Chem. Soc., **1951**, 73, 373.

4. Low-cost materials for boron adsorption from water

Low-cost materials for boron adsorption from water

Cristina Sanfeliu,[a,b,c] Ramón Martínez-Máñez,[a,b,c] Félix Sancenón,[a,b,c] Juan Soto,[a,b] Victoria Puchol,[d] Pedro Amorós,[d] M. Dolores Marcos,[a,b,c]

a Centro de Reconocimiento Molecular y Desarrollo Tecnológico (IDM), Unidad Mixta Universitat Politècnica de València, Universitat de València, Spain.
b Departamento de Química, Universitat Politècnica de València, Camino de Vera s/n E-46022 Valencia, Spain. (Tel.: (+34) 963877343)
c CIBER de Bioingeniería Biomateriales y Nanomedicina (CIBER-BBN), Spain.
d Institut de Ciència del Materials (ICMUV), Universitat de València, P.O. Box 22085, E-46071, Valencia, Spain. (Tel.: (+34) 963543617)

Received 4th May 2012, Accepted 7th Oct 2012
First published online 8th Oct 2012

Journal of Materials Chemistry, *2012*, ***22***, *25362-25372*

Abstract

Knowing the affinity of boron aqueous species to cis-diol organic groups, five different hybrid materials have been prepared by anchoring glucose groups onto the surface of silica matrices with a different surface topology: UVM-7 bimodal mesoporous silica, UVM-11 unimodal non-templated mesoporous silica, commercial silica fume and two silica xerogels with pores within the mesoporous range (13-50 nm). After optimizing the experimental conditions, a comparison was made of the boron adsorption capacities in water. The relationship of the structural and functionalization parameters is discussed and the importance of the surface topology in the final adsorption behaviour is revealed. Hence, despite the UVM-7 based material being the best boron adsorbent, the solid based on one of the xerogels is seen as a good candidate for preparing low-cost boron adsorbents.

4.1 **Introduction**

Although boron is an essential plant nutrient, the range between deficiency and toxicity is very narrow (e.g., 0.3–0.5 mgL-1 in citrus), and it has been found to be toxic for both plants and animals. For instance, it is known to be phytotoxic in small amounts and can induce serious damage such as stunted growth, chlorosis and necrosis.[1]

The World Health Organization (WHO) has offered a guideline boron concentration value of 0.3 mgL-1 in drinking water. Later, this standard was revised and became 0.5 mgL-1 because it would be difficult to achieve with the treatment technology available in areas with high natural boron levels.[2] Recently, the European Union (EU) classified boron as a pollutant for drinking water and adopted a standard of 1 mgL-1 in drinking water.[3]

Boron is widely distributed in nature. In aqueous environments, it is present mainly as boric acid in equilibrium with borate anion. Boric acid, $B(OH)_3$, in an aqueous solution presents a planar trigonal structure versus the tetrahedral structure of borate ion $B(OH)_4^-$. Aqueous boron species very easily produce esters with polyols

containing OH groups in the cis position (stereospecific reaction). These esters may be considered anionic chelates complexes with boron taking a tetrahedral configuration.[4-8]

Boron pollution is mainly due to anthropogenic sources as it is present in many household (cosmetics, insecticides, medicines etc.) and industrial products (coalfired steam power plants, chemical plants, rockets, fertilizers, etc.) and by-products. In particular, wastewaters from certain ceramic factories contain a high level of boron and, in regions where such industries concentrate, ground and subsoil pollution by boron is considered to be of maximum environmental concern. In line with this, one important aspect of pollutant management is the development of new useful environmental boron remediation agents for their application in a wide range of situations.

Boron removal technologies have been reviewed.[9] The main boron removal processes include adsorption,[10,11] coagulation,[12,13] reverse osmosis,[14-17] , use of membranes,[18-20] electrodialysis,[21] etc. Basically, the only method utilized to separate boron from liquid media has been the use of ion exchange resins.[22,23]

In a previous work, we presented an alternative system designed by using a new generation of adsorption materials based on mesoporous silica.[24] The design approach we followed in the synthesis of boron adsorbents was inspired by mesoporous solids' attractive properties (very large specific surface, functionalization capacity, etc.) for their use as matrices in anion remediation protocols.[25,26] In fact, after the pioneering work devoted to the Hg(II) adsorption[27,28] a great amount of research has been developed on the use of ordered mesoporous materials as adsorbent.[29-31] Additionally, given boron's ability to react with non-acidic polyalcohols, it was envisaged that the grafting of mesoporous scaffolds with saccharides could yield highly efficient boron removal systems.

In terms of industrial applications however, the high cost of final materials is a significant drawback. Mesostructured silica materials (MSM)[32] have been synthesized using surfactants as structure directing agents, while expensive silica

sources (TEOS, TMOS, etc.) have been the most frequently used reactants. At this point, there has been growing interest in recent years in implementing alternative "low-cost" active materials. The economic drawback could be partially solved by cutting the cost of the inorganic matrix and, eventually, by eliminating the organic template molecules in preparative strategies.

In this context, synthetic procedures excluding the use of surfactants or other template reagents can lead to porous silica-based xerogels where, evidently, the achieved porosity must rely only on the silica hydrolysis and condensation conditions used. In this way, the xerogels obtained from sodium silicate represent an inexpensive family of silica matrices which could be used as active sites scaffolding supports.

In this paper, the preparation and characterization of different types of adsorbents (**S1**, **S2**, **S3**, **S4** and **S5**) from diverse inorganic matrices are described. **S1** and **S2** are based on mesoporous materials (UVM-7 and UVM-11)[33-35] obtained from an alcoxide source, **S3** is based on a commercial nanoparticulated silica (silica fume, SF) and finally **S4** and **S5** are based on two silica xerogels (X4 and X5).[36]

Hence following our previous studies, we report herein a comparison of the capacity of boron adsorption from aqueous solutions of these different systems based on the affinity of borate for cis-diol groups. Our goal was to incorporate active sites into "low-cost" materials. In this sense, we will show how the boron adsorbents deriving from silica xerogels (**S4** and **S5**) display comparable performances to those obtained from expensive organosilica precursors (**S1** and **S2**).

4.2 **Experimental**

4.2.1 Reagents

For the synthesis of inorganic matrices, tetraethyl orthosilicate (TEOS), sodium silicate, n-cetyltrimethylammonium bromide (CTAB), triethanolamine ($TEAH_3$) and silica fumed (SF) were provided by Aldrich. Sodium hydroxide was purchased from Scharlab. For the functionalization of the materials, (3-aminopropyl)-triethoxysilane (APTES) and gluconolactone were purchased from Aldrich. The 1000 ppm boron standard solution was obtained from Scharlab, Determination of boron concentration was carried out with azomethine-H, purchased from VWR.

4.2.2 Synthesis of porous materials

The general procedure for synthesizing UVM-7 silicas, a modification of the so-called atrane route,[37] has been described in detail elsewhere.[32] A mixture of TEOS (10.7 mL; 0.05 mol) and $TEAH_3$ (22.3 mL, 0.17 mol) was heated at 150ºC for 10 min to prepare the silatrane complexes in $TEAH_3$ medium. Then, it was cooled down to 90ºC and 4.56 g of CTAB (0.0125 mol) were added. Later, 80 mL of water were slowly added with vigorous stirring at a mixing temperature of 80ºC. After some minutes, a white suspension resulted. This mixture was allowed to age at room temperature for 16 h. The resulting mesostructured powder was filtered, washed with water and ethanol, and air-dried. Preparation of the final porous material requires the removal of the surfactant from the as-synthesized powder, a process that was carried out by chemical extraction. A suspension of 10 g of the mesostructured silica was refluxed under stirring in a mixture of absolute ethanol (1 L) and concentrated (35%wt) hydrochloric acid (75 mL). After 2 h, the suspension was left at room temperature and filtered. The process was repeated with a refluxing time of 16 h.

For the UVM-11 material, the “atrane route” was also used but, in this case, the template surfactant molecules were avoided. Details of a typical synthesis leading to a UVM-11 nanoparticulated xerogel are described as follows: 33.08 mL (0.15 mol) of TEOS was added to liquid $TEAH_3$ (39.33 mL, 0.3 mol) and heated at 150ºC

for 5 min to form silatrane complexes. The resulting solution was cooled down to 80ºC. Then, 80 mL (4.5 mol) of water were added while stirring. After some hours, a transparent gel resulted. Finally, the occluded hydroalcoholic solvent was extracted from the gel by refluxing in ethanol (ca. 1 g of powder in 120 mL of ethanol; 24 h at 60ºC).

The synthesis of silica xerogels was carried out in a two-step process to allow the separation of the hydrolysis and condensation mechanisms. In a typical synthesis, the silica source was added under stirring to an aqueous solution containing HCl. The synthesis with sodium silicate as the silica precursor was carried out at different H_2O/Si and HCl/Si molar ratios. For xerogel X4, the molar composition of the synthesis mixture was Si:HCl:H_2O 1:4:162, and 1:6:194 for xerogel X5. In the first stage, the solution was stirred for 20 h at room temperature. In the second stage, the mixture was heated at 100°C until gelation of the mixture resulted. The resulting gels were filtered, washed several times with water and then with acetone, to be finally dried at room temperature.

4.2.3 Functionalization of silica scaffoldings

Sorbent materials were synthesized in two steps: in the first step, the support materials (UVM-7, UVM-11, SF, X4 and X5) were functionalized with (3-aminopropyl)triethoxysilane (APTES) in order to cover the material's surface with amine groups. In the second step, the grafted materials were reacted with gluconolactone to create active sites on the surface (Figure 1).38 Thus, 1 g of each material was suspended in 40 mL of acetonitrile and heated at 120ºC in a dean-stark apparatus to remove the adsorbed water by azeotropic distillation in an inert atmosphere (Ar gas). Then, 10.7 mmol of APTES were added at room temperature. After 16 h, the formed solids were filtered and washed with acetonitrile and water, and the different amine-functionalized silica matrices were separated. Finally, the amine-functionalized materials were reacted with 10 mmol of gluconolactone in 50 ml of methanol. The mixture was stirred for 48 h at room temperature. Afterwards, precipitates were filtered and washed with water. Solids **S1** to **S5** were obtained.

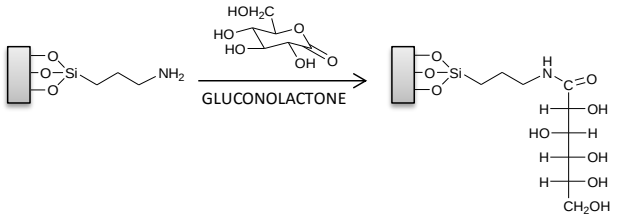

Figure 1. Schematic representation of the porous materials surface functionalization.

4.2.4 Boron adsorption assays

Boron adsorption studies of the materials were carried out by suspending 25 mg of each solid in 10 mL of boron solution at a certain concentration. Suspensions were stirred for 16 h. Then the mixture was filtered and the boron concentration in the solution was analyzed.

4.2.5 Boron determination

The boron concentration in the water solutions was determined using a Perkin Elmer Spectrophotometer and the azomethine-H as a colorimetric reagent according to the method described in the references. [39-41]

4.2.6 Kinetic studies on functionalized materials

Batch experiments were carried out for the kinetic assays on the solids. These experiments involved a suspension of 25 mg of each solid in 10 ml of a 5 ppm boron solution for each time. Suspensions were stirred and filtered at different times for 4 h.

4.2.7 Characterization Techniques

The X-ray powder diffraction (XRD) data were recorded with a Bruker D8 Advance diffractometer using Cu Kα radiation. XRD patterns were collected in steps of 0.02°2θ over the angular range of 0.65-10°2θ and an acquisition time of 25 s/step. The high- and low-magnification SEM images were recorded with a Jeol JSM 6300

microscope. Samples were previously coated with Au-Pd. A TEM study was carried out with a Philips CM10 instrument operating at 100 KV and equipped with a CCD camera. Samples were gently ground in dodecane, and microparticles were deposited on a holey carbon film supported on a Cu grid. Nitrogen adsorption-desorption isotherms (-196°C) were recorded with a Micromeritics ASAP-2010 automated instrument. Samples were degassed at 120°C and 10-6 Torr for 5 h prior to measurements. Surface areas were estimated according to the BET model, and pore size dimensions and pore volumes were calculated by using the BJH method from the adsorption branch of the isotherms. Thermogravimetric analyses were carried out on a TGA/SDTA 851e Mettler Toledo balance, with a heating program consisting of a heating ramp of 10°C per minute from 393 K to 1273 K and an isothermal heating step at this temperature over 30 min. The elemental analysis was performed in a CE Instrument EA-1110 CHN Elemental Analyser. Spectrophotometric measurements were taken with a Lambda 35 UV/Vis Spectrometer from Perkin-Elmer Instruments. ^{13}C MAS NMR spectrum was recorder on a Varian Unity 300 spectrometer operating at 128.3 MHz and using a magic angle spinning speed of 4.0 kHz.

4.3 **Results and discussion**

4.3.1 Materials Characterization

All the synthesized inorganic matrices and the final modified solids were characterized by standard procedures. The typical TEM and SEM images of representative materials are shown in Figure 2.

Then, the inorganic matrix of the **S1** adsorbent, the UVM-7 solid, can be described as bimodal porous silica constructed by the aggregation of pseudo-spherical mesoporous primary nanoparticles whose average diameter is ca. 15-20 nm (see Figure 2.a). The origin of the small intra-particle mesopore system lies in the template effect of surfactant aggregates. This pore system is defined by regular mesopores organized into a disordered hexagonal array. On the other hand, the

large inter-particle pores are generated as the nucleation and growth of the primary mesoporous nanoparticles proceeds.

As observed in Figure 2.b, the UVM-11 material can be described as a unimodal porous matrix constructed by the aggregation of pseudo-spherical primary nanoparticles whose average diameter is very small (ca. 4 nm), according to the room temperature conditions used during the ageing process.

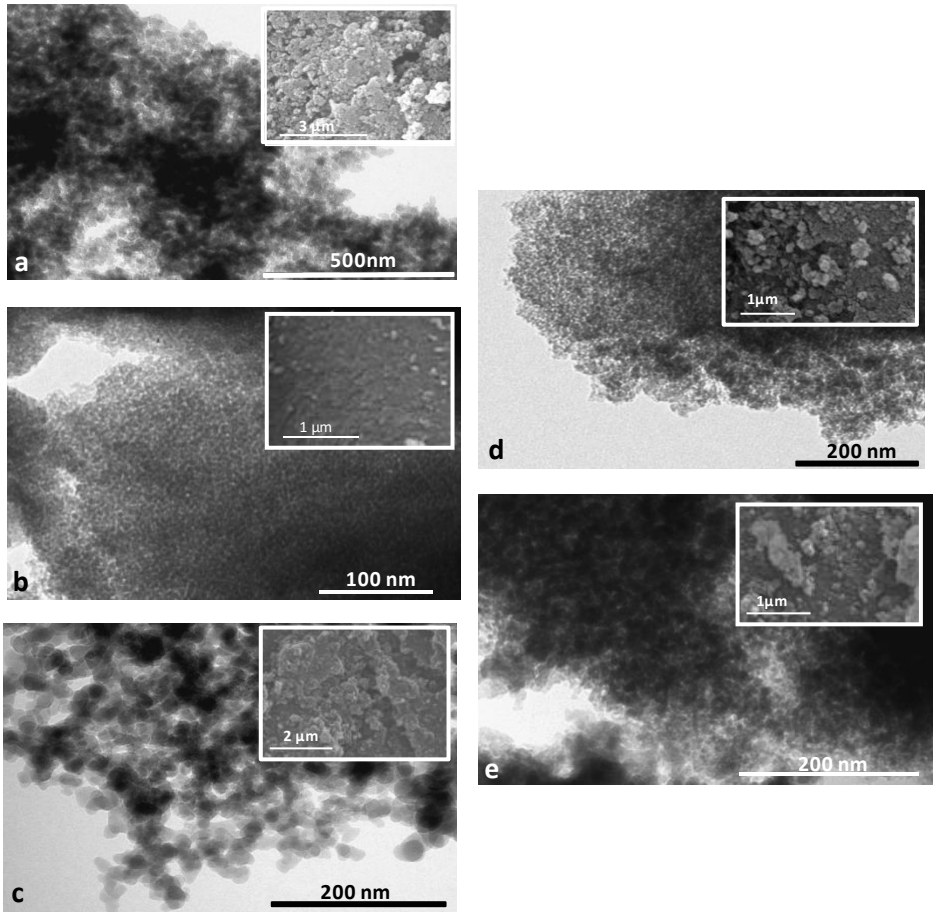

Figure 2. Typical TEM and SEM (in the inset) images of materials a) UVM-7, b) UVM-11, c) SF, d) X4 and e) X5.

On the other hand, it is known that the primary particles of SF (diameter 10-20 nm) are non-porous and form relatively stable aggregates (diameter 100-500 nm), developing larger sized agglomerates (diameter >1 μm) (Fig. 2.c).[42]

The SEM inspection of the silica xerogels (X4 and X5 in Figure 2.d and 2.e, inset) reveals the existence of a very open structure made up of interconnected clusters with macropores corresponding to the inter-cluster voids. This structure is typical of the silica xerogels prepared by a two-step process.[43] The clusters' internal structure is illustrated by the TEM images shown in Figure 2.d and 2.e. They reveal a highly disordered 3-D interconnected porous network. Clusters are the result of the aggregation of very small primary particles (<10 nm, showing an average size centred at ca. 4-5 nm for both synthesized gels) and porosity can be ascribed to the spaces between these particles.[44] Differences in porosity (see below) may be associated with the different proportion of reagents.

All these microscopy images clearly reveal the similar disordered nature of the inter-particle voids pore system generated in all cases by nanoparticles' aggregation. Hence, the silica xerogels synthesized with sodium silicate have structural properties (at the qualitative level) comparable to those obtained by using TEOS (i.e., porous architectures originating from the aggregation of silica nanoparticles). This is evidenced in Figures 3 and 4, where the nitrogen sorption isotherms and pore size distributions (PSDs) of the silica xerogels derived from sodium silicate (X4 and X5) are compared with those obtained by using TEOS (UVM-7 and UVM-11) and with the commercial silica fume. Table 1 summarizes the porous structure characteristics of all the silica matrices. The specific surface areas were calculated from a Brunauer–Emmet–Teller treatment of the isotherm (BET; specific surface area calculation),[45] and the volumes and pore sizes were calculated from the Barret–Joyner–Haselda method (BJH; volumes and pore size calculation).[46]

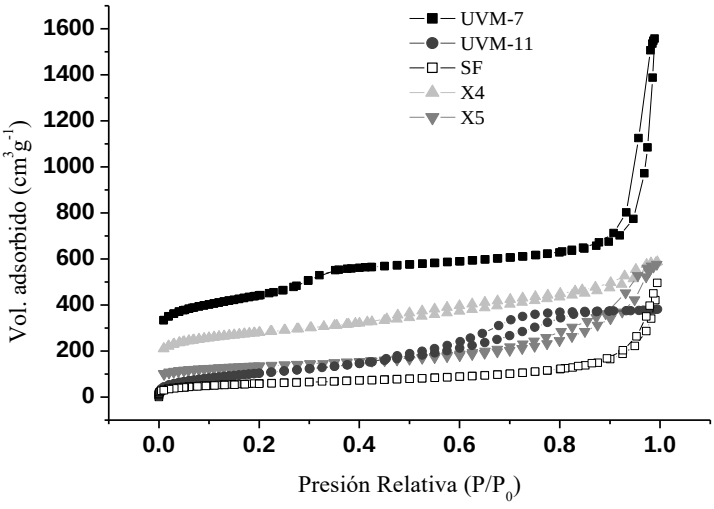

Figure 3. N_2 adsorption-desorption isotherms of the synthesized solids

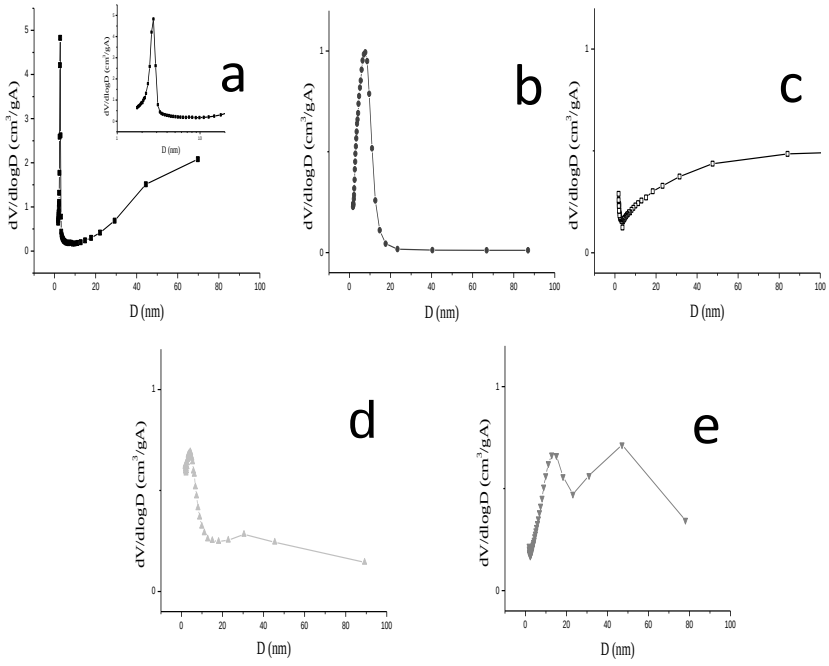

Figure 4. Pore size distribution of synthesized solids a) UVM-7, b) UVM-11, c) commercial silica fume, d) xerogel X4 and e) xerogel X5.

In the first place, the N_2 adsorption-desorption isotherms quantitatively confirm the bimodal character of the final UVM-7 material (Figure 3 and Table 1). As noted, the curve shows two well-defined adsorption steps. The first, at an intermediate relative pressure ($0.3 < P/P0 < 0.5$), is characteristic of the type IV isotherms and can be related to the capillary condensation of N_2 inside the templated mesopores. The second, at a high relative pressure ($P/P0>0.8$), corresponds to the filling of the large pores among the primary nanoparticles. The BJH pore size distribution shows how there are two well-differentiated pore systems. An intense and narrow signal, with a maximum at 2.77 nm, ascribed to the surfactant generated pores, and a very wide pore distribution expanding up to large mesopores (> 50 nm).

Material	BET (m^2/g)	Small pore [a] (nm)	$V_{Small\ Ppre}$ (cm^3/g)	V_{SP}/V_T (%)	Large pore [a] (nm)	$V_{Large\ Pore}$ (cm^3/g)
UVM-7	877.7	2.77[b]	0.72[b]	36	>50[c]	1.30[c]
UVM-11	392.5	7.70	0.58	100	-	-
SF	214.1	-	-	-	>50[c]	0.73[c]
X4	642.9	4.23	0.51	70	30.7	0.22
X5	298.9	13.2	0.47	58	47.2	0.34

[a] The pore sizes indicated in the table correspond to the maxima in the BJH pore size distribution calculated from the adsorption branch of the isotherms.
[b] Templated intraparticle pore
[c] Interparticle pore

Table 1. Pore structure data of the used silica matrices.

UVM-11, X4 and X5 silica matrices also exhibit nitrogen sorption isotherms of type IV with the H1 hysteresis loops, characteristic of mesoporous materials. However, some differences can be seen among the respective BJH pore size distributions. While the UVM-11 silica displays an asymmetric yet unimodal pore distribution with a maximum at 7.7 nm, the X4 and X5 xerogels present bimodal porosity, all within the mesoporous range. Hence, the BJH pore size distributions of the X4 and X5 solids display two well-defined peaks (at 4.23 and 30.7 nm for solid X4, and 13.2 and 47.2 nm for sample X5). By taking into account the absence of template molecules, the two pores in these xerogels must be considered inter-particle textural-like voids. In these last cases, porosity differences are due to the gel

preparative conditions affecting the hydrolysis, condensation and aggregation processes.

A comparison made of the Table 1 data indicates that, as previously mentioned, the pore structure properties (i.e., pore volume, pore size distribution, and specific surface area) of the silica xerogels synthesized for this work are comparable to those of the MSM usually employed for these applications (M41S, SBA-15, etc.). The pore volumes of both xerogels are similar, between 0.7 and 0.8 cm^3g^{-1}, and this value is of the same order as the intra-particle pore system of the UVM-7 material. In comparison, the pore volume of the UVM-11 material is the lowest. On the other hand, the specific surface area of both xerogels is different, while X4 shows a high value (642.9 m^2g^{-1}) close to that of the UVM-7 (877.7 m^2g^{-1}) material, the X5 xerogel presents a lower value (299 m^2g^{-1}) in the range of those of the UVM-11 (392.5 m^2g^{-1}) and SF (214.1 m^2g^{-1}) materials. Hence, apart from the UVM-7 material whose functionalization has already been assayed, we have four other matrices. X4 xerogel may be the most similar to that of the UVM-7 material. It has a large surface area and a bimodal pore structure with a small pore similar to that of the UVM-7 material, but a wider pore size distribution. Then, X5 xerogel is similar to X4, but has a smaller surface area, larger pore sizes and an even wider pore size distribution of the small pores; UVM-11 shows values between both xerogels, but presents a narrower pore size distribution. Finally, the SF material, with the same sized particles as the other materials, shows the widest pore size distribution due to very loosely connected particles.

4.3.2 Functionalization Process

For those solids showing only textural porosity, no XRD peaks could be expected when taking into account the absence of template species that are able to organize the silica network. However, certain organization must be expected when surfactant micelles have been used as templates, which was the case of the MCM-41 solids. Hence, Figure 5 illustrates the XRD patterns corresponding to a representative sample of the UVM-7 material a) before (mesostructured), b) after (porous) template removal and c) after the grafting protocol (solid **S1**). These XRD

patterns are characteristic of this kind of nanoparticulated mesoporous/mesostructured solids prepared through surfactant-assisted procedures and display, at least, one strong and broad diffraction peak in the low angle region. Apart from the intense peak, we can observe a broad small shoulder, which could be indexed as the (110) and (200) overlapped reflections of the typical hexagonal cell.[47] For the mesoporous solid (after the surfactant extraction process), this indexation leads to a lattice constant of a_o=50.9Å according to the hexagonal unit cell relation (a_o=2d100/√3). In the three cases, the XRD patterns indicate the relative order of the intra-nanoparticle mesopore (small pores) system and are clear proof of there being a certain pseudo-hexagonal order. Hence, we may infer that the organization of the intraparticle mesopores in solid **S1** (Figure 5c) is also preserved after the two-step functionalization process.

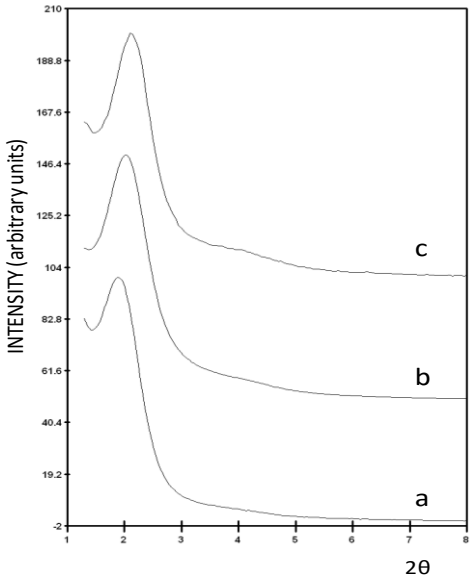

Figure 5. X-ray powder diffraction patterns of (a) as-synthesized (mesostructured) UVM-7, (b) chemically extracted UVM-7 silicas and (c) solid **S1**.

In order to confirm the functionalization reaction on the solid's surface, we carried out ^{13}C-NMR studies on the amine-functionalized UVM-7 matrix and on the **S1** adsorbent. The obtained spectra are offered in Figure 6. The ^{13}C-NMR spectrum of the amine-functionalized solid displays signals within the 11-50 ppm range assigned to the 3-aminopropyltriethoxysilane linker. On the other hand, solid **S1** shows

additional signals. Those between 62-75 ppm are assignable to the HO-C- units of the “saccharide” and that at ca. 170 ppm corresponds to the carbonyl of the amide group.

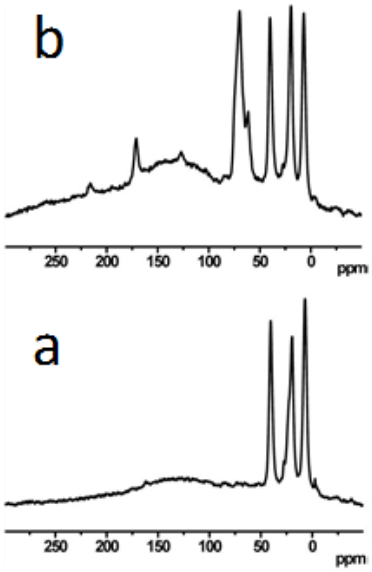

Figure 6. The 13C MAS NMR spectrum of (a) amino-functionalized UVM-7 solid and (b) **S1**.

In relation to determining the functionalization degree, the amount of the amine and glucose groups on the surface of active materials **S1** to **S5** was calculated by elemental and thermogravimetric analyses. By combining both methods, it is possible to determine the amount of binding groups attached to the surface in these materials, calculated as millimoles per gram of SiO_2 (mmolg^{-1} SiO_2) by means of Equation (1).

$$\alpha_A = \frac{\Delta W_i\% \times 1000}{\Delta W_{SiO_2}\% \times nM_i} \qquad (\text{mmolg}^{-1}\ SiO_2) \qquad (1)$$

where ΔWi% (i = C, N) represents the weight percentage of carbon or nitrogen, Mi is the corresponding atomic weight and n is the number of atoms of each element in one molecule. $\Delta WSiO_2\%$ is the inorganic SiO_2 content in weight percentage. The values of organic content as millimoles of amine and glucose per gram of SiO_2 for the solids **S1** to **S5** are shown in Table 2.

Adsorbent	α_{amine}[a]	$\alpha_{glucose}$[a]	α_g/α_a[c] (%)	β_{amine}[b]	$\beta_{glucose}$[b]
S1	2.45	1.29	53	1.68	0.88
S2	1.48	0.85	57	2.27	1.30
S3	0.77	0.5	65	2.32	1.51
S4	1.88	0.74	39	1.76	0.69
S5	0.88	0.52	59	1.77	1.05

[a] Units: mmol of function per gram of residue (SiO_2)

[b] Units: molecules$*$nm^{-2}

[c] Yield of the second functionalization reaction.

Table 2. Functionalization degree of the adsorvent materials.

From these data, it can be observed that the α_{amine} values correlate with the total BET area of the corresponding silica matrices (Table 1). This is due to the fact that 3-(aminopropyl)-triethoxysilane is a functional group of a relatively small size and with good accessibility to the whole surface; hence, no pore blocking or other related and undesired phenomena are produced. Thus, it seems that the topology of the porous surface has no influence on this first functionalization process. However, the $\alpha_{glucose}$ values display a more erratic behaviour, probably due to the fact that anchoring a bulkier fragment will produce more important blocking and steric effects. In fact, the reaction between the anchored amino-groups and the gluconolactone fragment has quite a different yield, ranging from 65% for solid **S3** to 39% for **S4**, which are the solids with the lowest and one of the highest specific surface, respectively. In order to gain a better insight of how the porous topology influences the functionalization process, we also calculated the average coverage, βA, as the number of molecules per nm^2 using Equation (2) in which α_A is the anchored group content (mmolg^{-1} SiO_2), S is the specific surface (m^2g^{-1}) of the corresponding silica matrices (Table 1) and N_A is the Avogadro's number. The results are also presented in Table 2.

$$\beta_A = \alpha_A \times 10^{-3} \times S^{-1} \times 10^{-18} \times N_A = \alpha_A \times S^{-1} \times 602{,}3 \qquad (2)$$

If the only factor affecting the functionalization degree in these solids was the specific surface area, a similar coverage value in each case from **S1** to **S5** should be found. However, very different values have been obtained for each adsorbent.

Thus, the solid with the highest amine value is that with the smallest specific surface (**S3**), while that with the smallest amine is the one with the greatest surface (**S1**). This can be explained by the fact that the matrix in solid **S3** presents a very wide pore size distribution and for which the whole surface is fully accessible. However, solid **S1** is a bimodal mesoporous material with an important percentage of its pore volume related with a very narrow intra-particle pore system (2.77 nm). Then, solid **S2** shows an amine coverage value very close to that of **S3**. In this case, the corresponding matrix is a mesoporous solid similar to that of **S1**, but with a unimodal pore distribution of around 7.7 nm. This pore size should be large enough to allow a first functionalization, which is almost as high as that for the silica matrix in **S3**. Next, solids **S4** and **S5** show similar intermediate amine values corresponding to medium pore sized mesoporous matrices.

We might even acquire a better understanding of the functionalization process by taking a closer look at both the yield of the functionalization reaction and the glucose values. Hence, the highest yield is shown by the **S3** material, indicating that it presents the highest accessibility for the amine groups and that only the steric impediments among the bulkier organic groups may be expected. In this sense, even when the total amount of anchored aminoglucose groups is not very large, the glucose value is very high, probably the highest possible value after considering the hindrance effects among the anchored glucose groups. Solid **S1** presents an intermediate yield because, even when the small pore system is the smallest of the whole family of silica matrices, this pore system only represents about 36% of the total pore volume; hence, a large amount of amine might be anchored onto the surface of the textural pores, thus allowing for a high accessibility of the amine groups. Then, solids **S2** and **S5** present a similar yield and glucose values as both adsorbents have been built on a porous matrix with large enough pore sizes to avoid pore blocking effects. Finally, the last one, **S4**, shows the smallest yield, even when the amount of amine groups is the second highest, which may be because 70% of the total pore volume is related with pores that are large enough in size to allow for a good first functionalization, but not to avoid pore blocking during the second anchoring reaction. In this way, even when amine coverage has an intermediate value for **S4**, glucose coverage is the smallest.

However this high functionalization degree of the active adsorbent materials, the morphology and architecture of the original porous silica supports are maintained after the two functionalization steps. The TEM images for organic modified materials **S1** to **S5** show (not included) that the materials' structure is preserved in all cases. Nevertheless, a significant decrease in pore size and volume values is noted if compared to those of the non-functionalized matrices, as expected. The values obtained from the N_2 adsorption isotherms of the functionalized materials are shown in Table 3.

Material	BET (m^2/g)	Small pore [a] (nm)	V_{SP} (cm^3/g)	Large pore [a] (nm)	V_{LP} (cm^3/g)
S1	183.9	-	-	32.3[c]	0.94[c]
S2	275.9	6.61	0.45	-	-
S3	145.6	-	-	50.0[c]	1.08[c]
S4	206.2	3.44	0.21	28.5	0.17
S5	128.5	11.6	0.25	44.2	0.29

[a] The pore sizes indicated in the table correspond to the maxima in the BJH pore size distribution calculated from the adsorption branch of isotherms.
[b] Templated intraparticle pore
[c] Interparticle pore

Table 3. Pore structure data of the silica matrices used.

These data reveal that the BET area diminishes with values up to 200 m^2/g for all the hybrid samples. The functionalization effect on materials' porosity is more marked for samples with smaller pore sizes (samples **S1** and **S4** with small original mesopores of 2.77 nm and 4.23 nm, respectively). In these cases, glucose anchoring leads to a significant blocking of small mesopores from the N_2 adsorption-desorption isotherms viewpoint. Besides, the porosity ascribed to medium- and large-sized pores is preserved in all cases, although an appreciable pore size volume and size decrease can be estimated by applying the BJH model.

4.3.3 Adsorbent Behaviour

Boron can be adsorbed on functionalized materials, considering that boric acid can form a complex with poly-ol groups. As Figure 7 depicts, boron is expected to form both bidentate and bis-bidentate complexes with the glucose groups attached to adsorbents. Hence, it is likely that those adsorbents with a greater functionalization degree will show a greater degree of boron adsorption. However, we will see that not only the amount of functionalization is important, but also the topology of the former silica matrix, which influences the accessibility of boron species to active sites.

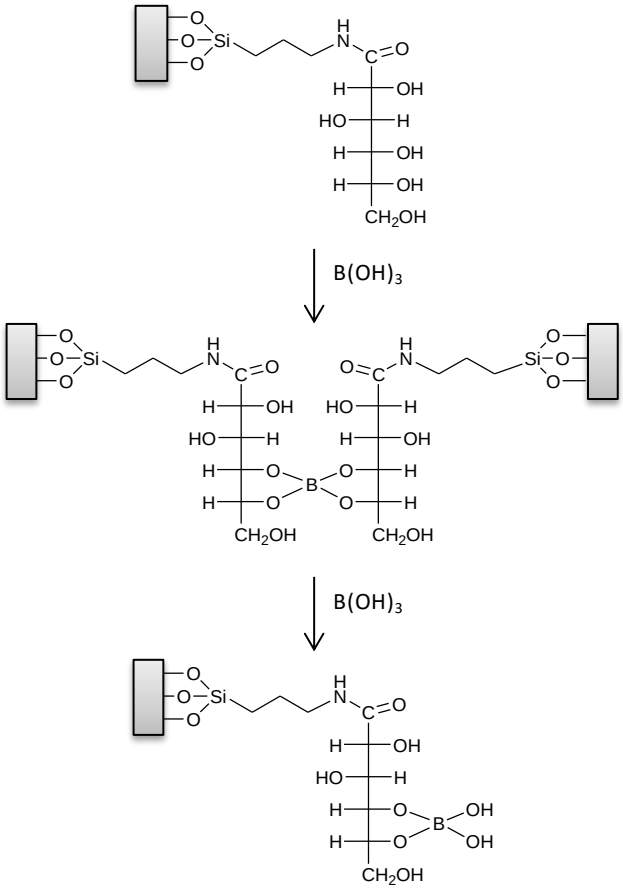

Figure 7. Proposed mechanism for the boron sorption by gluconamide-functionalized sorbents.

In any case, and although the binding mechanism of gluconamide with boric acid has not yet been clarified, it was envisaged that grafting the mesoporous scaffolds with saccharides would yield highly efficient boron removal systems. Then, even when those materials that from N_2 adsorption are apparently blocked with glucose, a significant boron capture can be expected as its adsorption follows a different sorption operative process. Hence, no important diffusion problems are expected for boric acid derivatives through a high hydrophilic environment provided by glucose moieties, the remaining silanol groups and trapped water molecules. All the materials modified with the N-(3-triethoxysilylpropyl)gluconamide groups were tested for their boron sorption efficiency. The expected inability of non-modified silica for B adsorption under the working conditions used has been experimentally confirmed. In order to compare the sorption properties of all the prepared organically modified solids, we firstly optimized the experimental parameters.

4.3.4 Effect of pH on sorption

The first experimental parameter to be optimized was the solution's pH. Then, the effect of pH on boron adsorption was investigated with a view to ascertaining the conditions for maximum boron removal. Variation of the adsorbed boron as a function of the pH value for the **S1** solid is shown in Figure 8. As this figure illustrates, the boron adsorption curve shows a maximum at around a neutral pH and a sharp drop towards high pH values.

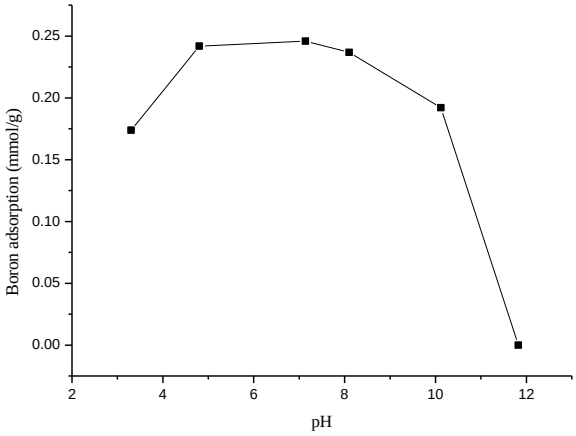

Figure 8. Boron sorption by **S1** as a function of pH.

Such behaviour can be explained by considering that boric acid, $B(OH)_3$, is a very weak, exclusively monobasic acid (pKa= 9.23) that does not act as a proton donor, but as a Lewis acid, by accepting hydroxyl groups in water to form the $B(OH)_4^-$ species.

By taking into account boric acid's Lewis character, it is likely that the acid's coordination with cis-diols will proceed by means of a nucleophilic attack of the alcohol group onto the $B(OH)_3$ species. As the electrophilic character of boron in the $B(OH)_4^-$ anion is already fulfilled, boron adsorption is expected to be optimum at the pH interval at which $B(OH)_3$ is the predominant species. At a high pH, boron mainly exists as $B(OH)_4^-$ and only a very low coordination of boron to the anchored glucose groups will occur.

Additionally, pH values above 10 will lead to the destruction of the inorganic scaffold. Finally, since protons are also a product in the boron chelation reaction with the anchored cis-diol groups, adsorption lowers at a low pH. Hence in the following experiments, the pH of the solution after adsorbent addition was maintained at ca. 6.5. Similar results were reported for boron adsorption on new boron-selective hybrid gel48 and gluconamine-modified MCM-41.[49]

As shown below, decreased sorption at low pH values was considered an indication of acidic water solutions' desorption capacity.

4.3.5 Effect of the adsorbent amount

Figure 9 depicts the boron removal percentage as a function of the adsorbent amount. For this study, each experimental point was obtained by assaying a fixed volume of boron solution (5 ppm in boron, 10 mL) with increasing sorbent amounts. As expected, the total amount of adsorbed boron increased when the sorbent amount increased. However, the variation of adsorbed boron was not linear with the material dosage and a decrease in the curves slope was observed in all cases. Hence, as the adsorptive capacity of the materials was not fully utilized at higher

adsorbent dosages, a low dose of adsorbents (0.025 g of material per 10 mL of 5 ppm boron solution) was chosen in the following studies.

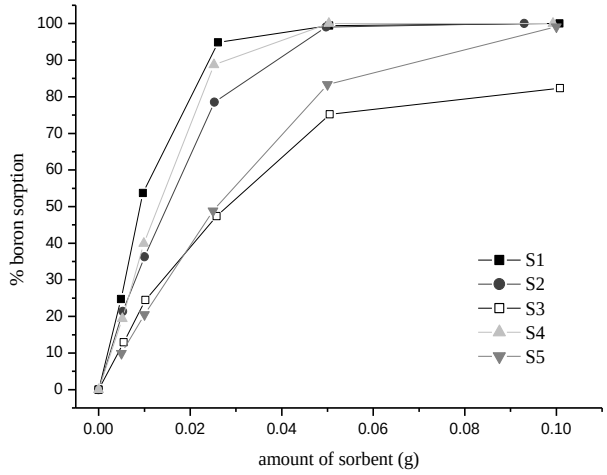

Figure 9. Sorption capacity of the gluconolactone-modified sorbents (as a percentage of the initial amount of boron in solution) as a function of the sorbent amount (initial boron concentration: 5.0 ppm; 10.0 mL).

4.3.6 Effect of contact time

The variation of boron adsorption as a function of time is shown in Figure 10. Boron sorption is a very quick process. All the adsorbents reach ca. 90% of total efficiency in the first 5 minutes. Then the adsorption equilibrium curve levels off after 15 minutes. The short time needed to achieve the equilibrium suggests that all the prepared functionalized mesoporous silicas have a high adsorption efficiency and good potential for removing boron from the aqueous phase. Moreover, the high adsorption rate observed supports the absence of diffusion barriers, even for small mesopores filled with glucose.

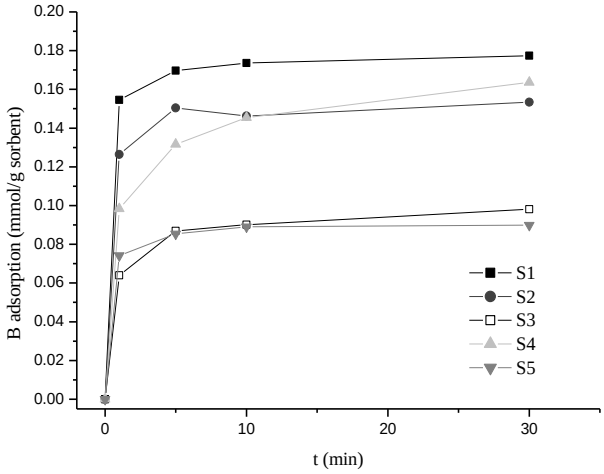

Figure 10. Boron removal as a function of time for functionalized solids S1 to S5.

4.3.7 Boron adsorption isotherms

The experiments to study boron sorption as a function of the initial boron concentration were performed in the batch mode, the amount of solid added to the boron solution in each measurement was kept constant at 0.025 g and the solution concentration varied within the 2.5–100.0 mgL^{-1} range. Boron uptakes are shown in Figure 11, where the boron adsorbed value per unit mass of the sorbent as a function of the boron initial amount in the solution is presented. No detectable boron adsorption was found for either the non-functionalized starting materials or the amine-functionalized matrices.

As seen in Figure 11, all the studied solids exhibit a similar behaviour, the amount of adsorbed boron increases with the boron concentration in the solutions, and saturation is reached in all cases. However, differences in the saturation value and also in the facility to reach that value can be inferred from the curves. Hence by focusing on the boron adsorption capacity (Table 4), our adsorbents may be classified into two different groups: those with greater adsorption ability, **S1**, **S2** and **S4** (0.38, 0.34 and 0.32 mmol of boron per gram of solid, respectively), and those with a lower capacity, **S3** and **S5** (0.22 and 0.18 mmolg-1, respectively).

Although very different materials are grouped together in this classification, as expected, this behaviour correlates very well with the degree of glucose functionalization (see glucose in Table 2)

Table 4 also shows the efficiency in the boron uptake calculated as the moles of adsorbed boron per mol of anchored glucose. As noted, all the materials present a maximum boron uptake of around 0.5. By assuming a good mobility for the small $B(OH)_3$ molecules towards the active sites, this value suggests that the preferred complexation process between boron and the glucose groups could be the formation of 1:2 boron to glucose complexes. This is the case of the solids with the highest glucose coverage, **S2** and **S3** (see the glucose values in Table 2). However, for solid **S4** with the lowest glucose surface density, the higher boron uptake efficiency value might suggest the presence of both the bis-bidentate and the bidendate complexes. Lower values from 0.5 in the **S1** and **S5** materials may require a more complex explanation; still we should take into account the very high degree of functionalization for **S1**, which would make it difficult to cover all the active sites.

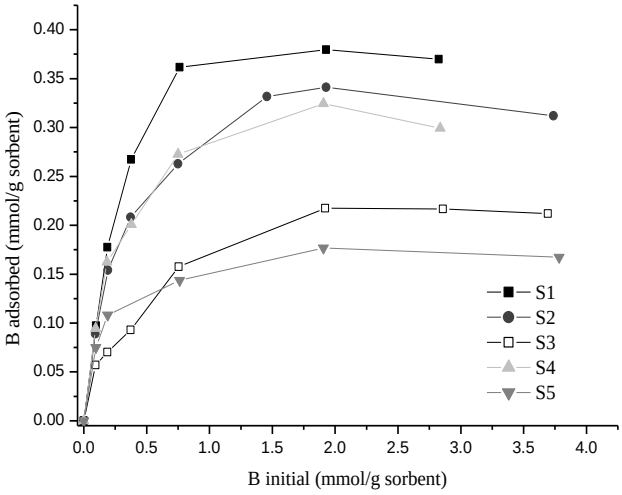

Figure 11. Boron adsorbed at 25ºC as a function of the initial boron concentration for functionalized solids **S1** to **S5**.

However, in order to achieve a more comprehensive analysis of the influence of the adsorbents' topology on boron adsorption, the Langmuir isotherm has been chosen as the most appropriate correlation. The Langmuir isotherm model is valid for monolayer sorption onto a surface with a finite number of identical sites and uniform adsorption energies:

$$\theta = \frac{q}{q_m} = \frac{KC_e}{1 + KC_e}$$

where q_m (mmol·g^{-1}) is the maximum sorption capacity corresponding to complete monolayer coverage, C_e (mol·dm^{-3}) is the equilibrium concentration, and K is the adsorption constant relating to the affinity between the adsorbate and the solid surface. The Langmuir model was selected for its simplicity and its previously demonstrated utility in describing adsorption processes for mesoporous materials. In order to apply this model to our adsorbents, the maximum boron adsorption capacity value from Figure 11 (q_m in Table 4) has been taken as the total number of active sites, the adsorbed boron in each measurement as the number of occupied sites and the concentration of the solution after the adsorption process as the equilibrium concentration of boron in the solution. From these values, the variation of the occupied centres fraction as a function of the boron concentration in solution at the equilibrium has been represented in Figure 12. The adjustment of these curves using the Langmuir isotherm provides an acceptable description of the experimental data, as seen from the correlation coefficients (R^2) and allows us to obtain the boron adsorption constants for materials **S1** to **S5** (Table 4).

Adsorbent	Uptake [a]	q_m [b] (mmol·g^{-1})	Log *K*	R^2
S1	0.44	0.38	4.37	0.9381
S2	0.52	0.34	3.71	0.9480
S3	0.48	0.22	3.22	0.9579
S4	0.59	0.32	3.87	0.9052
S5	0.41	0.18	3.96	0.9691

a Max. boron uptake/ binding site.

b Max. sorption capacity.

Table 4. Adsorption properties of solids **S1** to **S5**.

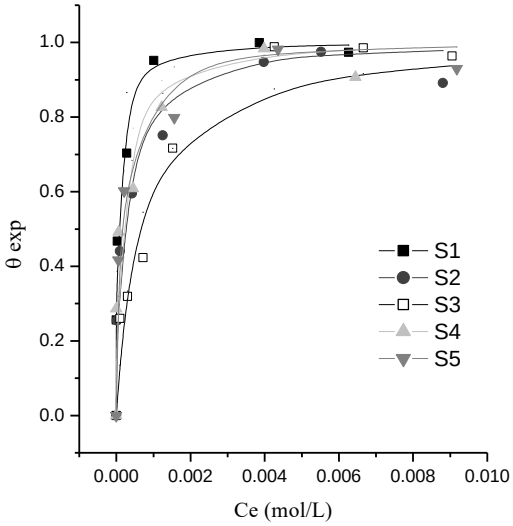

Figure 12. Boron Adsorption Isotherms for solids **S1** - **S5**. The inset shows the absorbents' initial performance

By focusing on these obtained constants, we distinguish three different adsorption behaviours among our solids. Firstly, solid **S1** shows the steepest curve in Figure 13, which corresponds to the highest adsorption constant value (logK = 4.37, see Table 4). Then, solids **S5**, **S4** and **S2** (logK values 3.96, 3.87 and 3.71, respectively) present a similar tendency; finally, solid **S3** (logK = 3.22) exhibits the most moderate variation. This behaviour does not correlate with either the amount of functionalization or the density of active sites, and only some correlation between this classification and the total pore volume of the used silica matrices (see Table 1) can be established. However, a very important conclusion can be drawn at this point: this classification groups our adsorbents according to their porous topology. Hence, the adsorbent with the highest constant is the adsorbent built on the UVM-7 material bimodal mesoporous solid; then the group with medium constant values gathers the adsorbents with the non-templated mesoporous materials; finally, and as a separate category, **S3** is the adsorbent with the matrix showing the widest pore size distribution.

By bearing in mind that K (the adsorption constant) accounts for the boron-solid interaction and that the study of the adsorption properties of solids **S1** to **S5** has been carried out under similar conditions, it is clear that solid **S1** binds boron more

strongly than any other solid, and that solid **S3** does so with the lowest strength, while solids **S2**, **S4** and **S5** are found in an intermediate situation. In order to explain the different responses of these solids to boron adsorption, it has to be taken into account that the main difference between them is due to the different matrices used to build the final adsorbents and that these differences rely on the surface properties arising from the matrices' mesoporosity. Though after functionalization, those porous systems with small pore sizes could be well-blocked, these solids must still retain the main features of the former matrices though conveniently modulated by the bonded ligand molecules. Hence the main characteristic of solid **S1** is the periodicity and homogeneity of the intra-particle pore system's shape and size. Once this matrix has been functionalized, the resulting nano-cavities must fit the coordination necessities of boron because, inside the mesopores, there must be greater probabilities of finding glucose molecules that are close enough to easily produce the high stable bis-bidentate complexes. However, solid **S3**, which could be considered to present a "flat" surface, should present more difficulties to fulfil the boron quelation. Between these two different materials, the **S2**, **S4** and **S5** solids also present glucose lined nano-cavities, as in the **S1** solid: on this occasion, however, the lack of size and shape homogeneity must diminish the complementarity between the adsorbate and the available active sites.

4.3.8 Adsorbents regeneration

As we have seen above in the study of the effect of pH on the boron sorption for our materials, the decrease in sorption at low pH values has been considered as an indication that adsorbents could be easily regenerated by simple acidic washing (Figure 13). Hence, complementary studies into boron desorption from adsorbents and their regeneration is also described and compared.

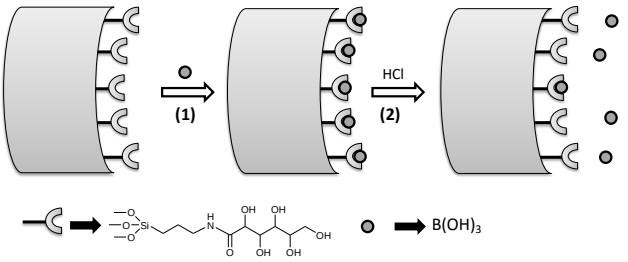

Figure 13. Protocol for boron removal in water (1) and subsequent regeneration of the sorbents (2).

The boron-loaded materials were dried and 0.1 g of each material was treated with 100 mL of a 0.01 M HCl solution for 24 h at room temperature to be then filtered. In order to test the regenerated solids' boron uptake activities, they were treated with a new 50 ppm boron solution to reproduce the saturation conditions, then the adsorbed boron was measured. The results of the recovery percentage, calculated as the boron adsorption capacity in the regenerated materials referring to each adsorbent's initial capacity, are offered in Figure 14. In this Figure we can observe a recovery percentage larger than 95% for the **S1** adsorbent. Solids **S2** and **S4** also show a quite high boron adsorption capacity, which is well above 80% of the original adsorption, and **S5** presents a recovery of almost 64%. Finally, the solid with the lowest recovery capacity, 42%, is solid **S3**. We tentatively attribute this low adsorption recovery to the degradation of the grafted molecules in these adsorbents due to the more open structure of the **S3** material, which does not protect the active sites against the environment.

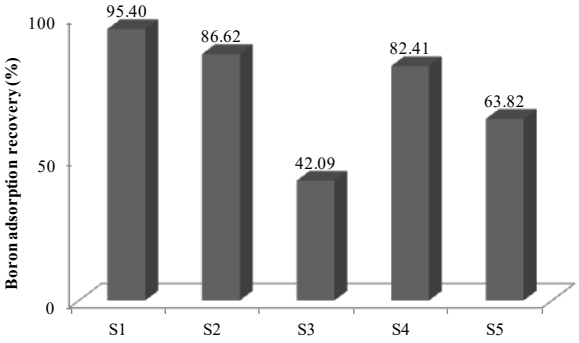

Figure 14. Boron adsorption capacity in the regenerated **S1** to **S5** solids expressed as the percentage of boron adsorption referring to each material's initial capacity.

From boron adsorption studies, it is clear that **S1** is best suited for adsorption applications. For this material, a maximum boron adsorption of 0.38 mmol per gram of material was observed. However from an economical viewpoint, it makes sense to use a cheap silica source rather than expensive organosilica compounds to prepare adsorbents (i.e., TEOS). Thus, adsorbent **S4** is suitable for industrial applications. Its structural properties are comparable to those of the solids obtained by using TEOS (UVM-7- and UVM-11-based adsorbents). It presents a maximum boron adsorption of 0.32 mmol per gram of adsorbent, which represents 84% of **S1** and 94% of **S2** maximum boron uptake. The reported reusability studies also show a large degree of recovery for solids **S1** and **S2** (95% and 86%, respectively), but **S4** remains at the same level of regeneration (82%).

In order to further corroborate the reusability of **S4** solid, consecutive cycles of adsorption and desorption have been performed.

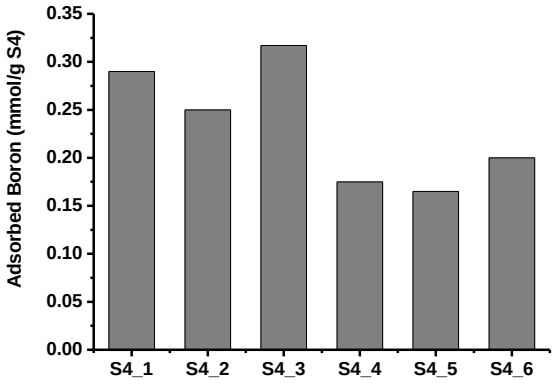

Figure 15. Boron adsorption capacity evolution for S4 solid during consecutive recovering cycles.

The results in Figure 15 show the amount of adsorbed boron per gram of desorbed material. Hence, though a small loss of adsorption capacity is detected, **S4** solid remains at good level of performance after several cycles.

In summary, although **S3** and **S5** show a poor boron adsorption capability, **S1**, **S2** and **S4** present not only high adsorption capacities, but also high recovery efficiencies. Furthermore, solid **S4**, prepared from sodium silicate, presents comparable adsorption properties to solids **S1** and **S2**, synthesized by using TEOS.

4.4 **Conclusions**

We have shown that functionalized mesoporous materials can act as adsorbents for boron removal from aqueous media. We have prepared several adsorbents, based on different kinds of inorganic matrices, to compare their boron adsorption efficiency after functionalization. The inorganic matrix of solids **S1** and **S2** has been prepared by the previously reported atrane route with TEOS and TEAH, and a surfactant (CTAB) as a templating agent for **S1**. Solid **S3** has been prepared from a commercial silica material, silica fumed. The silica scaffoldings of solids **S4** and **S5** have been obtained from inexpensive sodium silicate. The organic contents of ca. 0.47 to 1.03 millimole of active sites per gram of SiO_2 have been obtained in the final solids. Adsorption capability has been tested at different pH values and at

different adsorption times. Their efficiency in a neutral pH region and their high adsorption rates suggest an advantage for the boron removal application in environmental water samples because pH adjustments of samples and long contact times are not required.

Solids **S1** to **S5** have been tested as boron adsorption agents in water. The adsorption ability follows the order of **S1**>**S2**>**S4**>>**S3**>**S5**. **S4** shows a remarkable boron adsorption, comparable to that of **S1** and **S2**, suggesting that the replacement of templated mesoporous materials by silica xerogels make it possible to produce boron adsorbent agents for practical applications at a low cost. In addition, the recovery of adsorbents by a simple acidic wash has been shown, indicating a further minimization of costs for final adsorbents.

Acknowledgements

Financial support from the Spanish Government (Project MAT2009-14564-C04-01 and MAT2009-14564-C04-04) and the Generalitat Valenciana (Project PROMETEO/2009/016) is gratefully acknowledged. C.S. thanks the MICINN for a predoctoral fellowship.

References

1 R.F. Moseman*, Environ. Health Perspect. Suppl*., **1994**, 102, 113.

2 Guidelines for Drinking-Water Quality, 3rd Ed; Vol. 1. Recommendations; *World Health Organization: Geneva*, **2004**.

3 E. Weinthal, Y. Parag, A. Vengosh, A. Muti, W. Kloppmann, *Eur. Environ.,* **2005**, 15, 1.

4 S. Sahin, *Desalination*, **2002**, 143, 35.

5 D. Yu, D. Xue, *Acta Crystallogr*., **2006**, B62, 702.

6 D. Yu, D. Xue, H. Ratajczak*, J. Mol. Struct*., **2006**, 792–793, 280.

7 G. Yuan, D. Xue, *Acta Crystallogr*., **2007**, B63, 353.

8 D. Xue, K. Betzler, H. Hesse, D. Lammers, *Solid State Commun.*, **2000**, 14, 21.

9 Y. Xu, Jia-Qian Jiang., *Ind. Eng. Chem. Res*., **2008**, 47, 16.

10 S. Karahan, M. Yurdakoc, Y. Seki, K. Yurdakoc*, J. Colloid Interface Sci*., **2006**, 293, 36.

11 A. Sabarudin, K. Oshita, M. Oshima, S. Motomizu, *Talanta*, **2005**, 66, 136.

12 A.E. Yilmaz, R. Boncukcuoglu, M. M. Kocakerim, M. T. Yilmaz, C. Paluluoglu*, J. Hazard. Mater.*, **2008**, 153, 146.

13 M. D. Joshi, G. Chalumot, Y. Kim, J. L. Anderson, *Chem. Commun*., **2012**, 48, 1410.

14 L. Melnyk, V. Goncharuk, I. Butnyk, E. Tsapiuk, *Desalination*, **2007**, 205, 206.

15 M. Turek, P. Dydo, J. Trojanowska, A. Campen, *Desalination*, **2007**, 205, 192.

16 W. Bouguerra, A. Mnif, B. Hamrouni, M. Dhahbi, *Desalination*, **2008**, 223, 31.

17 N. Öztürk, D. Kavak, T. E. Köse, *Desalination*, **2008**, 223, 1.

18 J. Q. Meng, J. Yuan, Y. L. Kang, Y. F. Zhang, D. Y. Du, *J. of Colloid and Interface Science*, **2012**, 368, 197.

19 D. Hou, J. Wang, X. Sun, Z. Luan, C. Zhao, X. Ren, *J. of Hazard. Mater.*, **2010**, 177, 613.

20 E. Kir, B. Gurler, A. Gulec, *Desalination*, **2011**, 267, 114.

21 Y. Oren, C. Linder, N. Daltrophe, Y. Mirsky, J. Skorka, O. Kedem, *Desalination*, **2006**, 199, 52.

22 C. Yan, W. Yi, P. Ma, X. Deng, F. Li, *J. Hazard. Mater*., **2008**, 154, 564.

23 T.M. Suzuki, D.A. Pacheco, T. Yokoyama, Y. Miyazaki, K. Yoshimura*, J. Chem. Soc., Dalton Trans.*, **1999**, 1636.

24 G. Rodríguez-López, M.D. Marcos, R. Martínez- Máñez, F. Sancenón, J. Soto, L. A. Villaescusa, D. Beltrán and P. Amorós*, Chem. Commun*., **2004**, 2198.

25 C. Coll, R. Martínez- Máñez, M.D. Marcos, F. Sancenón, J. Soto, R. K. Mahajan*, Eur. J. Inorg. Chem.*, **2009**, 25, 3770

26 J.V. Ros-Lis, R. Casasús, M. Comes, C. Coll, M.D. Marcos, R. Martínez- Máñez, F. Sancenón, J. Soto, P. Amorós, J. El Haskouri, N. Garró, K. Rurack, *Chem. Eur. J.*, **2008**, 14, 8267.

27 X. Feng, G.E. Fryxell, L.Q. Wang, A.Y. Liu, K.M. Kemmer, *Science*, **1997**, 276, 923.

28 L. Mercier, T.J. Pinnavaia, *Adv. Mater*., **1997**, 9, 500.

29 A. Walcarius, L. Mercier*, J. Mater. Chem*., **2010**, 20, 4478.

30 Z. Wu, D. Zhao, *Chem. Commun*., **2011**, 47, 3332.

31 T. Yokoi, Y. Kubota, T. Tatsumi, *Appl. Catal. A: General*, **2012**, 421-422, 14.

32 G.J. Soler-Illia, C. Sanchez, B. Lebeau, J. Patarin, *Chem. Rev*. **2002**, 102, 4093.

33 L. Huerta, C. Guillem, J. Latorre, A. Beltrán, R. Martínez-Máñez, M. D. Marcos, D. Beltrán, P. Amorós, *Solid State Sciences*, **2006**, 8, 940.

34 D. Ortiz de Zárate, L. Fernández, A. Beltrán, C. Guillem, J. Latorre, D. Beltrán, P. Amorós*, Solid State Sciences*, **2008**, 10, 587.

35 El Haskouri, J. M. Morales, D. Ortiz de Zarate, L. Fernandez, J. Latorre, C. Guillem, A. Beltran, D. Beltran, P. Amoros, *Inorg. Chem.*, **2008**, 47, 8267.

36 A.B. Fuertes, *Chem. Mater.*, **2004**, 16, 449.

37 S. Cabrera, J. El Haskouri, C. Guillem, J. Latorre, A. Betrán, D. Beltrán, M. D. Marcos, P. Amorós, *Solid State Sci.*, **2000**, 2, 405.

38 B. Burczyk, K.A. Wilk, A. Sokolowski, L. Syper, *J. of Colloid and Interface Science*, **2001**, 240, 552.

39 B. Wolf, *Comm. Soil Sci. Plant Anal.*, **1974**, 5, 39.

40 D.L. Harp, *Anal. Chim. Acta*, **1997**, 346, 373.

41 R. N. Sah, P. H. Brown, *Microchem. J.*, **1997**, 56, 285.

42 V.M. Gun'ko, I.F. Mironyuk, V.I. Zarko, E.F. Voronin*, J. of Colloid and Interface Science*, **2005**, 289, 427.

43 A. Fidalgo, M. E. Rosa, L. M. Ilharco, *Chem. Mater*., **2003**, 15, 2186.

44 C. J. Brinker, G. W. Scherer, *Sol-Gel Science; Academic Press: New York*, **1990.**

45 S. Brunauer, P. H. Emmet, E. Teller, *J. Am. Chem. Soc.*, **1938**, 60, 309.

46 E. P. Barret, L. G. Joyner, P. P. Haselda, *J. Am. Chem. Soc*. **1951**, 73, 373.

47 C.T. Kresge, M.E. Leonowicz, W.J. Roth, J.C. Vartuli, J.S. Beck, *Nature*, **1992**, 359, 710.

48 H. Liu, X. Ye, Q. Li, T. Kim, B. Qing, M. Guo, F. Ge, Z. Wu, K. Lee, *Colloids and Surfaces A: Physicochem. Eng. Aspects.*, **2009**, 341, 118.

49 O. Kaftan, M. Açikel, A. E. Eroglu, T. Shawan, L. Artok, C. Ni, *Analytica Chimica Acta*, **2005**, 547, 31.

5. Boron Adsorption Mechanism Study in UVM-7 Gluconamide Adsorbent

Boron Adsorption Mechanism Study in UVM-7 Gluconamide Adsorbent.

*Cristina Sanfeliu,[abc] Ramón Martínez-Máñez,[abc] Félix Sancenón,[abc] Juan Soto,[abc] Pedro Amorós,[d] Thierry Azaïs,[e] Mª Dolores Marcos.[abc] **

a Centro de Reconocimiento Molecular y Desarrollo Tecnológico (IDM), Unidad Mixta UniversitatPolitècnica de València-Universitat de València, Spain.

b Departamento de Química, UniversitatPolitècnica de València, Camino de Vera s/n, 46022, Valencia, Spain.

c CIBER de Bioingeniería, Biomateriales y Nanomedicina (CIBER-BBN).

d Institut de Ciència del Materials (ICMUV), Universitat de València, P.O. Box 22085, E-46071, Valencia, Spain. (Tel.: (+34) 963543617)

e Sorbonne Universités, UPMC Univ Paris 06, CNRS, Collège de France, Laboratoire de Chimie de la Matière Condensée de Paris (LCMCP), 11 place Marcelin Berthelot, F-75005, Paris, France. (Tel.: (+33) 1 44 27 15 43).

**Corresponding Author: mmarcos@qim.upv.es.*

Submitted

Abstract

Boron chemistry has raised high interest due to the fact that being the difference between necessities and toxicity very narrow, it is widely used in industries. We have in previous work reported on an adsorbent for boron extraction from water by functionalization of a UVM7 mesoporous silica matrix with gluconamide moieties. The ability of this material to adsorb boron is based on its affinity for coordination of cis-diols present in the attached saccharide. In this paper depth study of the adsorption process has been accomplished. Several solids with increasing boron content have been prepared from the gluconamide functionalised UVM-7 material and an isothermal boron adsorption curve has been obtained. Additionally, ^{11}B and ^{13}C MAS NMR techniques have been used to the obtained solids and the simulation of the boron NMR and isothermal adsorption combined data has been accomplished to enlighten the boron adsorption process. A model including three different coordination environments, two possible adsorption sites and the presence of oligomeric boron species has allowed us to reproduce not only the isothermal boron adsorption curve but also the evolution of the integrated areas for the signals in the ^{11}B MAS NMR spectra obtained for the different boron containing-S1 materials.

5.1 **Introduction**

Boron has been extensively used in many industries, such as glass, ceramics, porcelain, cosmetics, semiconductors, carpets and fireproofing fabrics. Nowadays, the concentration of boron increases day by day in ground water because of both natural and anthropogenic reasons. Due to the use of boron containing products, boron waste has become a serious problem. Eventually, it may pollute drinking water sources and lead to a series of environmental and health problems.[1,2] Treatment methods for the removal of boron include coagulation-electrocoagulation, adsorption on oxides and membrane exchange resins.[3-5] Among them, the most effective method to remove boron from aqueous solutions

is the adsorption technique, because process requirements are simple and can be used in aqueous media with low concentration of boron.

Recently, hybrid functional mesoporous materials have been applied in adsorption protocols including the removal of boron from aqueous solutions by introduction of polyol functional groups onto the inner walls of mesoporous supports through post-grafting method.[6-9] This design is based on the ability of boric acid to form chelate complexes with organic molecules bearing vicinal hydroxyl groups through esterification reactions.[10] Hence, partial esterification may create 1:1 boron:polyol complexes in which a five or six members ring is formed. Complete esterification leads to the formation of bicyclic 1:2 boron:polyol complexes, as shown in Scheme 1.

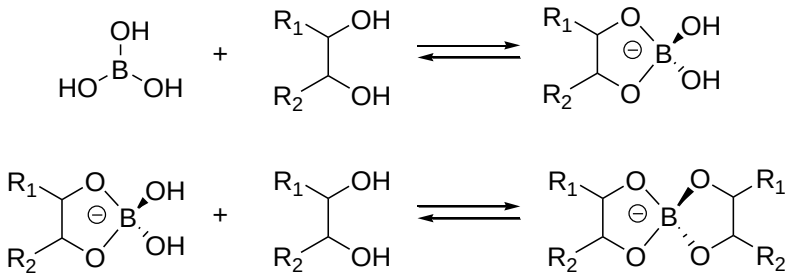

Scheme 1. Formation of mono- and bis-chelate borate esters with polyhydroxy compounds.

Boron mono-chelate complexes are quite labile and rapidly hydrolyze to their original components in aqueous solution while bis-chelate complexes are thermodynamically more stable and almost indissociable in water. While the complexation of boron by means of adjacent hydroxyl groups in the polyol is commonly assumed, it has been evidenced that complexation across alternate hydroxyl groups is also possible, as demonstrated by ^{1}H NMR spectroscopy, ^{11}B NMR spectroscopy, circular dichroism and polarimetry.[11-14]

Much research has been done on borate esters of sugars and sugar derivatives in solution.[15-18] However, there are very few reports about the adsorption mechanism of boric acid or borate onto functionalized materials in solid state. Yoshimura and coworkers[19] studied the interaction between N-Methylglucamine resin and borate. The combination of distribution and ^{11}B MAS NMR measurements revealed the

formation of a 1:1 tetradentate complex of $B(OH)_4^-$ with the N-methylglucamine group. Nevertheless, this study only showed the pH dependence of the borate esters formation in solid state, no ^{11}B MAS NMR measurements were presented with the resin and in the presence of different amounts of boric acid/borate solution. Thus, to the authors' knowledge, no study in solid phase on the mechanism of boric acid/borate adsorption onto functionalized materials has yet been reported.

We have previously reported the preparation of various materials and supports for boron removal from aqueous solutions.[20-22] These materials were built by grafting saccharides functionalities onto mesoporous silica scaffolds with different porous structures. However no emphasis was done then in terms of the adsorption mechanism and only an adsorption of boron by the formation of chelate complexes with the silica attached hydroxyl groups was stated. Having in mind the fact that the elucidation of the interactions between boron species and the anchored groups in the adsorbent materials should give important information for the development of new boron-selective efficient adsorbents, we have accomplished in this work the synthesis and characterization of boron adsorbent materials with different boron contents. This time we have made use of the very well-known UVM-7 mesoporous silica[23] functionalized with gluconamide moieties. In addition to the typical characterization techniques, the combination of boron-isothermal adsorption experiments with ^{11}B MAS NMR spectroscopic analysis[24-27] of each one of the obtained solids has resulted in a powerful tool to elucidate boron species present in the solid phase as a function of the boron concentration in the aqueous media. Hence we present in this paper the synthesis and characterization of the boron adsorbents and the corresponding analysis of the boron complexation process onto the active material. The data obtained gave important information about the interaction between boron species and the functional groups in the adsorbent.

5.2 **Experimental**

5.2.1 Chemicals

All chemicals for synthesis of the mesoporous materials, tetraethyl orthosilicate (TEOS), sodium silicate, n-cetyltrimethylammonium bromide (CTAB), and triethanolamine (TEAH3), were provided by Aldrich. For material functionalisation, (3-aminopropyl)triethoxysilane (**1**) and gluconolactone (**2**) were purchased from Aldrich. For preparation of boron solutions, boron standard solution of 1000 ppm was provided by Scharlab. To determine boron concentration, azomethine-H was purchased from VWR.

5.2.2 Materials characterization

X-ray powder diffraction (XRD) data were recorded on a Bruker D8 Advance diffractometer using Cu Kα radiation. XRD patterns were collected in steps of 0.02°2θ over the angular range 0.65-10°2θ and an acquisition time of 25 s/step. High and low-magnification SEM images were recorded by using a Jeol JSM 6300 microscope. Samples were previously coated with Au-Pd. A TEM study was carried out with a Philips CM10 instrument operating at 100 K and equipped with a CCD camera. Samples were gently ground in dodecane, and microparticles were deposited on a holey carbon film supported on a Cu grid. Nitrogen adsorption-desorption isotherms (-196 °C) were recorded with a Micromeritics ASAP- 2010 automated instrument. Calcined samples were degassed at 120 °C and 10-6 Torr for 5h prior to measurement. Surface areas were estimated according to the BET model, and pore size dimensions and pore volumes were calculated by using the BJH method from the adsorption branch of the isotherms. Thermogravimetric analyses were carried out on a TGA/SDTA 851e Mettler Toledo balance, with a heating program consisting of a heating ramp of 10 °C per minute from 393 to 1273 K and an isothermal heating step at this temperature over 30 min. The elemental analysis was performed in a CE Instrument EA-1110 CHN Elemental Analyser. Spectrophotometric measurements were carried out with a Lambda 35 UV/Vis Spectrometer from Perkin–Elmer Instruments.

5.2.3 NMR Measurements

NMR spectra were recorded on a 16,3 T Avance 700 Bruker spectrometer under magic angle spinning (MAS). Samples were packed in 3.2 mm zirconia rotors and spun at 22 kHz. Larmor frequencies were $\nu_L(^1H)$ = 700,13 MHz, $\nu_L(^{11}B)$ = 224,6 MHz, $\nu_L(^{13}C)$ = 176,07 MHz. ^{11}B spectra were recorded through a composite pulse sequence in order to suppress background probe signal. ^{13}C spectra were recorded using ^1H-to-^{13}C cross polarization (CP) experiments with a contact time of 1.5 ms. The spectra were proton decoupled during acquisition (SPINAL-64) with a ^1H radio-frequency field of $\nu(^1H)$ = 50 kHz. Recycle delays were 1,5 and 5 s for ^{11}B MAS and ^{13}C CP MAS experiments, respectively. The spectra were referenced (δ = 0 ppm) to TMS for ^{13}C and boric acid aqueous solution (0,1 M) for ^{11}B.

5.2.4 Molecular modelling

Eleven structural varieties of the possible boroester complexes were studied computationally by PM3 calculations applying the basis set included in the HYPERCHEM program package. Full geometry optimisations were performed on the isolated ions. Calculations were considered to be over when the gradient norm reached 0.1. The boroester complexes geometries were calculated in an aqueous environment. After geometry optimisation, the values (reflecting the stabilities of the complexes) were compared and related to experimental findings.

5.2.5 Preparation of UVM-7

The nanosized mesoporous UVM-7 silica was synthesized through a one-pot surfactant-assisted procedure in a homogeneous hydroalcoholyc reaction medium (water/triethanolamine). The general procedure, a modification of the so-called atrane route,[23] has been described in detail elsewhere. It is based on the use of a simple structural directing agent (such as n-cetyltrimethylammonium bromide, CTAB) and a complexing polyalcohol (triethanolamine), which originates silatrane complexes (relatively inert complexes that include triethanolamine-related ligand species) as hydrolytic

precursors. Together with its complexing ability, the presence of the co-solvent (triethanolamine) was a key in order to favour the formation of nanoparticulated materials. To open the intrananoparticle mesopores, the surfactant was extracted from the as synthesized mesostructured solid by chemical exchange using an HCl/ethanol solution (CTAB/H^+ exchange). Thus, 1 g of mesostructured UVM-7 powder was suspended in a solution containing 16 mL of HCl (37%) and 130 mL of ethanol (99%), and this mixture was heated at reflux (60 °C) for 2 h under stirring. Later, after renewal of the HCl/ethanol solution, and to complete the extraction process, the suspension was stirred and heated again at 60 °C for 16 h. The resulting mesoporous powder (UVM-7) was collected by filtration, washed with ethanol, and air-dried at 100 °C.

5.2.6 Preparation of S1

UVM-7 (1 g) was suspended in acetonitrile (40 mL) and heated at 120 ºC in a Dean-Stark apparatus in order to remove the adsorbed water by azeotropic distillation under an inert atmosphere (Ar gas). Then, to this suspension, (3-aminopropyl)triethoxysilane (**1**, 10.7 mmol) were added at room temperature. After 16 h, the solid **(SNH_2)** was filtered, washed (acetonitrile and water) and dried. As a last step, solid **SNH_2** (0.75 g) was suspended in methanol (50 mL), gluconolactone (**2**, 10 mmol) was added and the mixture was stirred at room temperature during 48 h. The final solid **S1** was filtered, washed with water and dried (see scheme 1).

5.2.7 Preparation of boron charged materials

Mesoporous solids containing various amounts of boron were prepared from **S1**. Boron adsorption was carried out suspending **S1** (100 mg) in boron solutions of selected concentrations (50 mL). The suspensions were stirred during 16 h and then filtered. Final solids, with different boron contents (**S1-B1, S1-B2, S1-B3, S1-B4, S1-B5** and **S1-B6**), were washed (water), dried and stored for further NMR measurements. The boron concentration in the remaining solution was determined by azomethine-H method and the difference between this value and the initial concentration gave the amount adsorbed in the final materials.

5.3 **Results and discussion**

5.3.1 Design and synthesis of the adsorbent material

The synthesis of the boron adsorbent material **S1** is shown in Scheme 1. Inorganic support UVM-7 mesoporous silica was selected due to its high loading capacity and its easy chemical functionalization. UVM-7 material is a mesoporous silica phase with a bimodal pore system prepared with tetraethylorthosilicate (as silica source) and hexadecyltrimethylammonium bromide (as templating agent). Hence, UVM-7 matrix can be described as bimodal porous silica constructed by aggregation of pseudo-spherical mesoporous primary nanoparticles whose average diameter is ca. 15–20 nm. The small intra-particle mesopore system has its origin in the template effect of the surfactant aggregates (acting as porogens, as consequence of their ulterior elimination). This pore system is defined by regular mesopores organized in a disordered hexagonal array. On the other hand, large inter-particle pores are generated as the nucleation and growth of the primary mesoporous nanoparticles proceeds. In practice, the formation of a continuous network from the soldered nanoparticles generates a disordered system of large void-pores (ranging from large-meso to macropores) accounting for the observed textural porosity.[29-31] The non-ordered nature of this large pore system is consistent with a formation mechanism implying collision and aggregation of primary nanoparticles, in which does not participate any supramolecular template able to transfer a certain organization. Thus, at micrometric scale, the UVM-7 silicas present rough surfaces resulting from the aggregation of pseudo-spherical clusters of mesoporous nanoparticles defining large true textural macropores among them.

On the other hand, knowing the affinity of boron aqueous species for cis-diol moieties we selected, as functional groups, glucose molecules. As could be seen un Scheme 2, the UVM-7 support was functionalized, in a first step, with aminopropyl moieties through reaction of the silanol moieties located on the surface with (3-aminopropyl)triethoxysilane (**1**). This functionalization step yield the **SNH_2**. In a second step, the amino groups of **SNH_2** were reacted with gluconolactone (**2**) yielding the final solid **S1.**

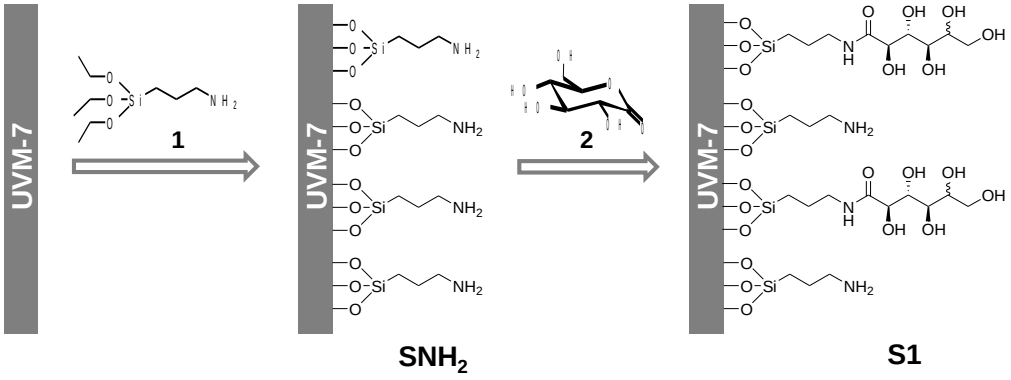

Scheme 2. Schematic representation of the synthesis of **SNH_2** and **S1** materials.

The reaction between the grafted amino groups in **SNH_2** and gluconolactone to produce the final material **S1** have a 53% yield (see below). The moderate yield of the amidation reaction is a clear consequence of the fact that formation of bulky gluconolactone moieties would induce an important pore blocking and steric hindrance. In spite of the fact that amine moieties in **SNH_2** are located mainly on the surface of the wide textural pores, the reaction of the more accessible NH_2 groups with gluconolactone should induce some pore blocking and, as a consequence, the progress of the reaction is somehow handicapped leading to a moderate yield. The final **S1** solid then is a bimodal pore material with gluconamide moieties grafted on its surface, containing cis-diol groups able to react with boron species yielding boroester entities.

5.3.2 Characterization of the sorbents

In Figure 1 a representative image of the typical bidimensional structure of the UVM-7 inorganic matrix is shown. In this figure it can clearly be seen how the small mesopore particles fuse together to give rise to the secondary interparticle pore

system. Inside the small particles the pseudo-hexagonal ordered intraparticle mesopore system can also be observed.

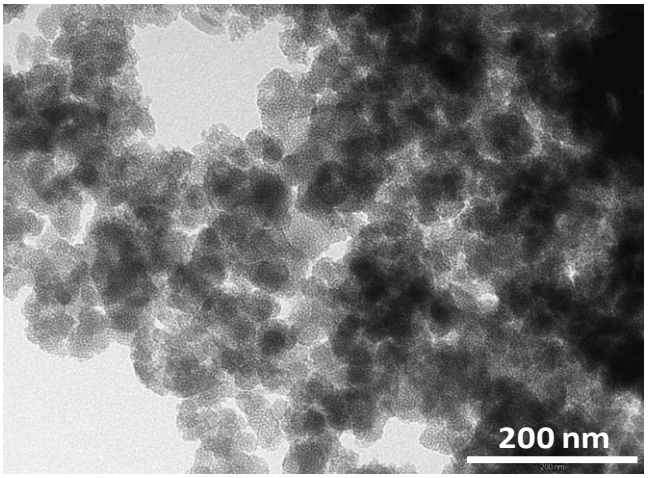

Figure 1. Representative TEM micrograph of the bimodal porous UVM-7 materials.

Figure 2 illustrates the PXRD patterns corresponding to a representative sample of the UVM-7 material (a) before (mesostructured), (b) after (porous) template removal and (c) after the grafting protocol (solid **S1**). These PXRD patterns are characteristic of this kind of nanoparticulated mesoporous/mesostructured solids prepared through surfactant-assisted procedures and display, at least, one strong and broad diffraction peak in the low angle region. Apart from the intense peak, we can observe a broad small shoulder, which could be indexed as the (110) and (200) overlapped reflections of the typical hexagonal cell. For the mesoporous solid (after the surfactant extraction process), this indexation leads to a lattice constant of ao = 50.9Å according to the hexagonal unit cell relation (ao = 2d100/√3). In the three cases, the PXRD patterns indicate the relative order of the intra-nanoparticle mesopore (small pores) system and are clear proof of the presence of a certain pseudo-hexagonal order. Hence, we may infer that the organization of the intraparticle mesopores in solid **S1** (curve c in Figure 2) is also preserved after the two-step functionalization process.

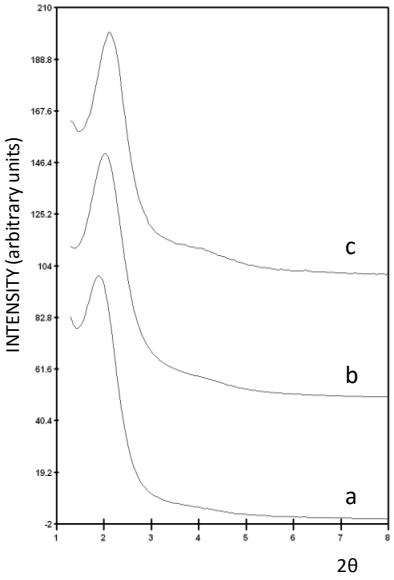

Figure 2. X-ray powder diffraction patterns of (a) as-synthesized (mesostructured) UVM-7, (b) chemically extracted UVM-7 silica and (c) funcionalizated solid S1.

The N_2 adsorption-desorption isotherms quantitatively confirm the bimodal character of the UVM-7 material (Figure 3). As it can be noted, the curve shows two well-defined adsorption steps. The first one, at an intermediate relative pressure ($0.3 < P/P0 < 0.5$), is characteristic of type IV isotherms and can be related to capillary condensation of N_2 inside the mesopores. The second step, at a high relative pressure ($P/P0 > 0.8$), corresponds to the filling of the large pores among the primary nanoparticles. The BJH pore size distribution shows the existence of two well differentiated pore systems. An intense and narrow signal with a maximum at 2.7 nm ascribed to the surfactant generated pores, and a very wide pore distribution expanding up to large macropores (> 50 nm).

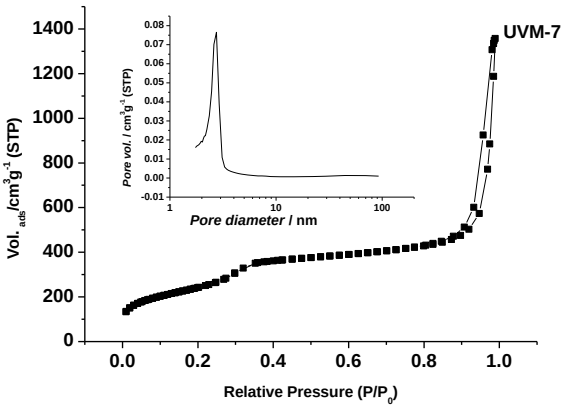

Figure 3. N_2 adsorption-desorption isotherms of UVM-7 extracted material. The inset shows the BJH pore size distribution from the adsorption branch of the isotherm.

The specific surface areas, volumes and pore sizes were calculated from a Brunauer–Emmet–Teller (BET; specific surface area) treatment of the isotherm,[32] and the Barret–Joyner–Haselda (BJH; volumes and pore size) method,[33] respectively and are shown in Table 1. UVM-7 materials show large surface area (880 m2 g-1) and more than 50 nm of interparticle pore diameter, which would allow a high degree of organic functionalization.

Material	BET ($m^2\ g^{-1}$)	Intraparticle pore[a] (nm)	small pore volume ($cm^3\ g^{-1}$)	Interparticle pore[a] (nm)	large pore volume ($cm^3\ g^{-1}$)
UVM-7	877.7	2.77	0.72	>50	1.30

Table 1. Pore structure data of the UVM-7 material.

For all the organic-inorganic hybrid materials, one key point associated with their characterization is the determination of the functionalization degree. The contents in organic groups (i.e. amine and gluconamide) in **SNH_2** and **S1** materials were determined by thermogravimetric and elemental analyses. From elemental analysis of C, H, N it is possible to determine the amount of binding groups contained in the corresponding material (calculated in millimoles per gram of SiO_2, mmol g^{-1} SiO_2) using equation (1).

$$\alpha_A = \frac{\Delta W_i\% \times 1000}{\Delta W_{SiO_2}\% \times n M_i} \text{ (mmol g}^{-1}\text{ SiO}_2\text{)} \qquad (1)$$

where ΔWi% (i = C, N) are the weight percentages of carbon or nitrogen, Mi is the corresponding atomic weight and n is the number of the corresponding atom type in one molecule. $\Delta WSiO_2\%$ is the inorganic SiO_2 content in weight percentage. These experiments allowed us to estimate the total amount of organic material in **SNH_2** and **S1**. At this respect, for **SNH_2** solid a degree of functionalization of 2.45 mmol of amine per gram of SiO_2 was obtained, whereas for **S1** 1.29 mmol of glucose per gram of SiO_2 was reached. Bearing in mind both contents, the yield of the amidation reaction can be calculated as being about 53%.

We also calculated the average coverage, β_{gluc}, as the number of gluconamide molecules per nm^2 using Equation (2) in which α_A is the anchored group content ($mmol \cdot g^{-1}$ SiO_2), S is the specific surface ($m^2 \cdot g^{-1}$) of the UVM-7 material (Table 1) and N_A is the Avogadro's number.

$$\beta_A = \alpha_A \times 10^{-3} \times S^{-1} \times 10^{-18} \times N_A = \alpha_A \times S^{-1} \times 602{,}3 \qquad (2)$$

Thus, solid **S1** presents 0.88 gluconamide molecules per nm^2, which corresponds to an average distance of 1.07 nm between vicinal groups attached to the surface.

The characterization of the organic matter in solids **SNH_2** and **S1** was examined through ^{13}CNMR studies of both materials. These studies allowed us to confirm the correct performance of both the functionalization reaction of the UVM-7 mesoporous matrix with APTES (reactant 1 in scheme 2) and also the amidation reaction of solid **SNH_2** with gluconolactone (reactant 2 in scheme 2). The ^{13}C CP MAS NMR spectra of solids **SNH_2** and **S1** are shown in Figure 4. ^{13}C NMR spectrum of solid **SNH_2** (curve a in Figure 4) displays three resonances in the 10-50 ppm that are assigned to the propyl chain that links the amino moiety to the inorganic scaffold. More in detail, the signal appearing at ca. 10 ppm can be ascribed to the carbon atom of the methylene moiety neighbour to the Si atom in the inorganic support, whereas the signal at ca. 45 ppm is due to the carbon atom of the methylene moiety directly linked to the amino group. On changing to solid **S1**, ^{13}CNMR spectrum

displays the same signals in the 10-50 ppm interval, ascribed to the propyl linker, whereas other signals in the 62-75 ppm interval and at ca. 170 appeared (see curve b in Figure 4). The new signals were ascribed to the gluconamide moiety in **S1**, formed through an amidation reaction between amine moieties and gluconolactone. The broad signals that appeared in the 62-75 ppm interval are ascribed to the C-OH carbons of the "saccharide" units, whereas the signal at ca. 170 ppm is due to the amide carbon that is produced in the amidation process.

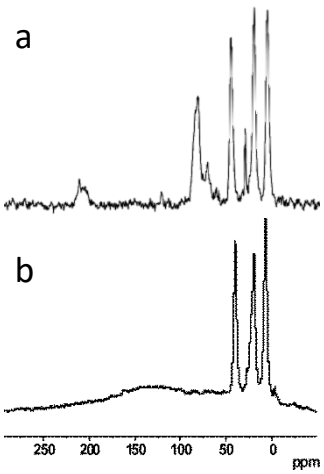

Figure 4. ^{13}C CP MAS NMR spectrum of (a) **SNH_2** and (b) **S1**.

5.3.3 Boron charged solids

Boron can be adsorbed on the functionalized materials bearing in mind that boric acid is able to link poly-ol groups forming a chelate complex.[34] Hence, it was expected for boron to form both mono-chelate and bis-chelate complexes with glucose groups attached to the adsorbent.[35,36] In order to clarify boron adsorption mechanism onto the solid and the stoichiometry of the formed complexes, various materials with different amounts of adsorbed boron were prepared and then analysed by ^{11}B and ^{13}C MAS NMR.

All boron-containing materials were prepared from **S1**. Hence, different samples of solid **S1** (100 mg each time) were suspended in boron solutions of diverse concentrations (50 mL, from $1.92 \cdot 10^{-4}$ to $3.8 \cdot 10^{-2}$ mol dm^{-3}), then filtered and, finally, washed to remove free boric acid and physisorbed borates. This protocol yielded six different solids (**S1-B1**, **S1-B2**, **S1-B3**, **S1-B4**, **S1-B5** and **S1-B6**) with different boron concentrations. In each case the corresponding boron content was determined following the azomethine method.[37] Table 2 shows the quantity of boron adsorbed in each of the prepared materials, first in absolute value as the amount of mmol of boron per gram of solid and then, as a value relative to the adsorbent gloconamide content (mmol of boron per mmol of gluconamide, taking into account a gluconamide content for **S1** of 0.86 mmol per gram of solid).

Material	B ads	
	mmol B/ g solid	mmol B/ mmol glucose
S1-B1	0.0189	0.02
S1-B2	0.0960	0.11
S1-B3	0.2600	0.30
S1-B4	0.3928	0.46
S1-B5	1.1458	1.34
S1-B6	1.8475	2.16

Table 2. Boron content in solids S1-B1 to S1-B6 (absolute and relative to the anchored glucose).

The high relative boron content obtained for solids **S1-B5** and **S1-B6** is indicative of a more than one boron coordination per anchored glucose group. In fact, polyalcohols are able to form complexes of 2:1, 1:1 and 1:2 stoichiometries upon borate complexation. The formation of one or several complexes in our solid materials may be a function of the boron/gluconamide ratio. At this respect, in solid **S1-B1** (with the lower boron/gluconamide ratio) the formation of bischelate 2:1 gluconamide-borate complex would be expected. Upon increasing borate concentration monodentate 1:1 gluconamide-borate complex would be formed, but this new complex could either replace the previous bis-chelate 2:1 gluconamide-borate complex or could both coexist in the adsorbent. At higher

boron/gluconamide ratios (as in solids **S1-B5** and **S1-B6**) more adsorption sites would be needed and monodentate 1:1 gluconamide-borate positions will be predominant.

5.3.4 ^{13}C NMR MAS studies

The different solids prepared in this paper (**S1** and **S1-B1** to **S1-B6**) have been studied by ^{13}C CP MAS NMR spectroscopy. At this respect, studies carried out in aqueous solutions indicated that upon borate ester formation shifts of 3-10 ppm to higher frequency are usually observed for the ^{13}C nuclei in the borate ester ring. For helping in the discussion, Figure 5 shows the schematic structure of the grafted gluconamide with the carbon atoms' numbering assignment.

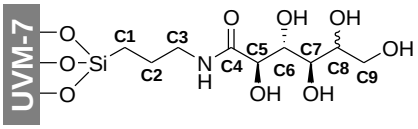

Figure 5. Structural formula of gluconamide group with a numbering scheme used in the text.

Figure 6 displays the ^{13}C CP MAS NMR spectra and Table 3 a full list of the corresponding chemical shifts of solids **S1, S1-B1, S1-B2, S1-B3, S1-B4, S1-B5** and **S1-B6**. The ^{13}C MAS NMR spectra of solid **S1** presents five signals coming from the different environments surrounding the carbon atoms. The signals of the propyl linker carbon atoms (C1, C2 and C3 in Figure 6) appear at ca. 10, 21 and 42 ppm. Dealing with the gluconamide signals, the methylene linked directly to a hydroxyl group (C9 in Figure 6) is related to the resonance centred at 63 ppm, whereas a broad signal centred at ca. 72 ppm is due to the overlapping of the resonances of the CH-OH (C5, C6, C7 and C8 in Figure 6). Finally, the signal of the carbon atom of the carbonyl group (C4 in Figure 6) is ascribed to the resonance at 174 ppm. Addition of small boron quantities (bellow the content of gluconamide), as in solids **S1-B1, S1-B2, S1-B3** and **S1-B4**, induced negligible changes in the carbon signals of the propyl linker. However, the signals of the carbon atoms bearing hydroxyl moieties suffer moderate downfield shifts. At this respect, the signal of C9 was

shifted from 63 to 64.2 ppm on changing from **S1** to **S1-B4**, whereas the signals of C5-C8 carbons were also shifted from 72 to 75.4 ppm. Also the carbonyl peak suffers a downfield shift from 174 to 175.2 ppm. These moderate downfield shifts (1.2 ppm for C9, 3.4 ppm for C5-C8 and 1.2 ppm for C4) of the carbon atoms of the gluconamide moiety were ascribed to the formation of bischelate (α,β)2-BL2 and monochelate (α,β)-BL complexes. At higher boron contents (such in solids **S1-B5** and **S1-B6**) the signals of the carbons of the gluconamide moieties suffers again moderate downfield shifts but the most important feature of the ^{13}C NMR spectra are the changes observed for the propyl linker for solid **S1-B6**. At this respect, the signals centred at 10 (C1), 21 (C2) and 42 (C3) ppm were shifted, respectively, to 11.0, 23.3 and 53.5 ppm. These downfield shifts are tentatively ascribed to the fact that a large amount of boron adsorbed would modify the chemical environment of the surroundings even for the carbon atoms of the propyl linker.

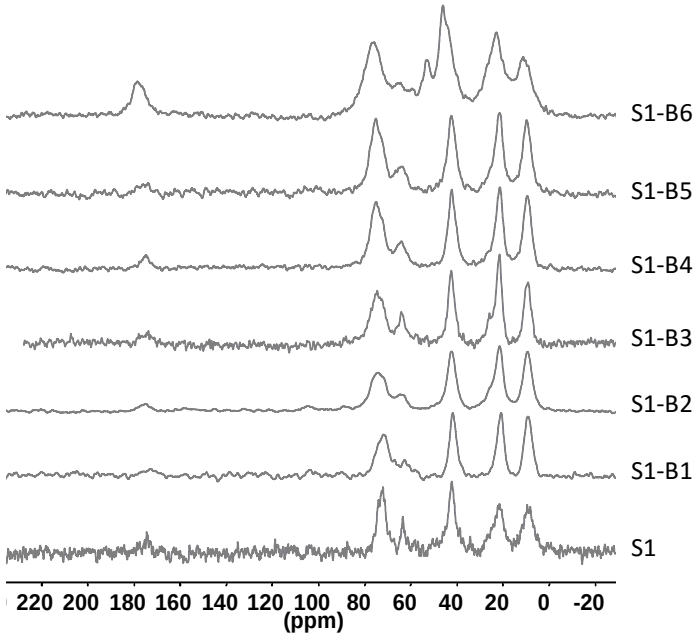

Figure 6. ^{13}C CP MAS NMR spectra of solids S1 to S1-B6.

material	δ C4 GLUC (ppm)	δ C5,6,7,8, GLUC (ppm)	δ C9 GLUC (ppm)	δ C3 APTES (ppm)	δ C2 APTES (ppm)	δ C1 APTES (ppm)
S1	174,0	72,6	63,5	42,6	21,6	9,6
S1-B1	174.0	72.6	63.4	42.3	21.4	9.6
S1-B2	175.2	74.6	64.8	42.9	21.7	9.6
S1-B3	175.2	74.9	64.5	42.8	22.0	9.5
S1-B4	175.2	75.4	64.2	42.5	21.6	9.6
S1-B5	176.6	75.3	64.0	42.5	21.6	9.8
S1-B6	178.8	76.8	65.8	53.5	23.3	11.0

Table 3. ^{13}C CP MAS NMR chemical shifts of solids S1 to S1-B6.

5.3.5 ^{11}B NMR MAS studies

Figure 7 displays the ^{11}B MAS NMR spectra of the six materials (**S1-B1** to **S1-B6**) prepared with increasing boron content inside the **S1** adsorption matrix.

There are several studies of the boron complexation with polyalcohols and saccharides in solution using ^{11}B NMR measurements. These studies have centred their attention on the identification of ^{11}B resonance signals in the different complexes with polyhydroxy compounds formed in solution. At this respect, Van Duin and co-workers,[24-25] studied the complexation of boron with a series of polyols and polyhydroxycarboxylates in aqueous solution and observed signals at -9.9 ppm, due to the formation of the bischelate $(\alpha,\beta)_2$-BL_2 complex, at -13.3 ppm, due to the formation of the monochelate (α,β)-BL complex, at -16.7 ppm, due to the formation of the monochelate (α,γ)-BL complex and at -18.5 ppm due to the formation of the bischelate $(\alpha,\gamma)_2$-BL_2 complex (see Scheme 3).

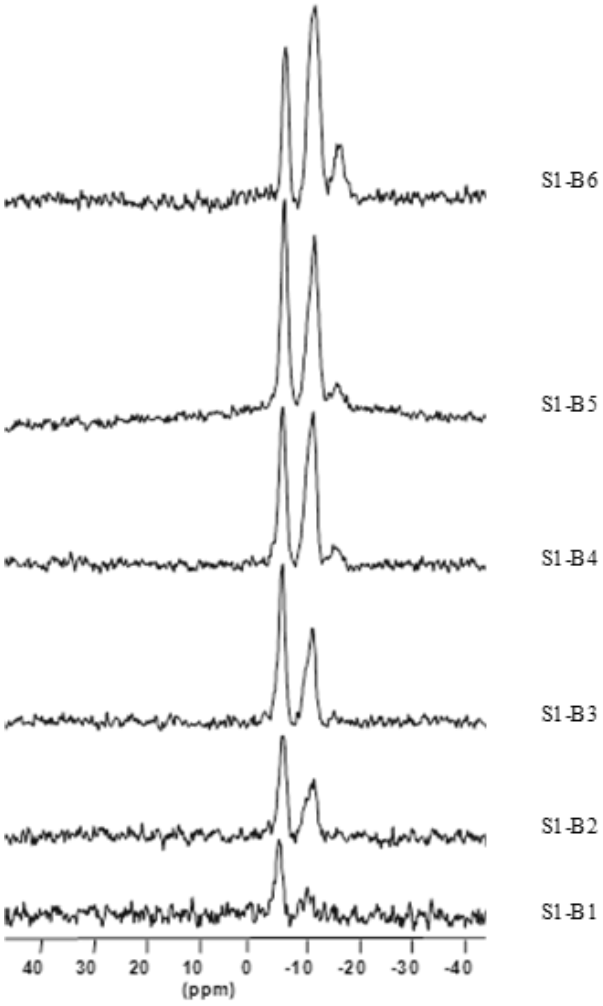

Figure 7. 11B MAS NMR spectra for solid **S1** containing different amounts of borate together with the resonances assignment.

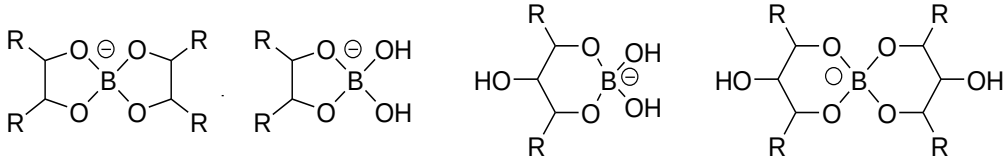

$(\alpha,\beta)_2$-BL_2 **(α,β)-BL** **(α,γ)-BL** **$(\alpha,\gamma)_2$-BL_2**

Scheme 3. Representative complexes formed between boric acid and polyol molecules.

As could be seen in Figure 7 solid **S1-B1**, with the lowest boron content, shows a broad signal centred at -5.8 ppm that may be ascribed, following the above mentioned studies in solution, to the bischelate $(\alpha,\beta)_2$-BL_2 complex. The formation of this bischelate complex, at lower boron concentrations, could be explained bearing in mind the high availability of gluconamide moieties and the stability of the bis-bidentate borate complex. Also, from the total concentration of anchored gluconamides in solid **S1**, and assuming a homogeneous repartition of the gluconamides moieties we could estimate an average distance between complexing molecules of 10.7 Å. Taking into account this distance, the gluconamide moieties are located in a spatial conformation that allowed the formation of the bis-chelate complex with borate. Addition of increasing quantities of boron (solids **S1-B2** and **S1-B3**) induces the clear emergence of a signal, almost visible in the first spectra, centred at -12 ppm. Following Van Duin assignation we may relate this signal to the formation of the mono-chelate (α,β)-BL complex. It can be seen in Figure 7 that when increasing the amount of available boron to be adsorbed onto the polyol moieties the relative area of the mono-chelate peak complex increases with respect to the area of the bis-chelate one. When doing the integration of the corresponding signals we can see that **S1-B2** and **S1-B3** complexes coexist in a nearly 1:1 bis-chelate to mono-chelate ratio (see Table 4 for the relative integration of the signals in the ^{11}B NMR spectra for the prepared solids). If we keep increasing the available amount of boron a new peak with a chemical shift of -17 ppm also appears (see Figure 7) that may be ascribed to the formation of the monochelate (α,γ)-BL complex. From Hyperchem calculations it can be seen that when occupying the (α,β)-dyol positions, the (α,γ)-dyol positions remain also available. See Figure 8.

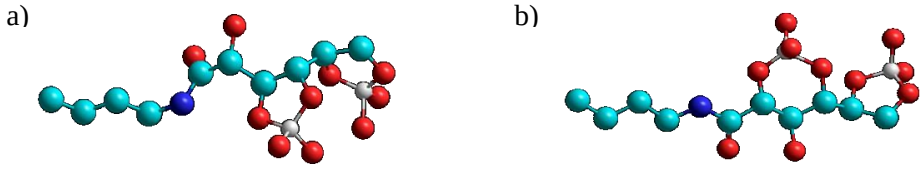

Figure 8. Hyperchem simulation of a) mono-chelate (α,β)-BL complex and b) monochelate (α,γ)-BL complex in the presence of an (α,β)-BL complex already formed at the end of the same gluconamide molecule.

Material	% (-5.8 ppm)	% (-12 ppm)	% (-17 ppm)
S1-B1	67.1	32.9	0.0
S1-B2	55.3	44.7	0.0
S1-B3	53.7	44.7	1.6
S1-B4	38.7	55.2	6.1
S1-B5	41.6	51.2	7.2
S1-B6	24.8	59.5	15.6

Table 4. Relative integration of the signals in the ^{11}B NMR spectra for the solids with increasing boron content.

Hence, we could say that the first site for boron to be adsorbed is the highly stable bis-chelate coordinating place and only when these positions are highly engaged the other mono-chelated sites start to be occupied, being the (α,β)-diol preferred against the (α,γ)-diol ones. This fact clearly indicates that (α,γ)-BL complex is the less stable and their formation is poorly favoured due to the fact that the small size of boron atom (when compared with oxygen and carbon) fits better with the formation of 5-membered ring chelate than with the 6-membered one.

However, the study of Van Duin and co-workers has been performed at experimental conditions for which the predominant species of boron is the boric acid, $B(OH)_3$. Yet, it is well known that when increasing the boron concentration a number of polyborates may appear in solution[37] and more complicated species may be considered when boron is made to react with polyol molecules (see Scheme 3). In this way, Salentine[39] has also used ^{11}B MAS NMR techniques to study the presence of polyborate species in solution. He reports the emergence of a broad signal centred at -18 ppm when the concentration of boron rise to 0.15 M. At our experimental conditions the presence of polyborate species should be taken into account. Hence, the upfield peak could also be considered as containing the resonance of chelates between the polyol molecules and different polyborate species (see Scheme 4).

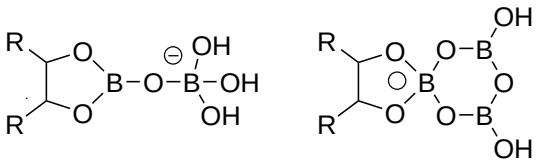

(α,β)-B_2L **(α,β)-B_3L**

Scheme 4. Possible complexes formed between polyol molecules and polyborates species.

As a conclusion, the ^{11}B and ^{13}C MAS NMR studies indicated that at least three main complexes were formed upon interaction with boron and the grafted gluconamide moieties in **S1.** Whereas the ^{13}C MAS NMR measurements have shown the degree of interaction between the boron species and the attached carbon chains, the ^{11}B MAS NMR spectra have provided us the information about the chemical nature of the formed complexes (bischelate or monochelate involving 1,2 or 1,3-diols).

5.3.6 Boron adsorption isotherm

In order to get a better insight in the boron adsorption process, the corresponding isothermal adsorption experiences have been performed. In Figure 9 the amount of adsorbed boron per gram of adsorbent is represented as a function of the equilibrium boron concentration in solution. The first part of the curve shows a typical profile of a Langmuir adsorption process. However, the last part of the curve that accounts for the formation of solids **S1-B5** and **S1-B6** shows an increasing profile that could correspond to a multilayer adsorption process. In Figure 9, on top of the experimental adsorption data, the curve corresponding to a model including the occupation of one type Langmuir position and a multilayer Freundlich adsorption has been drawn. This curve has been obtained by using the Solvert tool implemented in the Microsoft Excel program and the formula used was:

$$n(B_{ads})_{total} = \frac{n(B_{ads})_1 * K_1 * [B_{eq}]}{1 + K_1 * [B_{eq}]} + K_\beta * [B_{eq}]^{\frac{1}{\beta}} \quad (2)$$

In which $n(B_{ads})_{total}$ is the total number of mols of boron adsorbed per gram of adsorbent; $n(B_{ads})_1$ is the number of mols of boron adsorbed following a Langmuir

type behaviour and K_1 the corresponding adsorption constant; K_β is the Freundlich constant and β the corresponding Freunlich exponent; and $[B_{eq}]$ is the boron concentration of the solution in equilibrium with the corresponding solid. The adjustment was performed by minimizing the total standard deviation:

$$SD = \sqrt{\frac{\sum_1^6 \left[n(B_{ads})_{exp} - n(B_{ads})_{calc} \right]_i^2}{5}}$$

The values of the parameters in equation (2) obtained after the refinement are shown in Table 5. This model has been previously applied in order to fit the adsorption of boron from aqueous solution using chelate adsorbents. However, though the adjustment of the calculated data to the experimental values is quite good the information obtained is not very useful as the adsorption process must be more complex than that expressed by an only Langmuir constant and a general multilayer adsorption process. Our aim was to get a better insight in the boron adsorption process and try to differentiate between the several possible coordination positions that the anchored glucose molecules may offer to boron atoms. Hence, we have thought in combining the experimental adsorption data with the integrated areas obtained from the ^{11}B MAS NMR spectra.

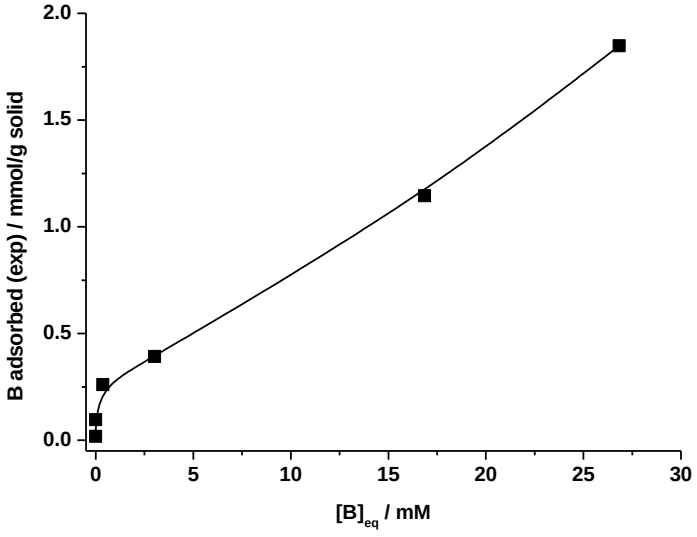

Figure 9. Boron adsorption isotherm: squares correspond with experimental boron content of solids S1-B1 to S1-B6 and solid line to the calculated boron content from the Langmuir-Freundlich model essayed for the boron adsorption.

Langmuir adsorption site	n (mmol/g solid)	0,27
	K	151
Freundlich Multilayer	K_β	0,026
	β	1,24
Minimized parameter	Global Standard Deviation	0,011

Table 5. Results obtained from the Langmuir and Freundlich model essayed for the boron adsorption.

As we have commented above, we assume the existence of two different and possibly simultaneous adsorption positions, one at the end of the glucose molecules (site 1) and the other involving the other hydroxyl groups that provide a more internal position (site 2). From all the possible combinations for the coordination of boron with the anchored glucose molecules we have assumed, first of all, that the bis-chelate complexes are formed at the external positions (site 1) as these will show an easier coordination with two neighbouring molecules for boron atoms. In Figure 10 the Hyperchem minimised bis-chelate complexes at different positions may be compared.

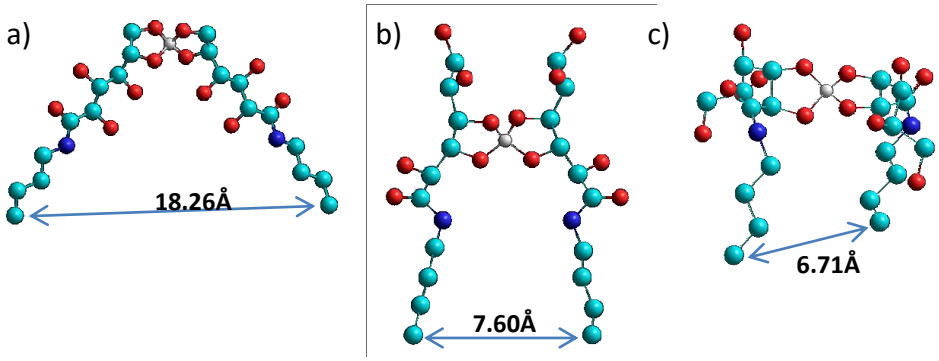

Figure 10. Hyperchem minimised bis-chelate boron complexes at different positions: a) (α,β-BL_2^-) (5,6); b) (α,β-BL_2^-) (3,4); c) (α,β-BL_2^-) (2,3).

We have also considered that this external position could also be competitively occupied by the mono-chelate (α,β)-BL complexes, and a competition equilibrium has also been considered. Secondly, for the *site 2*, formation of mono-chelated complexes has been considered and the equilibrium for the formation of both (α,β)-BL complex and (α,γ)-BL complexes have been taken into account. Hence, the equilibrium reactions we have used are:

Coordination equilibria at site 1:

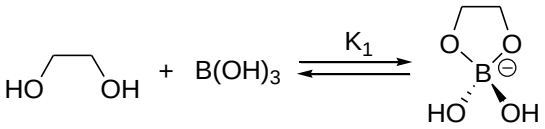

$$K_1 = \frac{\theta_{BLPE}}{(B(OH)_3)\theta_{LE}}$$

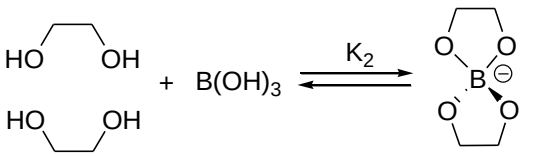

$$K_2 = \frac{\theta_{BL2}}{(B(OH)_3)\theta_{LE}}$$

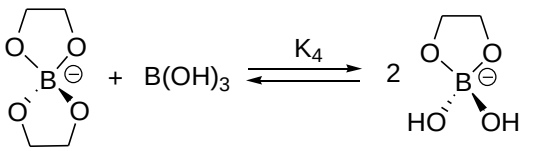

$$K_4 = \frac{\theta_{BLPE}}{(B(OH)_3)\theta_{BL2}}$$

Coordination equilibria at *site 2*:

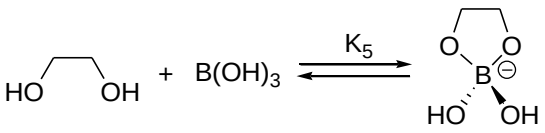

$$K_5 = \frac{\theta_{BLPI}}{(B(OH)_3)\theta_{LI}}$$

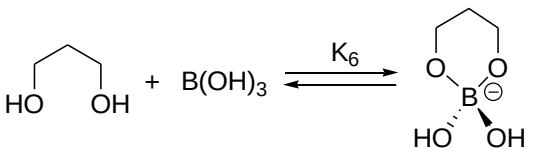

$$K_6 = \frac{\theta_{BLHI}}{(B(OH)_3)\theta_{LI}}$$

Where θ_i values states for the fraction of adsorption sites:

$$\theta_i = \frac{n_i}{n_{total}}$$

And *BL₂* refers to the (α,β)bis-chelate complex, *BLPE* and *BLPI* refers to the (α,β)mono-chelate complexes at the *site 1* and *site 2* respectively, *BLHI* refers to the (α,γ)mono-chelate complex and *LE* and *LI* for the free positions at *site 1* and *site 2*, respectively. With this model the evolution of the isothermal adsorption curve has been simulated taking into account the adsorbed boron atoms in both positions:

$$n(B_{ads})_{total} = n(B_{ads})_{site\ 1} + n(B_{ads})_{site\ 2} \qquad (3)$$

Being:

$$n(B_{ads})_{site\ 1} = n(B_{ads})_{BL_2} + n(B_{ads})_{BLPE} \qquad (4)$$

$$n(B_{ads})_{site\ 2} = n(B_{ads})_{BLPI} + n(B_{ads})_{BLHI} \qquad (5)$$

The values of the number of boron mols adsorbed in each position have been obtained by manual adjustment of the equilibrium constants above defined to get the best agreement to the experimental data:

$$(IA_{peak\ 1})_i * n(B_{ads})_{total\ i} = n(B_{ads})_{BL2\ i}$$

$$(IA_{peak\ 2})_i * n(B_{ads})_{total\ i} = n(B_{ads})_{BLPE\ i} + n(B_{ads})_{BLPI\ i}$$

$$(IA_{peak\ 3})_i * n(B_{ads})_{total\ i} = n(B_{ads})_{BLHI\ i}$$

Where $(IA_{peak\ 1})$, $(IA_{peak\ 2})$ and $(IA_{peak\ 3})$ are the integrated areas of the absorption signals centered at -5.8ppm (peak 1), -12ppm (peak 2) and -17ppm (peak 3) in the

^{11}B NMR spectra and $n(B_{ads})_{tota}$ is the total boron adsorbed. This calculation could reproduce the first part of the curves, however in order to simulate the final increase of the curves related with peak 2 and peak 3 the coordination of polyborate species to the adsorbent should be taken into account. Following the work published by Salentine[39] we considered that the adsorption appearing at -12ppm and -17ppm not only contains the adsorption coming from the (α,β)-monochelate and (α,γ)-monochelate complexes respectively but also the resonance coming from the boron trimer and pentamer. Then, new equilibria have been considered:

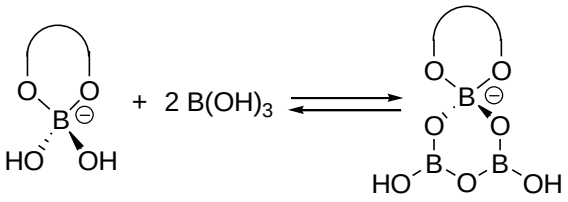

$$K_{O3} = \frac{\theta_{O3}}{(B(OH)_3)^2\theta_{BL}}$$

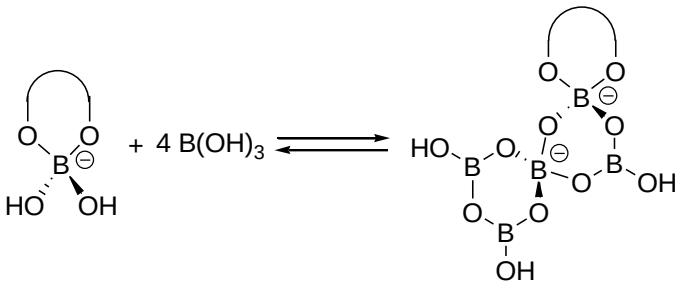

$$K_{O5} = \frac{\theta_{O5}}{(B(OH)_3)^4\theta_{BL}}$$

Where θ_{O3} and θ_{O5} state for the fraction of occupied sites by the trimers and pentamers species and θ_{BL} the fraction of occupied sites with any monochelate complexes. Hence, the adjustment considered has been:

$$(IA_{peak\ 1})_i * n(B_{ads})_{total\ i} = n(B_{ads})_{BL2i}$$

$$(IA_{peak\ 2})_i * n(B_{ads})_{total\ i} = n(B_{ads})_{BLPE\ i} + n(B_{ads})_{BLPI\ i} + n(B_{ads})_{B3L\ i}$$

$$(IA_{peak\ 3})_i * n(B_{ads})_{total\ i} = n(B_{ads})_{BLHI\ i} + n(B_{ads})_{B5L\ i}$$

Where $n(B_{ads})_{B3L}$ and $n(B_{ads})_{B5L}$ are the boron adsorbed in the form of trimer or pentamer species, respectively. Using this approach we show in Figure 11 the adjustment of the simulated values as solid lines to the experimental data, shown as discrete points. Also, in Table 6 the adjusted values for the above defined equilibrium constants used for the simulation of the data shown in Figure 11 are collected.

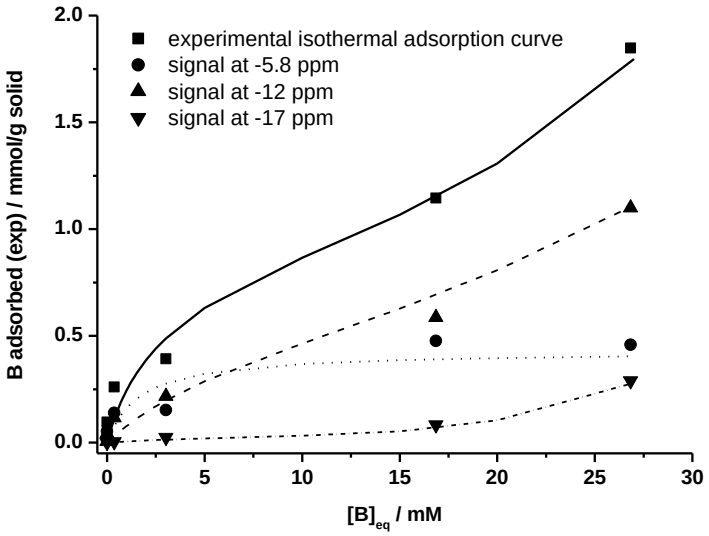

Figure 11. Isothermal boron adsorption on S1 solid: Experimental values (discrete symbols) and simulated ones (continuous lines) with the *site 1/site 2* model.

log K_2 (BL2)	-0.52
log K_4 (BLPE)	-4.00
log K_5 (BLPI)	-1.00
log K_6 (BLHI)	-2.15
log K_{O3} (B3L)	-2.96
log K_{O5} (B5L)	-6.15

Table 6. Results obtained from the *site 1/site 2* model essayed for the boron adsorption on **S1**.

From the values in Table 6 it can be seen that very different adsorption constants have been used to adjust the experimental data. As we have already discussed, the most stable complex to be form during the boron adsorption process correspond to the (α,β)bis-chelated species, being the monochelated ones less stable, and between them the (α,γ)mono-chelated complexes the least stable of them. Another important result is that the ability of the (α,β)mono-chelated complexes to displace the bis-chelated ones is low. In relation with the coordination of oligomeric species to the **S1** solid, the ability of the trimer species to be adsorbed onto the attached glucose molecules is considerable and higher than the ability of the pentameric oligomers.

5.4 **Conclusions**

As a summary, we have prepared an adsorbent for boron extraction from water by functionalization of a UVM7 mesoporous silica matrix with gluconamide moieties. The high affinity of boron towards polyols molecules makes of this material an excellent boron adsorbent. In order to get a better understanding of the adsorption process in this material several solids with increasing boron content have been prepared. ^{11}B and ^{13}C MAS NMR techniques have been used to elucidate the different coordination environments when boron is adsorbed onto the **S1** material and at least three different complexes have been identified, namely the bis-chelated (α,β)$_2$-BL$_2$ complex, the monochelate (α,β)-BL complex and the monochelate (α,γ)-BL one. Additionally, isothermal boron adsorption curves have been adjusted to a model including two different adsorption positions (*site 1* and *site 2*). Also, an additional adsorption of boron oligomeric species has been introduced in the model to take into account the increase of the adsorption curve in the presence of high boron concentrations. In this way, using three different coordination environments, two possible adsorption sites and the presence of oligomeric boron species it has been possible to reproduce not only the isothermal boron adsorption curve but also the evolution of the integrated areas for the signals in the ^{11}B MAS NMR spectra obtained for the different boron containing-**S1** materials.

ACKNOWLEDGEMENTS.

Financial support from the Spanish Government (Project MAT2009-14564-C04-01 and MAT2009-14564-C04-04, and MAT2012-38429-C04-01 and MAT2012-38429-C04-02) and the Generalitat Valenciana (Project PROMETEO/2009/016) is gratefully acknowledged. C.S. thanks the MICINN for a predoctoral fellowship.

References

1 P. D. Howe, *Biological Trace Element Research*, **1998**, 66, 153.

2 WHO, *Guidelines for drinking-water quality*, 4th ed., Malta, **2011**.

3 J. Wolska, M. Bryjak, *Desalination*, **2013**,310, 18.

4 B. Wang, X. Guo, P. Bai, *Colloids and Surfaces A: Physicicochem. Eng. Aspects*, **2014**, 444, 338.

5 Y. Xu, J.Q. Jiang, *Ind. Eng. Chem. Res*., **2008**, 47, 16.

6 T. Ben Amor, I. Dhaouadi, B. Lebeau, M. Tlili, M. Ben Amor*, Desalination*, **2014**, 351, 82.

7 D. I. Fried, A. Schlossbauer, T. Bein, *Microporous and Mesoporous Materials*, **2012**, 147, 5.

8 L. Wang, T. Qi, Y. Zhang, *Colloid. Surf. A*., **2006**, 275, 73.

9 O. Kaftan, M. Acikel, A.E. Eroglu, T. Shahwan, L. Artok, C. Ni, *Anal. Chim. Acta*., **2005**, 547, 31.

10 J. meseken, *Adv. Carbohydr. Chem*., **1949**, 4, 189.

11 J. Graham Dawber, Stuart I. E. Green, John C. Dawber and Sundus Gabrail*, J. Chem. Soc., Faraday Trans. I*, **1988**, 84(1), 41.

12 Y. Miyazaki, K. Yoshimura, Y. Miura, H. Sakashita, K. Ishimaru, *Polyhedron,* **2003**, 22, 909.

13 K. Benner, P. Klüfers, *Carbohydrate Research***, 2000**, 327, 287.

14 J. Graham Dawber, *J. Chem. Soc., Faraday Trans. I*, **1987**, 83, 771.

15 M.A. Becketta, C.C. Bland, K.S. Varma, *Polyhedron,* **2008**, 27, 2226.

16 N. Geffen, R. Semiat, M.S. Eisen, Y. Balazs, Il. Katz, C.G. Dosoretz, *Journal of Membrane Science,* **2006**, 286, 45.

17 Y. Miyazaki, H. Matsuo, T. Fujimori, H. Takemura, S. Matsuoka, T. Okobira, K. Uezu, K. Yoshimura, *Polyhedron*, **2008**, 27, 2785.

18 J. Graham Dawber, Stuart I. E. Green, *J. Chem. Soc., Faraday Trans. 1***, 1986**, 82, 3407.

19 K. Yoshimura, Y. Miyazaki, F. Ota, S. Matsuoka, H. Sakashita, *J. Chem. Soc., Faraday T rans*., **1998**, 94, 683.

20 G. Rodríguez-López, M.D. Marcos, R. Martínez- Máñez, F. Sancenón, J. Soto, L. A. Villaescusa, D. Beltrán and P. Amorós*, Chem. Commun.*, **2004**, 2198.

21 C. Sanfeliu, R. Martínez-Máñez, F. Sancenón, J. Soto, V. Puchol, P. Amorós, M. D. Marcos, *J. Mat. Chem*., **2012,** 22, 25362.

22 C. Sanfeliu, R. Martínez-Máñez, F. Sancenón, J. Soto, P. Amorós, M.D. Marcos, *Desalination*, **2015**, 374, 10.

23 S. Cabrera, J. El Haskouri, C. Guillem, J. Latorre, A. Betrán, D. Beltrán, M.D. Marcos, P. Amorós*, Solid State Sci.*, **2000**, 2, 405.

24 M. van Duin, J.A. Peters, A.P.G. Kieboom, and H. van Bekkum, *Tetrahedron,* **1984**, 40, 2901.

25 M. van Duin, J.A. Peters, A.P G. Kieboom, and H. van Bekkum, *Tetrahedron*, **1985**, 41, 3411.

26 W. G. Henderson, M. J. How, G. R. Kennedy*, and E. F. Mooney, *Carbohydrate Research*, **1973**, 28, 1.

27 Ron van den Berg, Joop A. Peters and Herman van Bekkum, *Carbohydrate Research*, **1994**, 253, 1.

28 D. G. Cory and W. M. Withney, *J. Magn. Reson*., **1988**, 80, 128.

29 L. Chu, M.I. Tejedor-Tejedor, M.A. Anderson, *Microp. Mater.,* **1997**, 8, 207.

30 I.C. Tilgner, P. Fischer, F. M. Bohnen, H. Rehage, W.F. Maier, *Microp. Mater*., **1995,** 5, 77.

31 R.K. Iler, *The Chemistry of Silica, John Wiley & Sons, New York*, **1979**.

32 S. Brunauer, P. H. Emmet, E. Teller, *J. Am. Chem. Soc.,* **1938**, 60, 309.

33 E. P. Barret, L. G. Joyner, P. P. Haselda*, J. Am. Chem. Soc*., 1951, 73, 373.

34 M. van Duin, J.A. Peters, A.P.G. Kieboom, H. van Bekkum, *Recl. Trav. Chim. Pays-Bas*, **1989**, 108, 57.

35 W.G. Henderson, M.J. How, G.R. Kennedy, E.F. Mooney. *Carbohydr. Res*., **1973**, 28, 1.

36 M. van Duin, J.A. Peters, A.P.G. Kieboom, H. van Bekkum. Tetrahedron, 40 (1984) 2901.

37 D.L. Harp, *Anal. Chim. Acta*, **1997**, 346, 373.

38 C. F. Baes, R.E. Messmer. *The hydrolysis of Cations. Ed. John Wiley & Sons Inc*, 1976.

39 C.S. Salentine, *Inorg. Chem.,* **1983**, 22, 3920.

6. Conclusions

The development of functional hybrid organic-inorganic materials is a relatively young field of research and has gained great interest in the last years, among others, in areas such as pollutant remediation. The present PhD thesis is intended to contribute to the expansion of these branches of research.

In the general introduction, the principles, of supramolecular chemistry have been described. The synthesis, functionalization and applications of mesoporous materials and other supports have been also reported. Furthermore, chemistry of boron and also the main methods for boron removal have been shown.

In the third chapter, the synthesis and characterization of a composite material for boron removal has been described. A ceramic foam has been used as macroscopic support for the active materials. Mesosporous material UVM-7 has been deposited on the monolithic support and then it has been functionalised with gluconamide as the active moiety for boron removal. The synthesis of this kind of composites shows a good reproducibility as all the tested monoliths present similar behavior and adsorption properties. When comparing with the parent adsorbent S1 (UVM-7), monoliths present lower adsorption kinetics. However they show comparable total adsorption capacity. The affinity of borate entities for the active sites in monoliths materials is lower than that for S1 which may indicate a different distribution of the active sites onto the composites. This different distribution may be related with a higher difficulty during the functionalization process due to a more intricate pathway for the organic moieties to reach the mesoporous surface. The capacity of composites to be recycled for new uses is quite good and makes this material a promising candidate to be tested in a continuous boron elimination process.

In the fourth chapter, the preparation of low cost materials for boron adsorption from water is reported. Several adsorbents have been prepared, based on different kinds of inorganic matrices. The inorganic matrix of solid S1 has been prepared by the previously reported atrane route with TEOS and $TEAH_3$ making used of a surfactant mediated template mechanism to obtain the porosity. For solid S2 the atrane route has been also used but in this case the porosity has been controlled with usual synthesis paramenters without the presence of surfactant molecules.

Solid S3 has been prepared from a commercial silica material, silica fumed. The silica scaffoldings of solids S4 and S5 have been obtained from inexpensive sodium silicate with a two step (hydrolysis and condensation) process. Once the inorganic matrices were synthetized they were functionalized with gluconamide, the active groups for boron adsorption. Solids S1 to S5 have been tested as boron adsorption agents in water. The adsorption ability follows the order of S1>S2>S4>>S3>S5. Hence low cost material S4 shows a remarkable boron adsorption, comparable to those of higher cost S1 and S2, suggesting that the replacement of templated mesoporous materials by silica xerogels make it possible to produce boron adsorbent agents for practical applications at a low cost. In addition, the recovery of adsorbents by a simple acidic wash has been shown, indicating a further minimization of costs for final adsorbents.

Finally, in the fifth and last chapter, a study of boron adsorption mechanism in UVM-7 gluconamide has been carried out. ^{11}B and ^{13}C MAS NMR techniques have been used to elucidate the different coordination environments when boron is adsorbed onto the active material and at least three different complexes have been identified.The boron adsorption data of S1-B1 to S1-B6 solids have been reproduced by using a Langmuir-Freundlich multilayer model. However, a better insight in the adsorption process has been obtained by combining experimental adsorption data with integrated areas from ^{11}B MAS NMR spectra. Taking into account the adsorption of oligomeric boron species it has been possible to reproduce the increase of the adsorption curve of high boron concentration. In this way, using three different coordination environments, two possible adsorption sites and the presence of oligomeric boron species it has been possible to reproduce not only the isothermal boron adsorption curve but also the evolution of the integrated areas for the signals in the ^{11}B MAS NMR spectra obtained for the different boron containing materials.